TECHNISCHE UNIVERSITÄT MÜNCHEN
TUM School of Life Sciences

The intestinal clock drives microbial rhythms to maintain host gastrointestinal homeostasis

Baraa Altaha

Vollständiger Abdruck der von der TUM School of Life Sciences der Technischen Universität München zur Erlangung des akademischen Grades eines

Doktors der Naturwissenschaften (Dr. rer. nat.)

genehmigten Dissertation.

Vorsitz: Prof. Dr. Martin Klingenspor

Prüfende der Dissertation:
1. Prof. Dr. Dirk Haller
2. Prof. Dr. Nina Henriette Uhlenhaut

Die Dissertation wurde am 19.02.2024 bei der Technischen Universität München eingereicht und durch die TUM School of Life Sciences am 03.06.2024 angenommen.

"The reward of the young scientist is the emotional thrill of being the first person in the history of the world to see something or to understand something. Nothing can compare with that experience."

Cecilia Payne-Gaposchkin

Abstract

The internal body clocks time activity, behavior, and physiology in a circadian (~24-hour) manner. Mismatch between these internal clocks and external timing cues can disrupt the circadian system, for example in the case of shift work or frequent jet lag. Circadian disruption promotes various diseases, including type 2 diabetes and obesity. This is not surprising, considering the impact of the circadian system on key regulators of gastrointestinal homeostasis, including metabolic functions and microbial composition. In fact, the gut microbiome oscillates diurnally. However, little is known about the factors that drive microbial rhythms. Additionally, the cause-effect relationship between microbial dysbiosis and metabolic diseases during circadian disruption remains largely unknown.

Here, we differentiate between internal and external timing cues in assessing how they drive microbial rhythms. Using 16S rRNA analysis of fecal microbiota from mice kept in constant darkness and under starvation conditions, we provide the first evidence of the circadian origin of microbial rhythms, identifying environmental signals as mere modulators of these oscillations. We also show that intestinal-specific clock knockout abolishes microbial rhythmicity, pinpointing the intestinal clock as the dominant driver of microbial rhythmicity. Remarkably, we discover that genetic and environmental circadian disruptions can desynchronize the intestinal clock. Circadian disruption also results in a loss of microbial composition and function rhythmicity, thereby reinforcing the role of the intestinal clock in driving microbial rhythms. Notably, circadian disruption alters taxa involved in the metabolism of short-chain fatty acids and lipids in both models, with these findings being further confirmed by PICRUST 2.0 and targeted metabolite analyses.

These results suggest that a loss of microbial rhythmicity alters metabolic homeostasis. Indeed, both circadian disruption mouse models show increased body weight. Germ-free colonization experiments mechanistically link body weight gain to the loss of microbial rhythmicity during circadian disruption. Interestingly, circadian disruption-associated microbiota in turn disrupts peripheral clock-gene expression in recipient mice, indicating a bidirectional relationship between microbiota rhythmicity and peripheral clocks.

In summary, we highlight the essential role of the intestinal clock for rhythmic microbial composition. Moreover, our results suggest that the metabolic phenotype observed in shift work is promoted by the loss of microbial rhythmicity and consequently its functionalities, with this loss originating from intestinal clock desynchronization.

Zusammenfassung

Die innere Uhr des Körpers steuert das Aktivitätsverhalten und die Physiologie auf zirkadiane (~24 Stunden) Weise. Wenn die internen Uhren nicht mit den externen Zeitgebern übereinstimmen, wie z. B. bei Schichtarbeit und häufigem Jetlag, wird das zirkadiane System gestört. Eine Störung des zirkadianen Systems begünstigt verschiedene Krankheiten, unter anderem Typ-2-Diabetes und Fettleibigkeit. Dies ist nicht überraschend, wenn man bedenkt, dass das zirkadiane System wichtige Regulatoren der gastrointestinalen Homöostase beeinflusst, darunter Stoffwechselfunktionen und die Zusammensetzung des Mikrobioms. Tatsächlich oszilliert das Darmmikrobiom tageszeitlich. Allerdings ist wenig über die Faktoren bekannt, die die mikrobiellen Rhythmen steuern. Ebenso ist die Ursache-Wirkungs-Beziehung zwischen mikrobieller Dysbiose und Stoffwechselkrankheiten während einer Störung des Tagesrhythmus noch weitgehend unbekannt.

Hier unterscheiden wir zwischen internen und externen Zeitgebern, die mikrobielle Rhythmen steuern. Mit Hilfe der 16S rRNA-Analyse der fäkalen Mikrobiota von Mäusen, die in konstanter Dunkelheit und unter Hungerbedingungen gehalten wurden, liefern wir erste Beweise für den zirkadianen Ursprung der mikrobiellen Rhythmen und identifizieren Umweltsignale als reine Modulatoren dieser Oszillation. Wir zeigen auch, dass das Ausschalten der Darmuhr die mikrobielle Rhythmik aufhebt, wodurch die Darmuhr als dominante Triebkraft der mikrobiellen Rhythmik identifiziert wird. Bemerkenswerterweise stellen wir fest, dass genetische und umweltbedingte zirkadiane Störungen die Darmuhren desynchronisieren. Die Störung der zirkadianen Uhr führt auch zu einem Verlust der mikrobiellen Zusammensetzung und Funktionsrhythmik. Dadurch wird die Rolle der intestinalen Uhren bei der Steuerung mikrobieller Rhythmen gestärkt. Bemerkenswert ist, dass die Störung der zirkadianen Uhr in beiden Modellen Taxa verändert, die am SCFA- und Lipid-

Stoffwechsel beteiligt sind, was durch PICRUST 2.0 und gezielte Metabolit-Analysen weiter bestätigt wurde. Diese Ergebnisse lassen vermuten, dass sich der Verlust der mikrobiellen Rhythmik auf den Stoffwechsel auswirkt. In der Tat ist das Körpergewicht in beiden Mausmodellen erhöht, wenn die Zirkadianität gestört ist. In Experimenten zur keimfreien Besiedlung wird die Zunahme des Körpergewichts mechanistisch mit dem Verlust der mikrobiellen Rhythmik während der circadianen Störung in Verbindung gebracht. Interessanterweise stört die mit der zirkadianen Störung assoziierte Mikrobiota die Expression peripherer Uhrengene in den Empfängermäusen, was auf eine bidirektionale Beziehung zwischen der Rhythmizität der Mikrobiota und den peripheren Uhren hinweist.

Zusammenfassend lässt sich sagen, dass wir die wesentliche Rolle der Darmuhr für die rhythmische Zusammensetzung des Mikrobioms hervorheben. Darüber hinaus deuten unsere Ergebnisse darauf hin, dass der metabolische Phänotyp, der bei Schichtarbeitern beobachtet wird, durch den Verlust der mikrobiellen Rhythmik und folglich ihrer Produkte gefördert wird, was auf die Desynchronisierung der Darmuhr zurückzuführen ist.

Contents

TABLE OF CONTENTS

1. Introduction

1.1. The circadian system

Various physiological processes follow a ~24-hour rhythm. These circadian (*circa* = about; *dies* = day) rhythms are generated by endogenous clocks, which are located in most organisms and cells (Dunlap 1999). Those circadian clocks are internal, self-sustained, and entrainable by external factors, typically environmental cues or so-called *Zeitgebers* (German for 'time-giver') (Aschoff 1960).

But why do we possess a circadian system? these clocks have evolved to prepare for recurring changes in environmental conditions such as light, food, and social activities (Damiola, Le Minh et al. 2000, Stokkan, Yamazaki et al. 2001, Dibner, Schibler et al. 2010). Mammals have a complex hierarchal circadian system with a central pacemaker in the hypothalamus, the suprachiasmatic nuclei (SCN) (Stephan and Zucker 1972). After receiving light input, the SCN regulates diurnal activity and feeding behavior and orchestrates subordinated peripheral clocks, present in other tissues and organs, through humoral and neuronal signals (Schibler, Ripperger et al. 2003). Therefore, SCN ablation results in a complete loss of rhythmic activity (Stephan and Zucker 1972) and desynchronizes peripheral clocks (Kolbe, Leinweber et al. 2019). Light and food serve as the main *Zeitgebers* for central and peripheral clocks, respectively. For example, reversing the light-dark (LD) cycle completely shifts the SCN clock (Green and Gillette 1982), while restricting food intake adjusts peripheral clocks to the feeding schedule without affecting the central clock (Damiola, Le Minh et al. 2000).

1.1.1. Clock molecular mechanism

On the molecular level, the circadian clock consists of a subset of clock genes organized in autoregulatory feedback loops. In the main loop, the transcription factors Circadian Locomotor Output Cycles Kaput (CLOCK) and Brain and Muscle ARNT-Like 1 (BMAL1) dimerize to

activate the expression of Period (*per*) and Cryptochrome (*cry*) genes by binding to E-box elements in their promoter. After a time delay, the corresponding PER and CRY proteins build heterodimers in the cytoplasm. Then PER:CRY complexes translocate to the nucleus to suppress *bmal1* and *clock* transactivation (Figure 1) (Duguay and Cermakian 2009). The degradation and translocation of these complexes are controlled by casein kinases (CKI) and protein phosphatases (PP), thus impacting the intrinsic period (Partch, Green et al. 2014). On the secondary loop, the BMAL1/CLOCK heterodimers also activate the activator ROR ALPHA and the inhibitor REV ERB alpha. These transcription factors act on the *bmal1* promoter by binding to the RORE DNA binding element.

Mutations in the clock genes alter the circadian rhythms with different effects. For example, deletion of a major clock component such as *bmal1* in mice leads to complete arrhythmicity (Bunger, Wilsbacher et al. 2000). Other examples of the impact of clock genes on rhythmicity are summarized in Table1. The molecular clock regulates the transcription of thousands of so-called clock-controlled genes (CCGs). Therefore, in any given cell type or organ, hundreds to thousands of genes are expressed rhythmically, which leads to the estimation that ~50% of all genes oscillate in at least one organ (Zhang, Lahens et al. 2014). Consequently, most cellular and physiological processes show 24-hour oscillations, including cell proliferation, immune cell functionalities, intestinal barrier functions, and microbial composition and function (Wu, Cai et al. 2010, Summa, Voigt et al. 2013, Thaiss, Zeevi et al. 2014, Stokes, Nunes et al. 2021).

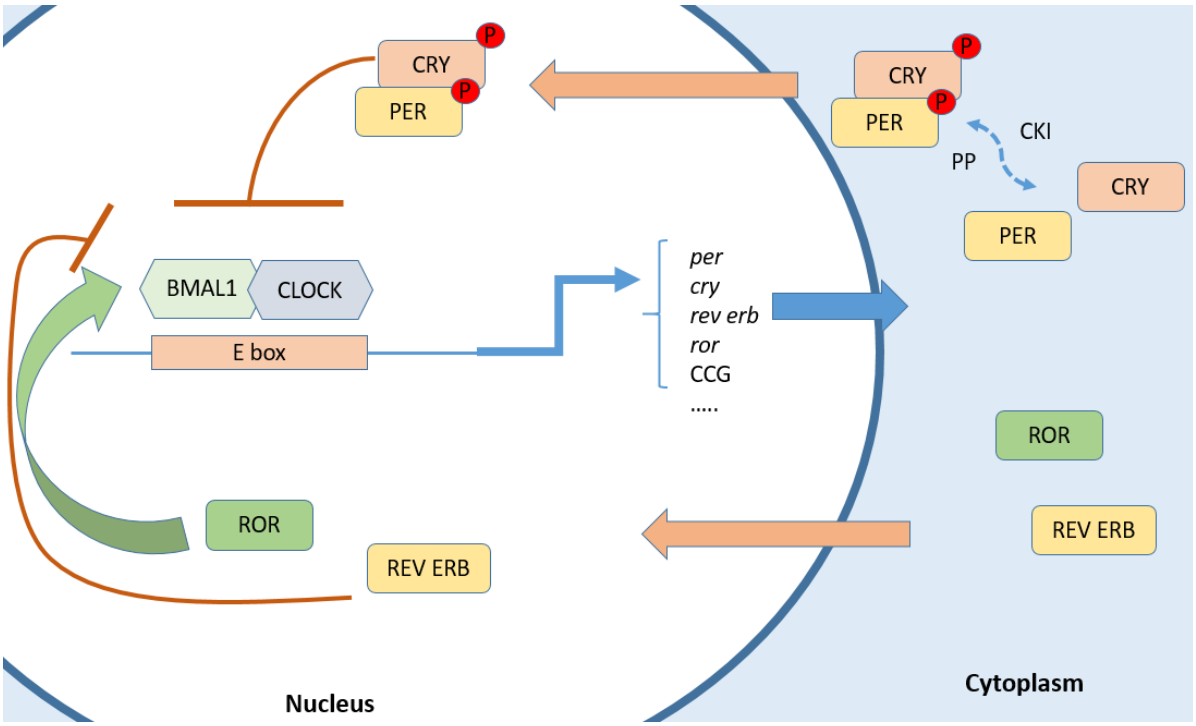

Figure 1: Mammalian circadian clock molecular mechanism
CLOCK and BMAL1 dimerize to activate the expression of per, cry, rev erb, ror, and other CCGs by binding to E-box elements in their promoter. PER and CRY proteins in the cytoplasm heterodimerize and translocate to the nucleus after phosphorylation (P) by CKI, which protein phosphatases (PP) counteracts. In the secondary loop BMAL1/CLOCK heterodimers activate ror alpha and rev erb alpha, which bind to RORE DNA binding element to activate and inhibit bmal1 transcription, respectively.

Table 1: Gene-specific effects of clock-gene disruption

Gene	Effect	Reference
clock	- Mutation in one allele lengthens the period. - Mutation in both alleles results in complete arrhythmicity after two weeks in constant darkness (DD). Notably, a light pulse restores rhythmicity temporarily.	(Vitaterna, King et al. 1994)
bmal1	- Complete arrhythmicity in DD. - Reduced activity in the LD cycle. - Light pulse cannot rescue the phenotype.	(Bunger, Wilsbacher et al. 2000)
per1-3	- *Per1*-deficient mice have ~1-hour shorter circadian period, with reduced precision. These mice express rhythmic clock-gene expression in DD. - *Per2* mutation reduces the circadian period, followed by arrhythmicity in mice in DD. Consequently, these mice have arrhythmic clock-gene expression in DD. Notably, a light pulse restores the rhythmicity temporarily. - *Per1/per2* mutant mice are rhythmic in LD. However, they become arrhythmic directly upon release in DD.	(Zheng, Albrecht et al. 2001) (Zheng, Larkin et al. 1999)
cry1-2	- *Cry 1* knockout mice possess ~1hour shorter free-running period. - *Cry1-2* double knockout are immediately arrhythmic in DD. - *Cry2* knockout mice possess ~1 hour longer free-running period.	(Vitaterna, Selby et al. 1999) (Thresher, Vitaterna et al. 1998)
rev erb	- *Rev erb* α -/- mice possess a functional molecular clock with altered amplitude of some clock genes. - *Rev erb* α -/- mice are rhythmic in DD and constant light. However, they have a shorter free-running period. - *Rev erb* α -/- mice show an altered response to phase shift.	(Preitner, Damiola et al. 2002)
ror	- *Ror β* -/- mice are rhythmic in LD and DD, with a lengthened circadian period and altered response to light pulses. - *Ror α* mutant mice are rhythmic in LD and DD, with a shorter circadian period and aberrant responses to photic manipulation. - *Ror γ* -/- mice show normal circadian behavior.	(Akashi and Takumi 2005, Masana, Sumaya et al. 2007, Liu, Tran et al. 2008)

1.1.2. Peripheral clocks are essential for organ-specific functions

Peripheral clocks have been discovered in most cells and tissues, controlling organ-specific gene oscillations. For example, the liver clock drives rhythmic metabolic processes. In fact, deletion of the liver clock impairs glucose and lipid homeostasis (Manella, Sabath et al. 2021). Moreover, the pancreatic clock plays an indispensable role in insulin production and glucose sensing (Sadacca, Lamia et al. 2011), showing the essentiality of peripheral clocks for organ functions.

Research to discover organ-specific clocks has also led to the discovery of the intestinal clock (Moore, Pruszka et al. 2014). What's the role of the intestinal clock? Although few studies have investigated its function, the intestinal clock seems to control the cell cycle and gut uptake system, as well as skeletal muscle metabolism (Kawai, Kinoshita et al. 2019, Ko, Jochum et al. 2021, Stokes, Nunes et al. 2021). Table 2 summarizes the current literature on the intestinal clock. Considering the numerous rhythmic gut functionalities (Hoogerwerf 2010, Pacha and Sumova 2013, Peterson and Artis 2014, Segers and Depoortere 2021), little is known about the role of the intestinal clock in these rhythms. Therefore, future research should decipher its impact on intestinal and other tissue functions.

1.1.3. Shift work disrupts the circadian system

Shift work or frequent jet lag impairs internal clocks while the body adjusts to the new LD cycle. In fact, not only do different tissues adjust to this new cycle at different speeds (Yamazaki, Numano et al. 2000), but clock genes also resynchronize at different speeds within the same tissue (Kiessling, Eichele et al. 2010). Therefore, shift work results in global circadian disruption. Several studies have shown the deteriorating effects of circadian disruption to the extent of increased mortality in aged mice (Davidson, Sellix et al. 2006). This is not surprising, considering that circadian disruption weakens host defenses and promotes various diseases

(Kiessling, Dubeau-Laramee et al. 2017, Codoner-Franch and Gombert 2018, Parkar, Kalsbeek et al. 2019). For example, circadian disruption exaggerates the inflammatory response to lipopolysaccharides (LPS) in mice due to a dysregulated innate immune system (Castanon-Cervantes, Wu et al. 2010). Epidemiological studies have associated shift work with the development of obesity and other metabolic syndromes (Peplonska, Bukowska et al. 2015, Sooriyaarachchi, Jayawardena et al. 2022). Furthermore, circadian disruption promotes weight gain and glucose intolerance in mice (Oike, Sakurai et al. 2015). It is still unclear how the circadian disruption induces metabolic abnormalities, although Thaiss and colleagues have shown involvement of the gut microbiota (Thaiss, Zeevi et al. 2014).

Table 2: Diurnal intestinal clock disruption alters host homeostasis

Author	**Gender**	**Mouse model**	***Zeitgeber* time (ZT)/circadian time (CT)**	**Findings**
(Chen, Yu et al. 2021)	Male	*bmal1*$^{fl/fl}$ *.villin-cre*	LD cycle 6 time points	- The intestinal clock controls carboxylesterase (*ces1*) gene diurnal rhythmicity.
(Kawai, Kinoshita et al. 2019)	Male	*bmal1*$^{fl/fl}$ *.villin-cre*	LD cycle 6 time points	Loss of the intestinal clock results in: - Loss of vitamin D response (*vdr*) gene rhythmicity. - Loss of *vdr* target-gene rhythmicity. - Decrease in transcellular calcium absorption. - Loss of serum calcium rhythmicity. - Activation of bone resorption. - Reduction in bone mass.
(Ko, Jochum et al. 2021)	Male and female	*bmal1*$^{fl/fl}$*.ts4-cre*	LD cycle 1 time point	- Colonic deletion of *bmal1* impairs bone formation in male, but not female, mice.

(Martchenko, Martchenko et al. 2021)	Male and female	*bmal1$^{fl/fl}$. gcg-cre*	LD cycle 2 time points	Loss of the circadian clock in intestinal L-cells results in: - Loss of time-dependent secretion of glucagon-like peptide-1 (GLP1). - Reduction in colonic CD4+ abundance and increase in *ifn, il6* expression. - Increase in *Actinobacteria* abundance. - Decrease in abundance of short-chain fatty acids (SCFAs) and bile acids.
(Stokes, Nunes et al. 2021)	Gender not specified	*apc^{min} ,bmal1$^{fl/fl}$ .villin-cre*	LD cycle 1 time point	- Loss of the intestinal clock promotes tumor initiation. - Absence of the intestinal clock results in lower *wnt* and higher *hippo* pathway activity.
(Penny, Domingues et al. 2022)	Gender not specified	*bmal1$^{fl/fl}$ .villin-cre*	LD cycle 4 time points	- The intestinal clock does not control rhythmic fecal IgA secretion.
(Yu, Zhang et al. 2019)	Male	*bmal1$^{fl/fl}$ .villin-cre*	LD cycle 6 time points	- Absence of the intestinal clock disrupts *mrp2* rhythmicity.
(Yu, Wang et al. 2021)	Male	*bmal1$^{fl/fl}$ .villin-cre*	LD cycle 6 time points	- The intestinal clock regulates diacylglycerol acyltransferase (*dgat2*) rhythmicity. - Absence of the intestinal clock protects from high-fat-diet-induced obesity, due to reduced fat absorption.

1.2. The gut microbiota

Over the course of evolution, various species evolved mutualistic relationships with tissue-resident microbiota, including in the gut. The gut microbiota consists of a complex, dynamic array of bacteria, viruses, fungi, and bacteriophages that inhabit the gastrointestinal tract (Lozupone, Stombaugh et al. 2013). Here, we will focus on the gut bacteria and refer to them as the gut microbiome or the gut microbiota. Although some of these bacteria are opportunistic pathogens, which can lead to infection and even sepsis in some circumstances (Guarner and Malagelada 2003), the gut microbiome plays an essential role in host physiology and metabolism such as maintaining gut integrity (Natividad and Verdu 2013), defending against pathogens, vitamin production, energy and nutrient extraction from the diet (den Besten, van Eunen et al. 2013), and regulating the development of host immunity (Gensollen, Iyer et al. 2016).

1.2.1. The gut microbiota impacts host physiology

Various studies using germ-free animals and antimicrobial cocktails have highlighted the functional contribution of the gut microbiota to host physiology (Gensollen, Iyer et al. 2016). Germ-free mice possess physiologically and anatomically altered gastrointestinal tracts (Gensollen, Iyer et al. 2016). For example, germ-free mice have an enlarged cecum, thinner intestinal walls, and reduced epithelial renewal compared with conventionalized controls (Gustafsson, Midtvedt et al. 1970, Thompson and Trexler 1971). Notably, administration of an antimicrobial cocktail yields germ-free-like characteristics, highlighting the indispensable role of the microbiota on host physiology (Kennedy, King et al. 2018). In addition, the gut microbiota plays an essential role in gastrointestinal immune cell recruitment and in developing a competent immune system (Gensollen, Iyer et al. 2016). In fact, germ-free mice have smaller spleen and mesenteric lymph nodes, a lower number of lymphoid cells, and fewer immunoglobulins

(Horowitz, Bauer et al. 1964, Gordon, Bruckner-Kardoss et al. 1966, Gensollen, Iyer et al. 2016). Matsumoto and colleagues have shown low intestinal MHCII expression in germ-free mice intestinal epithelial cells (IEC) (Matsumoto, Setoyama et al. 1992). Furthermore, the gut microbiota induces the excretion of antimicrobial peptide, REG IIIγ, by paneth cells (Cash, Whitham et al. 2006).

Interestingly, germ-free mice lack functional circadian clocks (Leone, Gibbons et al. 2015). Antibiotic administration to wild-type mice has further confirmed the importance of gut microbiota for intestinal clock functionality (Mukherji, Kobiita et al. 2013), pointing to a potential bidirectional relationship between the gut microbiota and the intestinal clock. Altogether, microbiota-host crosstalk is essential for host physiological functions, either through direct interactions with the host or through its metabolic functions.

1.2.2. Gut microbiota metabolic functions

The genomic diversity of the gut microbiota provides novel enzymes and new biochemical pathways (AL-Taha, Wadi et al. 2018). These pathways increase food utilization by fermenting indigestible dietary products and utilizing epithelial-produced mucus (Cummings, Pomare et al. 1987). Thus, the gut microbiota increases the amount of absorbable substrates and, consequently, the recovered metabolic energy for the host, while supplying nutrients and energy for microbial growth and proliferation. Although the gut microbiota is involved in several metabolic processes, here we will focus on SCFA fermentation and bile acid production.

1.2.3. Short-chain fatty acids (SCFAs)

The gut microbiota ferments non-digestible carbohydrates and generates SCFAs, including acetate, butyrate, and propionate (Cummings, Pomare et al. 1987, Cummings, Beatty et al. 1996).

SCFAs can also be produced by anaerobic metabolism of peptides and proteins (Macfarlane, Cummings et al. 1986). The effect of SCFAs on health has been extensively studied since discovering their receptor FFAR 2/3 in several cell types (Macfarlane, Cummings et al. 1986, Nilsson, Kotarsky et al. 2003).

In terms of their role, SCFAs impact gut integrity, glucose metabolism, immune functions, and disease development (Cummings, Pomare et al. 1987, Sanna, van Zuydam et al. 2019). For example, colonocytes utilize SCFAs, especially butyrate, as energy sources (Clausen and Mortensen 1995). Butyrate also enhances intestinal barrier functions by regulating tight junction protein expression (Wang, Wang et al. 2012). Butyrate and propionate promote intestinal glycogenesis, improving energy and glucose homeostasis (De Vadder, Kovatcheva-Datchary et al. 2014). Interestingly, SCFAs are also transported to the bloodstream, exerting extra-intestinal functions such as liver gluconeogenesis and lipogenesis (den Besten, Lange et al. 2013). As another example, acetate stimulates adipocyte leptin secretion, regulating energy balance and food intake (Zaibi, Stocker et al. 2010). Thus, and not surprisingly, the alteration of SCFAs has been linked to obesity and type 2 diabetes (de la Cuesta-Zuluaga, Mueller et al. 2018, Sanna, van Zuydam et al. 2019, Kaczmarczyk, Dabek-Drobny et al. 2022).

1.2.4. Bile acids

Many studies focus on bile acids as an important class of microbial-produced metabolites. Bile acids are synthesized by the liver from cholesterol and further metabolized by the gut microbiota (Wahlström, Sayin et al. 2016). Bile acids then act as signaling molecules to regulate host sterol, glucose, and energy homeostasis (Lambert, Amar et al. 2003, Ma, Saha et al. 2006). Bile acids also shape the gut microbiota by promoting bile-metabolizing bacteria, killing bile-sensitive bacteria, and inducing antimicrobial transcription through the bile acid receptor FXR (Inagaki,

Moschetta et al. 2006). However, bile acids and the microbiota do not interact in a unidirectional way. For its part, the gut microbiota regulates several enzymes involved in bile acid synthesis and uptake, in addition to its role in bile acid metabolism (reviewed by (Wahlström, Sayin et al. 2016)). For example, modulating the gut microbiota decreases weight gain through the bile acid-FXR signaling pathway (Li, Jiang et al. 2013). Moreover, germ-free experiments further prove that microbial-mediated bile acid modification alters obesity and glucose metabolism (Parséus, Sommer et al. 2017). Thus, and not surprisingly, bile acid alteration has been associated with metabolic disorders. For example, obese mice possess higher levels of the secondary bile acid deoxycholic acid (DCA) (Yoshimoto, Loo et al. 2013). Bile acid receptor deletion (FXR) results in hypercholesterolemia and hyperglycemia (Lambert, Amar et al. 2003, Ma, Saha et al. 2006). In summary, the interaction between the gut microbiota and bile acids is essential for maintaining host metabolic homeostasis.

1.3. Host-microbe interaction

The cross-talk between the gut microbiota and the host ensures a homeostatic, mutualistic relationship. Accordingly, gut microbial dysbiosis has been associated with several diseases such as inflammatory bowel disease (IBD), diabetes, and obesity, with detrimental effects (Fan and Pedersen 2021). For example, most IBD mouse models do not develop inflammation in germ-free conditions (Keubler, Buettner et al. 2015).

These microbe-host interactions have created multiple opportunities to modify the gut microbiota for our health. Consequently, several microbial-based interventions have been studied, with promising results (Nishida, Inoue et al. 2018). It is therefore of the utmost importance to identify the factors that shape the microbial ecosystem.

1.3.1. Factors shaping the gut microbiota

The gut microbiota is controlled dynamically at multiple levels. Its formulation begins directly after birth upon exposure to the mother's microbiota (Browne, Shao et al. 2022). Over time, the microbial diversity of the gut expands tremendously, outnumbering by 10 times the eukaryotic cells in the human body (Yao, Cai et al. 2021). However, many factors can shape our gut microbiota throughout our lives, including diet, environment, age, health status, and other host's intrinsic factors (Parkar, Kalsbeek et al. 2019). For example, a diet switch can shift microbial composition within a day (Turnbaugh, Ridaura et al. 2009). A recent meta-analysis has demonstrated the consistent effects of a high-fat diet on microbial composition (Bisanz, Upadhyay et al. 2019). Moreover, the gut microbiota changes substantially at both extremes of life (Claesson, Cusack et al. 2011, Savage, Lee-Sarwar et al. 2018). Health status, too, impacts the microbial balance. For example, several studies have detected altered microbial composition and functions in obesity, type 2 diabetes, and IBD (reviewed in (Fan and Pedersen 2021)). Importantly, the gut microbiota is also influenced by host's intrinsic factors, including their immune system and internal clocks (Thaiss, Zeevi et al. 2014, Thaiss, Zmora et al. 2016, Fulde, Sommer et al. 2018).

1.3.2. The gut microbiota and the circadian system

How does the circadian system influence the gut microbiota? Recently, it has been demonstrated that the gut microbiota oscillates diurnally in humans and mice (Thaiss, Zeevi et al. 2014, Reitmeier, Kiessling et al. 2020). This microbial rhythmicity seems to be imprinted through the host's circadian clocks, diet, feeding time, and several environmental factors (Thaiss, Zeevi et al. 2014, Zarrinpar, Chaix et al. 2014, Leone, Gibbons et al. 2015).

Wu and colleagues have shown that luminal and mucosal-associated microbial rhythms depend on the presence of the LD cycle (Wu, Tang et al. 2018). Notably, gender also impacts microbial

diurnal oscillations, with females showing more robust oscillations in the fecal microbiota (Liang, Bushman et al. 2015). Interestingly, the rhythmicity of specific taxa depends on gut IgA secretion, especially IgA-bound bacteria. Thais and colleagues have pointed out that feeding behaviors control taxa-specific rhythmicity (Thaiss, Zeevi et al. 2014). On the one hand, feeding behavior is governed by the central clock through the sleep-wake cycle. On the other hand, rhythmic food intake is the main *Zeitgebers* controlling peripheral clocks (Damiola, Le Minh et al. 2000), suggesting a potential impact of the circadian system. Indeed, a functional host's circadian system is required for microbial rhythmicity, and circadian disruption abolishes this rhythmicity (Thaiss, Zeevi et al. 2014, Liang, Bushman et al. 2015, Voigt, Summa et al. 2016). For example, Voigt has shown that environmental circadian disruption alters microbiota composition under a high-fat, high-sugar diet (Voigt, Forsyth et al. 2014). In addition, mice with genetic circadian disruption possess arrhythmic microbiota (Thaiss, Zeevi et al. 2014).

Despite this evidence, several factors that might play a critical role in microbial rhythmicity remained to be addressed such as the roles played by the central clock, the peripheral clocks, and other environmental factors.

1.3.3. Microbial rhythmicity

What is the role of microbial rhythmicity? Kuang and colleagues have shown that the gut microbiota induces rhythmic histone acetylation in the small intestine, synchronizing nutrient uptake and metabolic gene expression (Kuang, Wang et al. 2019). Moreover, the gut microbiota controls NFIL3 rhythmicity through the circadian system, regulating lipid uptake and body composition (Wang, Kuang et al. 2017). The gut microbiota produces SCFAs rhythmically. SCFAs, in turn, alter peripheral clock-gene expression (Leone, Gibbons et al. 2015, Tahara, Yamazaki et al. 2018). These results suggest a bidirectional relationship between the host

circadian system and microbial rhythmicity to maintain a fine balance, preserving host metabolic and intestinal homeostasis.

A few studies have directly investigated the role of microbial rhythms. For example, Thais and colleagues have linked arrhythmic microbiota to body weight gain during chronic jet lag (Thaiss, Zeevi et al. 2014). Loss of microbial rhythmicity has also been found in type 2 diabetic patients; interestingly, microbial arrhythmicity can provide a risk signature for developing type 2 diabetes (Reitmeier, Kiessling et al. 2020). In summary, microbial rhythmicity seems to affect the metabolic homeostasis of the host, yet more research is needed to shed more light on its role and to decipher the mechanisms by which it impacts the host.

2. Aims and scope of dissertation

The gut microbiota oscillates between day and night. Although microbial rhythms are affected by the circadian system and feeding time, little is known about the factors driving these rhythms. **We hypothesize that circadian intrinsic factors play a major role in driving microbial oscillations.** To address this point, we differentiated in this study between the intrinsic and extrinsic factors that might impact microbial rhythms, especially light, food, and the local intestinal clock. Firstly, we assessed the effect of the LD cycle on microbial oscillations by comparing microbial rhythms from mice in a 12:12 LD cycle and DD. Secondly, we identified the impact of rhythmic food intake on microbial rhythms by comparing the results of mice under the starvation protocol and those with *ad libitum* food access. Finally, we investigated the role of the intestinal clock on microbiota oscillations by comparing the microbial changes between intestinal clock-proficient and clock-deficient mice.

Shift work and chronic jetlag disrupt the circadian system, microbial rhythmicity, and metabolic homeostasis (Kiessling, Eichele et al. 2010, Thaiss, Zeevi et al. 2014, Voigt, Forsyth et al. 2014). Although studies have linked microbial arrhythmicity to metabolic disease (Thaiss, Zeevi et al. 2014, Reitmeier, Kiessling et al. 2020), the cause-effect relationship between these factors during circadian disruption remains unclear. **Here, we hypothesize a bidirectional relationship between the circadian system and microbial rhythmicity to maintain metabolic balance**. To address this, we investigated the microbial-host interaction using genetic and environmental circadian disruption mouse models. Moreover, we directly assessed the role of microbial rhythmicity on host metabolism by colonizing germ-free mice with circadian disruption-associated microbiota.

3. Materials and method

3.1. Ethics statement

Animal experiments were approved by the Bavarian Animal Care and Use Committee (No. TVA ROB-55.2Vet-2532.Vet_02-18-14) and by the Ministry of Agriculture, Environment, and Rural Areas (MELUR) of the state of Schleswig-Holstein (project license:42-5/18_Oster) for the experiments conducted at the Technical University of Munich and University of Lübeck, respectively.

3.2. Animal experiments

All mice were single-housed with *ad libitum* access to water and a chow diet (Ssniff, Soest, Germany). Unless specified, animals were maintained under specific pathogen-free (SPF) conditions in accordance with the FELASA recommendation. Littermate animals of comparable age were used to minimize the cage effect on microbiota composition (Ubeda, Lipuma et al. 2012). To limit gender effects, only male mice were used for all experiments. Unless mentioned, animals were kept in a normal LD 12:12 cycle with 300 lux light intensity. The lights were turned on at 5 a.m. (ZT 0) and turned off at 5 p.m. (ZT 12). Mice were checked daily and monitored weekly for changes in body weight.

3.2.1. *Syt10 ^{cre}-bmal1$^{IEC\ +/-}$* and *syt10 ^{cre}-bmal1$^{IECfl/-}$* mice

SCN-specific *bmal1* knockout mice and their control littermates (respectively: *syt-10 cre/wt* x *bmal1fl/-*, referred to in the text as *bmal1$^{SCNfl/-}$* ; and *syt-10 cre/wt* x *bmal1+/-*, referred to in the text as *bmal1$^{SCN+/-}$*) on C57BlL6 genetic background were generated as described before (Husse, Zhou et al. 2011) at the University of Lübeck. On the second day of DD, mice were sacrificed at the indicated CT points.

3.2.2. *Bmal1 $^{IEC-/-}$* and *bmal1 $^{IECfl/fl}$* mouse generation

Intestinal epithelial-cell-specific *bmal1* knockout C57BL/6J mice and their control littermates (*bmal1fl/fl* x *villin cre/wt* and *bmal1fl/fl x villin wt/wt*, referred to in the text as *bmal1$^{IEC-/-}$* and *bmal1$^{fl/fl}$*, respectively) were generated at the Technical University of Munich as previously described (Kawai, Kinoshita et al. 2019). At the age of eight weeks, mice were single-housed and

had free access to a running wheel. On the second day of DD, mice were sacrificed at the indicated CT points.

3.2.3. Simulated shift work (SSW)

Wild-type C57BL6 mice were bred at the Technical University of Munich. At the age of eight weeks, mice were single-housed and had free access to a running wheel. SSW mice were kept in LD cycle for two weeks (from week 8 to week 10) and then exposed to SSW for at least six weeks. At the age of 10 weeks, we changed the light intensity to 100 lux. SSW was accomplished by shifting the LD cycle in advance or delaying it by 8 hours every five days. Thus, on the first day of jet lag in the phase advance paradigm, we shifted ZT 12 from 5 p.m. to 9 a.m. Then, after five days, we introduced the mice to a phase delay by shifting ZT 12 from 9 a.m. to 5 p.m., as illustrated in Figure 2.

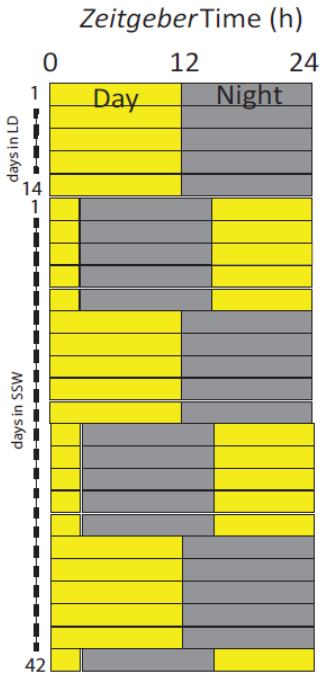

Figure 2: Graphical illustration of SSW protocol
LD cycle of SSW protocol, every row represents one day. Yellow represents the time with the lights on, while gray represents the time with the lights off

3.2.4. LD and DD conditions

We kept *bmal1*$^{IEC-/-}$ mice and their littermate controls, *bmal1*$^{IECfl/fl}$, in LD 12:12 for two weeks at the age of 8-10 weeks. At the age of 10-12 weeks, mice were kept in DD. Afterward, at the age of

12-14 weeks, they were switched to constant light for another two weeks. Finally, the mice were maintained in LD.

3.2.5. Food deprivation

Fecal samples were collected from 12-13-week-old *bmal1*$^{IEC-/-}$ and control mice for starvation experiments. On the first day of DD at CT 0, the food was removed from the cages. Fecal samples were collected at the indicated time points, starting at CT 13 on the second day of DD until CT 10 (for 13 hours of starvation till 34 hours), as indicated in Figure 3.

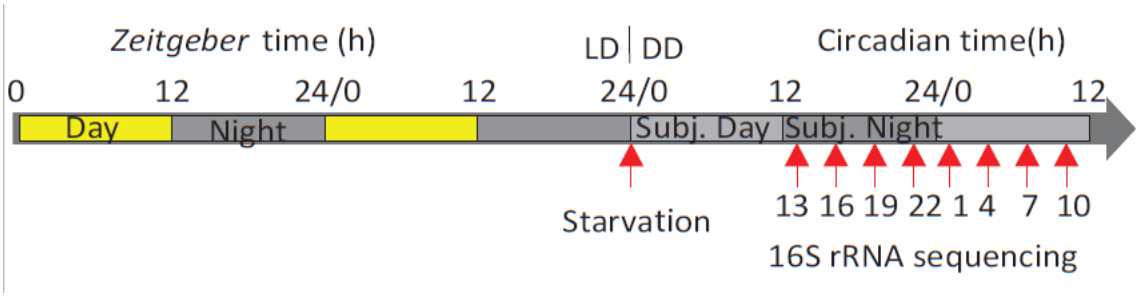

Figure 3: Food deprivation protocol
LD cycle and food availability of the starvation protocol, with red arrows indicating the time of fecal sample collection. Yellow represents the time with the lights on, while gray represents the time with the lights off.

3.2.6. Germ-free wild-type mice

Germ-free wild-type C57BL6 mice were kept single-housed in gnotobiotic isolators at the Technical University of Munich and provided *ad libitum* access to a standard autoclaved chow diet (Ssniff, Soest, Germany). Before starting the experiment, germ-free status was confirmed by fecal cultivation in a Wilkins-Chalgren Anaerobe (WCA) broth (OXOID, UK) and by gram staining from fecal suspensions. Mice were colonized at the age of 10 weeks and maintained for six weeks. Fecal samples were collected in LD at the age of 15 weeks. Finally, we sacrificed the mice on the second day of DD at the indicated CT points.

3.3. Gavage preparation

Cecal microbiota from SPF mice sacrificed at ZT 13 were diluted by 1:10 in 40% sterile glycerol. A mixture of diluted cecal microbiota from 4-5 mice was centrifuged at 300 rcf for 3 minutes to remove the debris. The supernatant was further centrifuged at 8,000 rcf for 10 minutes. Finally,

we diluted the pellet in sterile PBS. After adjusting the gavage material to 7 x 10^6 bacteria/µl, germ-free mice were gavaged with 100 µl per mouse.

3.4. Behavior analysis

Activity measurements were performed according to Jud and colleagues (Jud, Schmutz et al. 2005). We analyzed running-wheel activity using ClockLab software (Actimetrics). Periods were determined based on the 10-14 days of every condition (tau was calculated with X^2 periodogram and further confirmed by fitting a line to activity onsets), as well as active period duration (alpha), activity amount and activity ratio of subjective day/night (subjective night in DD condition is the active period between the onset and offset of activity).

3.5. Tissue collection

Mice were sacrificed at 16-20 weeks old by cervical dislocation. On the second day of DD, we sacrificed *bmal1*$^{SCNfl/-}$, *bmal1* $^{IEC-/-}$, germ-free mice, and their controls at the shown CT points. For the SSW experiment, control mice were sacrificed at the indicated ZT points, and we sacrificed mice undergoing SSW on the first day after the final phase advance shift at the indicated time point of the LD control group. Finally, tissues were collected, snap-frozen on dry ice, and then stored at -80°C until further processing.

3.6. Food intake and fecal sample collection

Average food intake was calculated from the amount of food consumed over five consecutive days. Fecal samples were collected at the indicated ZT points in LD. For the experiment performed in DD, fecal samples were collected at the indicated CT points after adjusting for every mouse's specific free-running period. This is because the internal period of mice within the same group can vary by 0.5 hours per day, and this can accumulate after several days in DD. Fecal samples of mice undergoing SSW were collected on the first day after the phase advance shift at the indicated time point of the LD control group. We collected fecal samples every 3 hours over the course of a day.

3.7. Complete gastrointestinal transit time (GITT)

To measure GITT, we gavaged the mice with 100 µl of natural carmine red (6%, Sigma-Aldrich) after dissolving it in 0.5% methylcellulose (Sigma-Aldrich), according to Li and colleagues (Li, Chalazonitis et al. 2011). Before the gavage, mice were starved for 6 hours. Fecal pellets were

collected from the cage every 10 minutes to check for redness. The time between the gavage (T0) and the presence of red color in the fecal pellets was considered to be the GITT.

3.8. Gut permeability

Ussing chambers were used to measure gut permeability, as described previously (Ussing and Zerahn 1951, Clarke 2009, Muller, Zietek et al. 2016). In brief, after dissecting the mice, 1.5 cm was freshly collected from the proximal colon. After cutting the tissue open, it was mounted in the Ussing chamber (six chamber system: Scientific instruments). A freshly prepared carbogen-gassed Krebs buffer (2.4 mM Na2HPO4, NaH2PO4, 5.4 mM KCl, 1.2 mM CaCl2, 114 mM NaCl, 1.2 mM MgCl2, 21 mM NaHCO3, 10 mM glucose, 0.6 mM pH 7.4) was used to support the tissue at 37°C. Then, 250 µl of 1.7673 mM fluorescein was added to the luminal side. Samples were collected from the serosal part of the buffer at 45 and 60 minutes to determine fluorescence intensity and tissue permeability.

3.9. Plasma glucose and triglycerides measurement

After sacrificing the mice at the indicated time point, fresh blood was collected by a 6%-EDTA-rinsed needle directly from the portal vein. Next, blood samples were centrifuged at 4,000 rcf for 10 minutes to collect plasma, which was stored at -80°C until further analysis. Non-fasting plasma glucose and triglycerides levels were measured using Fluitest ® GLU (Analyiticon, Germany) and Triglyceride gpo-pap (LT-SYS®, Germany) according to the manufacturers' recommendations.

3.10. Energy assimilation

Total fecal samples produced over the course of five days were collected. After drying the fecal pellets for five days at 55°C, we ground the dried fecal pellets with TissueLyserII (Qiagen, Retsch, Haan, Germany), then pressed the results into one-gram pellets. A 6,400 Calorimeter (Parr Instrument Company, Moline, IL, USA) was used to calculate gross fecal energy. Finally, after measuring the food intake over the course of fecal sample collection, we calculated the assimilation efficiency using the following formula:

$$\text{Assimilation efficiency (\%)} = ((\text{Food intake [g]} * \text{Efood [kJ} * \text{g} - 1]) - (\text{Feces production [g]} * \text{Efeces [kJ} * \text{g} - 1]))/(\text{Food intake [g]} * \text{Efood [kJ} * \text{g} - 1]) \text{ x } 100$$

3.11. Gene expression analysis and quantitative real-time PCR (qPCR)

Total RNA was extracted from snap-frozen tissues using a Trizol protocol. Briefly, tissues were placed in a 2 ml RNase-free screw-cap tube with beads and 400 µl Trizol (TRI reagent ®, Sigma). Samples were homogenized at 6 m/s for 40 seconds using a FastPrep®-24 bead beater (MP Biomedicals) with a cooling adapter. Next, we added 80 µl of chloroform to the samples and kept them on ice for 5 minutes before centrifuging for 30 minutes at 4°C and 16,000 rcf. After centrifuging, 200 µl of the top clear layer was added to 200 µl isopropanol. Then, samples were centrifuged for 30 minutes at 4°C and 16,000 rcf to precipitate the RNA. After discarding the supernatant, pellets were washed three times with 900 µl of 70% EtOH. Finally, the RNA pellets were suspended in 30 µl RNase-free water.

Next, 1,000 ng of RNA was used to generate cDNA using the cDNA synthesis kit Multiscribe RT according to the manufacturer's recommendation (Thermofischer Scientific). Using the Universal Probe Library system (UPL), qPCR was performed in the Light Cylcer 480 system (Roche Diagnostics, Mannheim, Germany) according to the manufacturer's instructions. All genes were measured using the UPL system with qPCR master mix (Brilliant III Ultra-Fast, Agilent Technologies, USA). Gene expression was normalized to the housekeeping gene elongation factor 1-alpha *(ef1a)*. Table 3 summarizes the primers and probes used:

Table 3: Primers and probes used to measure gene expression

Gene	Forward primer	Reverse primer	Probe
Elongation factor 1-alpha *(ef1a)*	5'- GCCAAT TTCTGGTTGGAATG-3'	5'-GGTGACTTTCCATCCCTTGA-3'	67
Intestinal-type fatty acid-binding protein (*ifabp)*	5'-GGTTTCTGGTAATGAACTAATCCAG-3'	5'-AAATCTGACATCAGCTTAGCTCTTC-3'	1
Peroxisome proliferator activated receptor Gamma (*pparg*)	5'- AAGACAACGGACAAATCACCA-3'	5'- GGGGGTGATATGTTTGAACTTG-3'	7
Fatty acid binding protein 2 (*fabp2*)	5'- ACGGAACGGAGCTCACTG-3'	5'-TGGATTAGTTCATTACCAGAAACCT-3'	56
Glucose transporter 2 *(glut2*)	5'-TTACCGACAGCCCATCCT-3'	5'-TGAAAAATGCTGGTTGAATAGTAAAA-3'	3
Cryptochrome circadian regulator 1 (*cry1*)	5'- ATCGTGCGCATTTCACATAC-3'	5'- TCCGCCATTGAGTTCTATGAT-3'	85
D site of albumin promoter (Albumin D-Box) binding protein (*dbp*)	5'- ACAGCAAGCCCAAAGAACC-3'	5'- GAGGGCAGAGTTGCCTTG-3'	94
Period 2 *(per2)*	5'-TCCGAGTATATCGTGAAGAACG-3'	5'- CAGGATCTTCCCAGAAACCA-3'	5
Nuclear receptor subfamily 1 group D member 1 *(rev-erbα)*	5'- AGGAGCTGGGCCTATTCAC-3'	5'-CGGTTCTTCAGCACCAGAG-3'	1
Brain and muscle ARNT-Like 1 *(bmal1)*	5'-ATTCCAGGGGGAACCAGA-3'	5'-GGCGATGACCCTCTTATCC-3'	15
Sodium/glucose cotransporter protein 1 *(sglt1)*	5'-CTGGCAGGCCGAAGTATG-3'	5'-TTCCAATGTTACTGGCAAAGAG-3'	49

3.12. High-throughput 16S ribosomal RNA (rRNA) gene amplicon sequencing analysis

To isolate genomic DNA from fecal samples, we used the protocol suggested by Godon and colleagues (Godon, Zumstein et al. 1997), with slight modifications. In brief, we added 600 µl of DNA stabilizer solution (Stratec Biomedical) to snap-frozen fecal samples in a 2 ml screw-cap tube with ~ 500 mg silica beads (0.1-mm-diameter; BioSpec Products). Next, 250 µl of 4 M guanidine thiocyanate, 0.1 M Tris, and 500 µl of 5% N-lauroyl sarcosine salt were added. Samples were vortexed and incubated for 1 hour at 70°C and 700 rpm. Afterward, samples were disrupted mechanically at 6.5 m/s for 40 seconds three times using a FastPrep®-24 bead beater (MP Biomedicals) with a cooling adapter. After that, we added a polyphenol adsorbent (15 mg of Polyvinylpolypyrrolidine) (PVPP, Sigma Aldrich) and centrifuged the samples for 3 minutes at 15,000 rcf. Finally, the supernatant was incubated with 2 µl RNAse (10mg/ml) for 30 minutes at 37°C and 700 rpm to remove the RNA.

For DNA purification, we used NucleoSpin gDNA columns (Machery-Nagel, No. 740230.250) according to the manufacturer's instructions. To amplify the 16S rRNA of 24 ng of DNA, we used the 341F-ovh and 785r-ov primers, targeting the V3-V4 region, in two-step PCR. Pooled samples were sequenced with Illumina HiSeq in paired-end mode (2 x 250 bp) based on Rapid V2 chemistry, as described previously (Reitmeier, Kiessling et al. 2020). To assure reproducibility, two negative controls were included per 46 samples; the negative control consists of the DNA stabilizer.

To analyze 16S rRNA data, we used high-quality sequences with at least 5,000 read counts. We used the NGS Toolkit (Version 3.5.2_64) to process FASTQ files with a 5-trim score at the 5' end and 3' end for both read R1 and R2. Next, the FASTQ mergepair script of USEARCH was used to remove chimera (Edgar 2010, Edgar, Haas et al. 2011). Then, we denoised, deduplicated, clustered, and merged quality-filtered reads to generate zero-radius operational taxonomic units (zOTUs) (Edgar 2010, Edgar 2016). Using zOTUs provides the maximum resolution possible from 16S rRNA data by denoising (correct sequencing error) and classifying unique sequences of 100% similarity as different microbial taxa. Taxonomy was assigned either to the Ezbiocloud database or the Greenbase database to compare our results with published data from Thaiss and colleagues (Thaiss, Zeevi et al. 2014). Finally, we used the RHEA pipeline to analyze the data (Lagkouvardos, Fischer et al. 2017). Low-abundant zOTUs were excluded; these were defined as zOTUs with a mean relative abundance of less

than 0.1% and a prevalence of less than 10%. Sequences were aligned to generate phylogenetic trees based on the maximum likelihood approach from MUSCLE by MegaX software (Kumar, Stecher et al. 2018). For tree visualization, we used Evolview (http://www.evolgenius.info/evolview) (Subramanian, Gao et al. 2019). Quantitative analysis of zOTUs was performed based on spike analysis, as described earlier (Heddes, Altaha et al. 2021).

3.13. PICRUST 2.0

PICRUST 2.0 was used to predict metagenomic functionality. In brief, the metagenome was constructed based on zOTU sequences to predict functional genes, while zOTU normalized copy numbers were used to quantify zOTU genes. Finally, genes were assigned enzyme commission (EC) numbers and further assigned to Metacyc pathways. Metacyc pathways were used for calculating LDA effective score (LEFSE) after removing super-class pathways, using the following online tool: (http://huttenhower.sph.harvard.edu/galaxy) (Segata, Izard et al. 2011).

3.14. Metabolite measurements

3.14.1. Sample preparation

Mouse fecal samples were weighed in 2 ml bead-beater tubes (Lysing Matrix D, MP Biomedicals). To correct for losses from the work-up, we added 1 ml of methanol-based dehydrocholic acid extraction solvent with a concentration of 1.3 µmol/l as an internal standard. We extracted fecal samples by bead beating 3 times at 6m/s for 20 seconds, with a 30-second break in-between, using a FastPrep-24 5G bead-beating grinder (MP Biomedicals) and CoolPrep adapter.

3.14.2. Bile acid measurement

For a 100 µl sample extract, we added 20 µl of isotopically labeled bile acids (7 µM each). To measure targeted bile acids, we used the QTRAP 5500 triple quadrupole mass spectrometer (Sciex, Darmstadt, Germany), which is coupled to the ultra-high-performance liquid chromatography system (ExionLC AD, Sciex, Darmstadt, Germany), in accordance with Reiter and colleagues (Reiter, Dunkel et al. 2021). Bile acids were detected and quantified using the multiple reaction monitoring (MRM) method. We used an electrospray ion voltage of -4,500 V with ion source parameters set at (450°C), curtain gas (35 psi), entrance potential (-10 V),

gas 1 (55 psi) and gas 2 (65 psi). To separate the analytes, we used a 100 × 2.1 mm, 100 Å, 1.7 µm, Kinetex C18 column (Phenomenex, Aschaffenburg, Germany).

For chromatographic separation, a constant flow (0.4 ml/min) of the mobile phase consisting of water (eluent A) as well as acetonitrile/water (95/5, v/v, eluent B) was used; both eluents contained 0.1% formic acid and 5 mM ammonium acetate. The elution buffer (B) was increased gradually. Starting at 3.5 minutes at 25%, it was increased over 2 minutes to 27%; after another 2 minutes, we increased it to 35% and kept it for 10 minutes. Then the buffer concentration was increased to 43% over 1 minute and was held for another 1 minute, then it was increased over 2 minutes to 58%, and held isocratically for 3 minutes at 58%. We increased the concentration to 65%, 80% and 100%, at 17.5, 18 and 19 minutes, respectively. A 100% concentration was held for 1 minute before starting the equilibration at 20.5 minutes for 4.5 minutes. Then, 1 µl sample was injected into the column oven at 40°C, with the auto-sampler at 15°C. Analyst 1.7 software (Sciex, Darmstadt, Germany) was used for instrumental control and data acquisition, in accordance with Reiter and colleagues (Reiter, Dunkel et al. 2021).

3.14.3. SCFA measurement

SCFAs were quantified by the 3-NPH method (Han, Lin et al. 2015). We mixed 15 µl isotopically labeled standards (ca 50 µM) and a 40 µl fecal extract with 20 µL of 200 mM 3-NPH HCL solution and 20 µl 120 mM EDC HCl-6% pyridine solution. Samples were shaken for 30 minutes at 1,000 rpm and at 40°C with Eppendorf Thermomix (Eppendorf, Hamburg, Germany); we then added 900 µl of acetonitrile/water (50/50, v/v). Samples were centrifuged for 2 minutes at 13,000 U/minute, and the supernatant was used for subsequent analysis. We used the same system described above for bile acid measurement, with an electrospray voltage of -4500 V, a temperature of 500°C and a curtain gas set to 35 psi, with ion source gas 1 to 55 and ion source gas 2 to 65.

To optimize MRM parameters, we used commercially available standards. We used a 100 × 2.1 mm, 100 Å, 1.7 µm, Kinetex C18 (Phenomenex, Aschaffenburg, Germany) column for chromatographic separation with 0.1% formic acid, and 0.1% formic acid in acetonitrile, as elution solvents A and B, respectively. We used a flow rate of 0.4 ml/min with an injection volume of 1 µL. The elution buffer B concentration was held at 23% for 3 minutes, then increased to 30% at 4 minutes. At 6.5 and 7 minutes, the B concentration was further increased to 40% and 100%, respectively. After holding the B concentration at 100% for 1 minute, we started column equilibration. We set the column oven temperature to 40°C while the auto-

sampler was at 15°C. Analyst 1.7 software (Sciex, Darmstadt, Germany) was used for instrumental control and data acquisition, in accordance with Reiter and colleagues (Reiter, Dunkel et al. 2021).

3.15. Statistical analysis

We used GraphPad Prism, V 9.0.0 and R for statistical analysis. Using the RHEA pipeline, microbial diversity was determined based on generalized UniFrac (G. UniFrac) distance calculation, differences between group was assessed by PERMANOVA test and matrix dissimilarity was illustrated by MDS plots including a bar for dissimilarity distance (Lagkouvardos, Fischer et al. 2017). For a diurnal circadian profile of G. UniFrac, data were compared to ZT 1 or CT 1. To determine diurnal and circadian patterns and to calculate the phase for each 24-hour graph, a cosine-wave equation with a fixed 24-hour period was used:

$$y = \text{baseline} + (\text{amplitude} \cdot \cos(2 \cdot \pi \cdot ((x - [\text{phase shift})/24)))$$

The rhythmicity of clock genes, CCGs, phyla, family, richness, zOTUs, and metabolites were calculated with the cosine-wave equation. However, we used the following harmonic regression equation to calculate rhythmicity for some CCGs:

$$y = \text{baseline} + (\text{amplitude A} * \cos(2 \cdot \pi \cdot ((x - (\text{phaseshift A}) / 24))) + (\text{amplitude B} * \cos(4 \cdot \pi \cdot ((x - [\text{phase shift B})/ 24))))$$

To indicate the rhythmicity of individual 24-hour period graphs, a connected straight line is used, while a dashed line is used to indicate arrhythmicity. The rhythmicity of all zOTUs and pathways was calculated with JTK_CYCLE V 3.1.R (Hughes, Hogenesch et al. 2010). To compare overall rhythmicity between datasets, we used an adjusted version of the CompareRhythms R script (Pelikan, Herzel et al. 2021), by running DODR after JTK_CYCLE analysis (Singer and Hughey 2019). For Manhattan plots, the phase was calculated based on cosine-wave regression, while amplitude and p-value were calculated by JTK_CYCLE V 3.1.R (Hughes, Hogenesch et al. 2010).

Notably, to better visualize the data, we removed the p-value = 1 in the Manhattan plots. To visualize samples and zOTU trees, we used the *online platform "evolgenius.info"* (Subramanian, Gao et al. 2019). We generated heatmaps with the "heatmapper.ca" online tool (Babicki, Arndt et al. 2016), after sorting the data on the peak phase of the control. We generated abundance plots using the function "*check.associations()"* from the SIAMCAT R

package (Wirbel, Zych et al. 2020). The non-parametric Mann-Whitney test was used to analyze the difference between the two groups. Group differences over different times and conditions were compared using a two-way ANOVA. P-values ≤ 0.05 are considered statistically significant.

4. Results

4.1. Microbial rhythms are generated by the circadian system

The gut microbiota oscillates diurnally in animal models and humans (Thaiss, Zeevi et al. 2014, Leone, Gibbons et al. 2015, Reitmeier, Kiessling et al. 2020). However, this microbial rhythmicity could result from rhythmic external cues, *Zeitgebers*, such as the LD cycle, or be generated by the circadian system (Aschoff 1960), and thus persist in the absence of environmental timing cues. To address this point, we compared microbial rhythms from the same mice kept in a rhythmic LD cycle and, for two weeks, in DD (Figure 4). In both light conditions, we found comparable host rhythmic factors that might impact microbial composition such as food intake, locomotor activity, and total GITT (Heddes, Altaha et al. 2022).

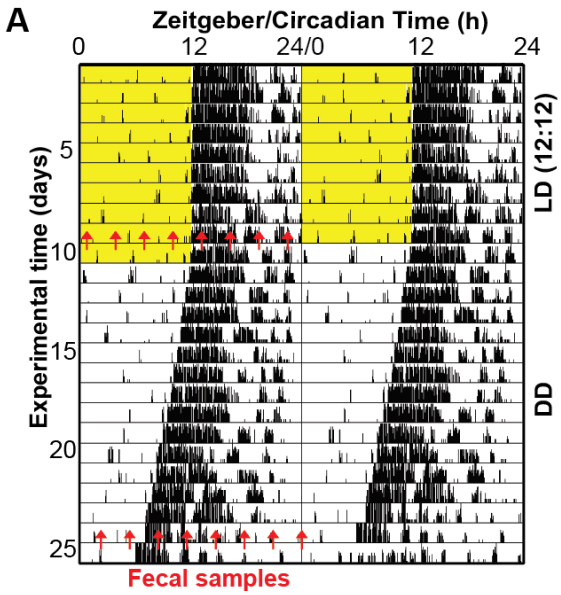

Figure 4: Fecal sample collection protocol
Representative actogram of activity behavior of WT mice in LD and DD, illustrating fecal sample collection time points. Each row represents one day, with tick marks illustrating running wheel activity. Yellow shading represents light, while white shading represents darkness. Red arrows point to the time of fecal sample collection.

To assess microbial composition and rhythmicity, we performed 16S rRNA gene sequencing of fecal samples collected from eight time points over the course of the day (Figure 4). Interestingly, microbial composition clustered according to the sampling time points instead of the light condition (Figure 5A). To assess the variation in microbial composition between samples, we quantified G. UniFrac to ZT 1.

Our results identified rhythmic changes in microbial composition in LD and DD (Figure 5B). Importantly, the diurnal rhythm of microbial richness and Shannon effective persisted in DD, pointing to their circadian origin (Figure 5C). Rhythms also continued in DD at the phylum level, with Bacteroidetes and Firmicutes, the most dominant phyla, oscillating in antiphase (Figure 5D). Despite the popularity of analyzing microbiota composition according to relative abundance, this approach generates some caveats for the assessment of rhythmicity. For example, the oscillations of highly abundant taxa may mask the rhythmicity of other microbial communities with lower abundance, as demonstrated by previous research (Liang, Bushman et al. 2015). Therefore, we used synthetic DNA spikes to relatively quantify the 16S rRNA copy number in accordance with Tourlousse and colleagues (Tourlousse, Yoshiike et al. 2017), referred to hereafter as "quantitative analysis". Both relative and quantitative analysis revealed similar rhythmicity among highly abundant phyla and families such as *Lachnospiraceae* and *Muribaculaceae,* in LD and DD (Figure 5D-E). Notably, in a few families such as *Prevotellaceae,* rhythms were only evident in the diurnal cycle (LD) but not the circadian (DD) cycle, indicating environmental control of these rhythms (Figure 5E).

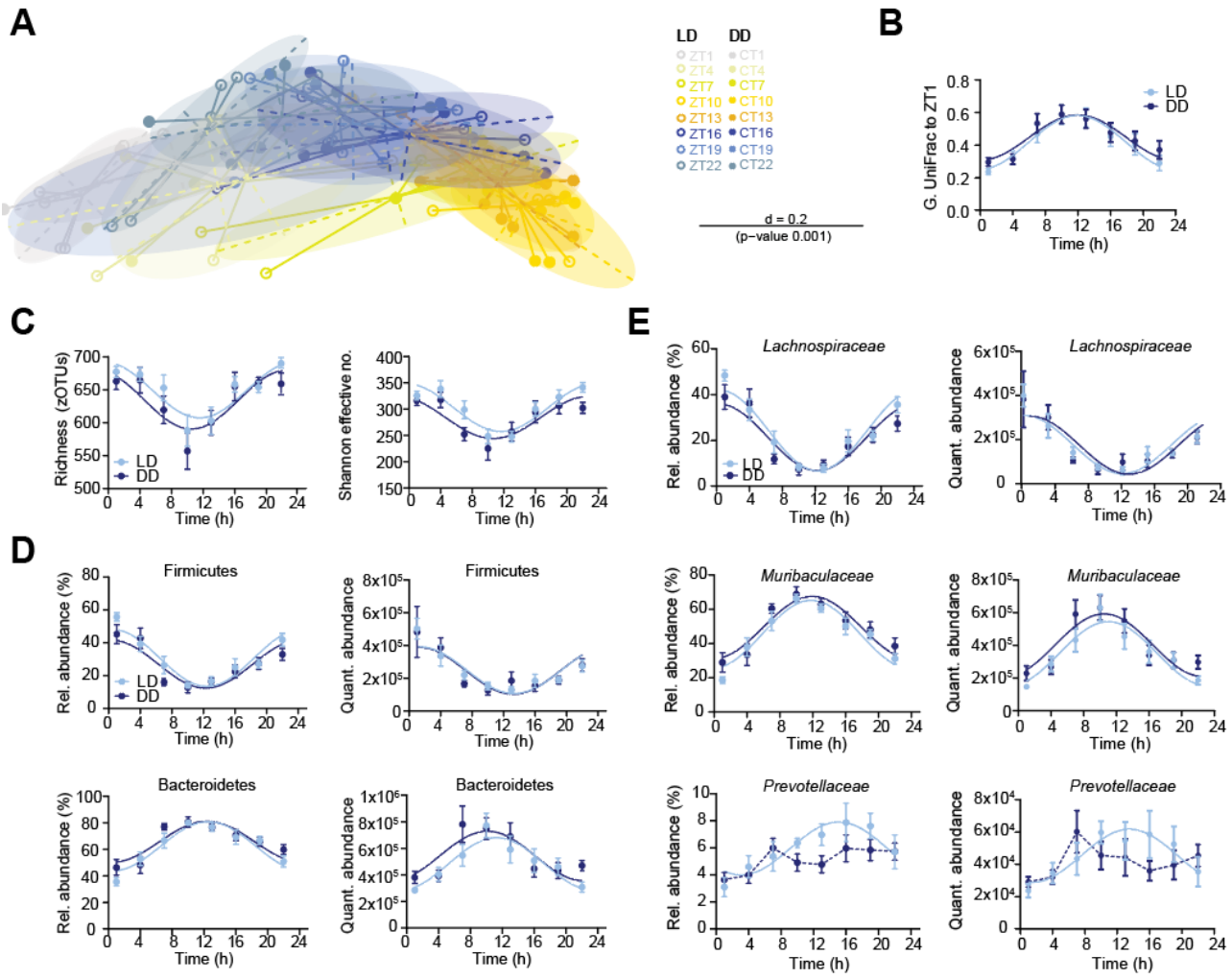

Figure 5: Circadian nature of microbial oscillations

(A) MDS plot of beta diversity based on G. UniFrac distances of the fecal microbiota composition of WT mice in LD and DD, stratified by the time points. Diurnal/circadian profile of microbial G. UniFrac distances (B), alpha diversity (C) as well as the major phyla and families (D-E) in relative and quantitative abundance. Wild-type mice in LD and DD are represented by light and dark blue, respectively. N = 6 mice/genotype/time point. Cosine-wave regression was used to assess rhythmicity. Solid lines indicate significant rhythms (p-value ≤ 0.05), while dashed lines indicate arrhythmicity. Data are illustrated as mean ± SEM.

After removing less abundant taxa, the remaining zOTUs showed rhythmic oscillation in LD and DD, according to relative and quantitative analyses (Figure 6 A-C, Figure 7 A-C). Notably, the peak abundances of zOTUs were distributed widely over the course of the day. For example, bacteria mainly belonging to *Muribaculaceae* peaked during the day while those belonging to *Lachnospiraceae* peaked at night (Figure 5E, Figure 6A-C, Figure 7A-C). These results suggest that different taxa dominate at different times of the day.

Importantly, the majority of zOTUs (> 60%) were significantly rhythmic in LD as well as DD (Figure 6A-C, Figure 7 A-C), pointing to the circadian force behind these rhythms. Notably, a lower percentage of rhythmic microbial taxa was found in the literature (Thaiss, Zeevi et al. 2014, Leone, Gibbons et al. 2015). To investigate this discrepancy, our results were compared to the published dataset from Thaiss and colleagues (Thaiss, Zeevi et al. 2014). The two different methods used to assign taxa, operational taxonomic units (OTUs) and zOTUs, show a similarity of 97% and 100% for taxa assignment, respectively, resulting in disparities in the percentage of rhythmic OTUs and zOTUs (Figure 6D). However, both studies show a comparable total abundance of oscillating bacteria (Figure 6D).

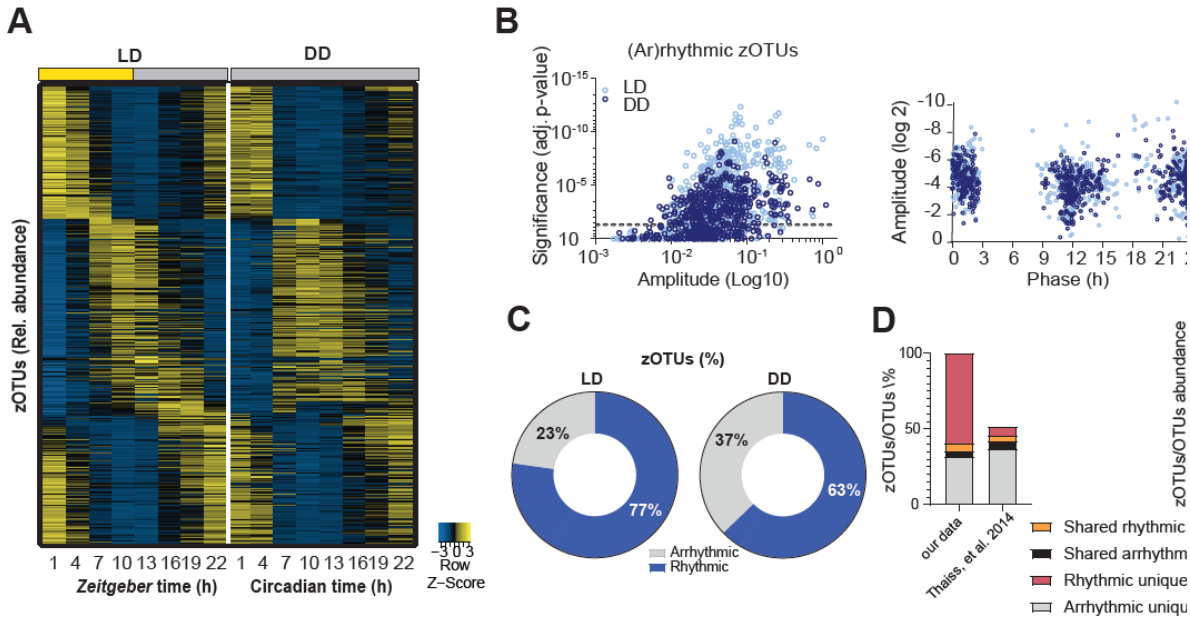

Figure 6: Robust zOTU oscillations in LD and DD according to relative abundance analysis
(A) Heatmap illustrates 580 zOTUs' relative abundance (relative abundance mean > 0.1% and prevalence > 10%). zOTUs are ordered based on the phase of zOTUs in the LD group; data are normalized based on the peak of each individual zOTU. (B) Significant adj. p-value, amplitude (calculated by JTK_CYCLE) and phase distribution (calculated by cosine regression) of all zOTUs in both light conditions. Dashed lines represent JTK_CYCLE adj. p-value = 0.05. (C) Pie charts represent the percentage of rhythmic and arrhythmic zOTUs in LD and DD. (D) Bar charts illustrate the difference in percentage and abundance of microbial zOTUs rhythmicity between our data and previously published data of Thaiss and colleagues (Thaiss, Zeevi et al. 2014). Wild-type mice in LD and DD are represented by light and dark blue, respectively. N = 6 mice/genotype/time point.

The quantitative analysis further validated the rhythmicity of most rhythmic zOTUs identified by relative analysis in our study (Figure 7 A-C), e.g., taxa belonging to the genera *Fusimonas*, *Alistipes*, and *Oscillibacter*. Testing zOTUs' rhythmicity using JTK_CYCLE (Hughes, Hogenesch et al. 2010), we further confirmed that the circadian system generates the majority of the microbial rhythm (Figure 5-7, Suppl. Figure 1). Comparing rhythms using DODR (Thaben and Westermark 2016) also confirmed the circadian nature of microbial rhythmicity, with 95% of zOTUs having similar rhythmicity in LD and DD, e.g., taxa belonging to *Eubacterium* and *Lachnospiraceae* (Figure 7 D, Suppl. Figure 1).

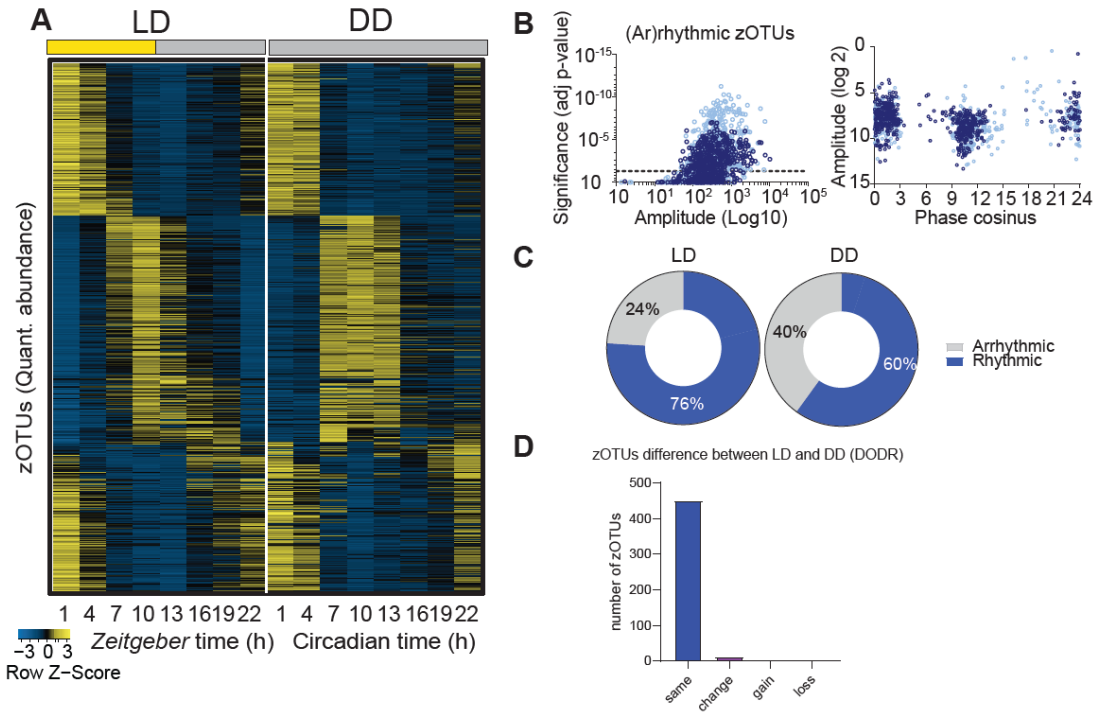

Figure 7: Robust zOTU oscillations in LD and DD according to quantitative abundance analysis
(A) Heatmap illustrates 580 zOTUs' quantitative abundance (relative abundance mean > 0.1% and prevalence > 10%). zOTUs are ordered based on the phase of zOTUs in the LD group; data are normalized based on the peak of each individual zOTU. (B) Significant adj. p-value, amplitude (calculated by JTK_CYCLE) and phase distribution (calculated by cosine regression) of all zOTUs in both light conditions. Dashed lines represent JTK_CYCLE adj. p-value = 0.05. (C) Pie charts represent the percentage of rhythmic and arrhythmic zOTUs in LD and DD. (D) Bar charts represent zOTUs' rhythmicity comparison between light conditions according to adjusted CompareRhythms R script based on DODR. Wild-type mice in LD and DD are represented by light and dark blue, respectively. N = 6 mice/genotype/time point.

4.2. The gut microbiota oscillates rhythmically in the absence of rhythmic food intake

Light and food represent the main *Zeitgebers* that impact the central and peripheral circadian clocks, respectively (Damiola, Le Minh et al. 2000, Schibler, Ripperger et al. 2003). Our results showed a mild effect of the LD cycle on microbial rhythms (Figure 5-7). Feeding time, on the other hand, alters the phase of rhythmic microbiota (Thaiss, Zeevi et al. 2014), suggesting dependency of microbial rhythms on rhythmic food intake. Thus, we investigated the relationship between bacterial oscillations and rhythmic food intake by studying microbiota rhythmicity in the absence of food and light. Therefore, fecal samples were collected from starved mice on the second day of DD (Figure 8A). Despite the changes in microbial composition following starvation, the gut microbiota clustered according to the time points in both feeding conditions (Figure 8 B-C).

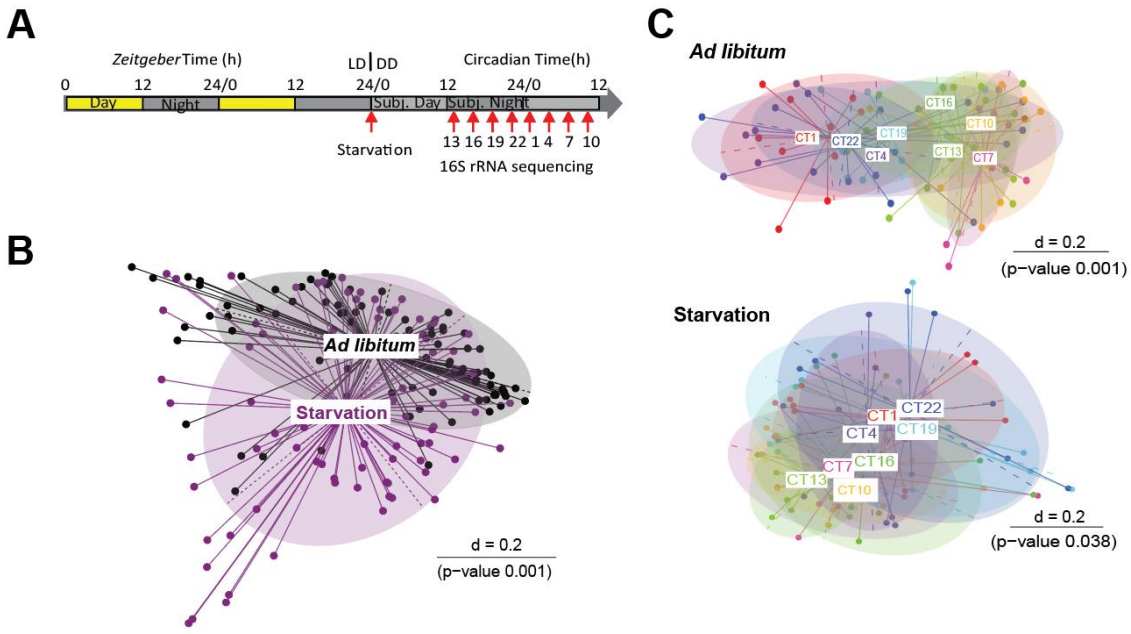

Figure 8: Food deprivation alters microbiota composition

(A) Graphical illustration of food deprivation (starvation) protocol, with red arrows indicating the time of fecal sample collection. Yellow represents the time with the lights on, while gray represents the time with the lights off. (B-C) MDS plots of beta diversity based on G. UniFrac distances of the fecal microbiota composition stratified by feeding condition (B) and time points (C) of wild-type mice under starvation and ad libitum food intake. Eleven mice per feeding condition were used to collect 81-83 fecal samples over eight time points.

Although the absence of rhythmic food intake resulted in arrhythmic microbial diversity (Figure 9A), rhythms persisted in the dominant phyla, highly abundant families, and the majority of zOTUs, independent of the feeding conditions (Figure 9 B-D). Notably, rhythmic food intake enhanced the rhythmicity of 16% of zOTUs (Figure 9E). However, highly abundant taxa, e.g., *Ruminococacaceae* and *Muribaculaceae*, oscillated under starving conditions (Figure 9F-G). Altogether, our data demonstrate that light and food slightly influence gut microbiota fluctuations, pointing to intrinsic factors driving microbial rhythms.

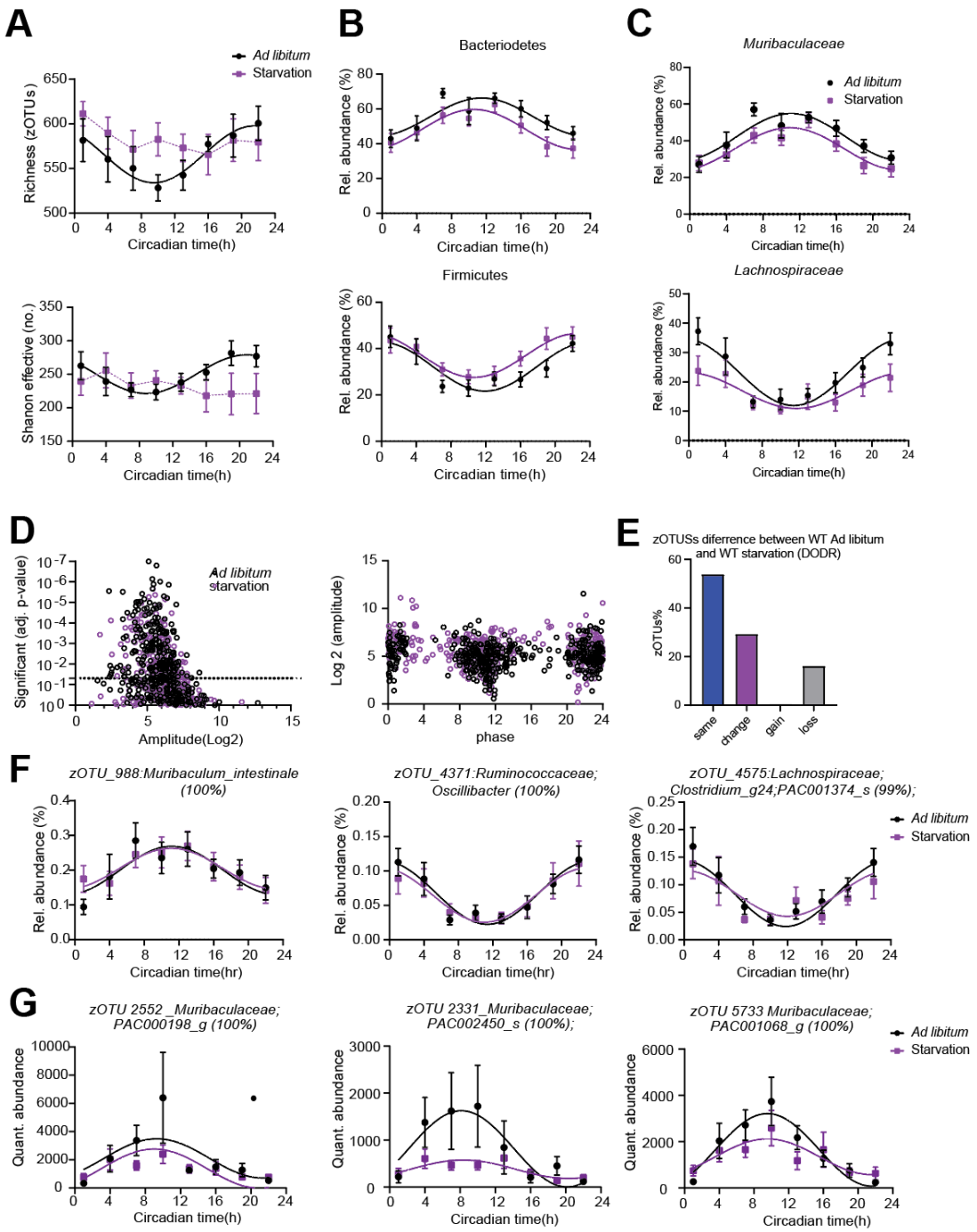

Figure 9: Rhythms persist in the absence of rhythmic food intake.

(A-C) Circadian profile of microbial alpha diversity (A) and the major phyla (B) and families (C) in relative abundance. (D) Significant adj. p-value, amplitude (calculated by JTK_CYCLE) and phase distribution (calculated by cosine regression) of all zOTUs in both feeding conditions. Dashed line represents JTK_CYCLE adj. p-value = 0.05. (E) Bar charts represent comparison of zOTU rhythmicity between feeding conditions based on adjusted CompareRhythms R script based on DODR. (F-G) Circadian profile of zOTUs' relative (F) and quantitative (G) abundance. Wild-type mice under starvation and ad libitum food intake are represented by purple and black, respectively. For relative data (A-F), 11 mice per feeding condition were used to collect 81-83 fecal samples over eight time points. For quantitative data (G), five mice per feeding condition were used to collect 37-39 fecal samples over eight time points. Cosine-wave regression was used to assess rhythmicity. Solid lines indicate significant rhythms (p-value ≤ 0.05), while dashed lines indicate arrhythmicity. Data are illustrated as mean ± SEM.

4.3. The intestinal clock drives microbial rhythmicity

Host circadian clocks play an important role in microbial fluctuations (Thaiss, Zeevi et al. 2014, Liang, Bushman et al. 2015). Recent research has led to the discovery of a gastrointestinal-specific circadian system, so called the gut clock (Moore, Pruszka et al. 2014). The gastrointestinal tract represents a critical interface for host-microbe interaction, controlling microbial composition (Coleman and Haller 2017). Thus, the gastrointestinal tract could drive microbial rhythmicity. To test this hypothesis, we used mice with an intestinal-specific clock deletion (*bmal1*$^{IEC-/-}$). *Bmal1*$^{IEC-/-}$ mice have rhythmic locomotor activity and food intake behavior, as well as normal GITT and stool weight, pointing to a functional central clock (Heddes, Altaha et al. 2022).

In *bmal1*$^{IEC-/-}$ mice, core clock genes were expressed arrhythmically in the proximal colon, cecum, and jejunum, while liver clock genes oscillated rhythmically, conforming to intestinal-specific clock disruption (Heddes, Altaha et al. 2022). Moreover, genes impacting host-microbe crosstalk such as *muc2, tlr2, hdac3,* and *nfil3,* lost rhythmicity in *bmal1*$^{IEC-/-}$ mice (Forman, deSchoolmeester et al. 2012, Mukherji, Kobiita et al. 2013, Hardbower, Asim et al. 2016, Wang, Kuang et al. 2017, Wu, Wu et al. 2018, Kuang, Wang et al. 2019, Heddes, Altaha et al. 2022). Importantly, the absence of a functional intestinal clock altered microbial composition in LD and DD (Figure 10A, Figure 11A) and disrupted the rhythmicity of species richness (Figure 10B). Although the major phyla Firmicutes and Bacteroidetes were rhythmic in *bmal1*$^{IEC-/-}$ mice, according to relative abundance analysis, quantitative analysis revealed the loss of Firmicutes' rhythmicity in the absence of the gut clock in LD and DD (Figure 10C, Figure 11B). The loss of the intestinal clock also resulted in lower quantitative abundance of Firmicutes and Bacteroidetes, which accords with the data from whole body-clock disrupted mice (Liang, Bushman et al. 2015), pointing to the importance of the quantitative analysis

(Figure 10C). Similarly, quantitative analysis revealed the loss of rhythm for families such as *Ruminococcaceae* and *Lachnospiraceae* (Figure 10D).

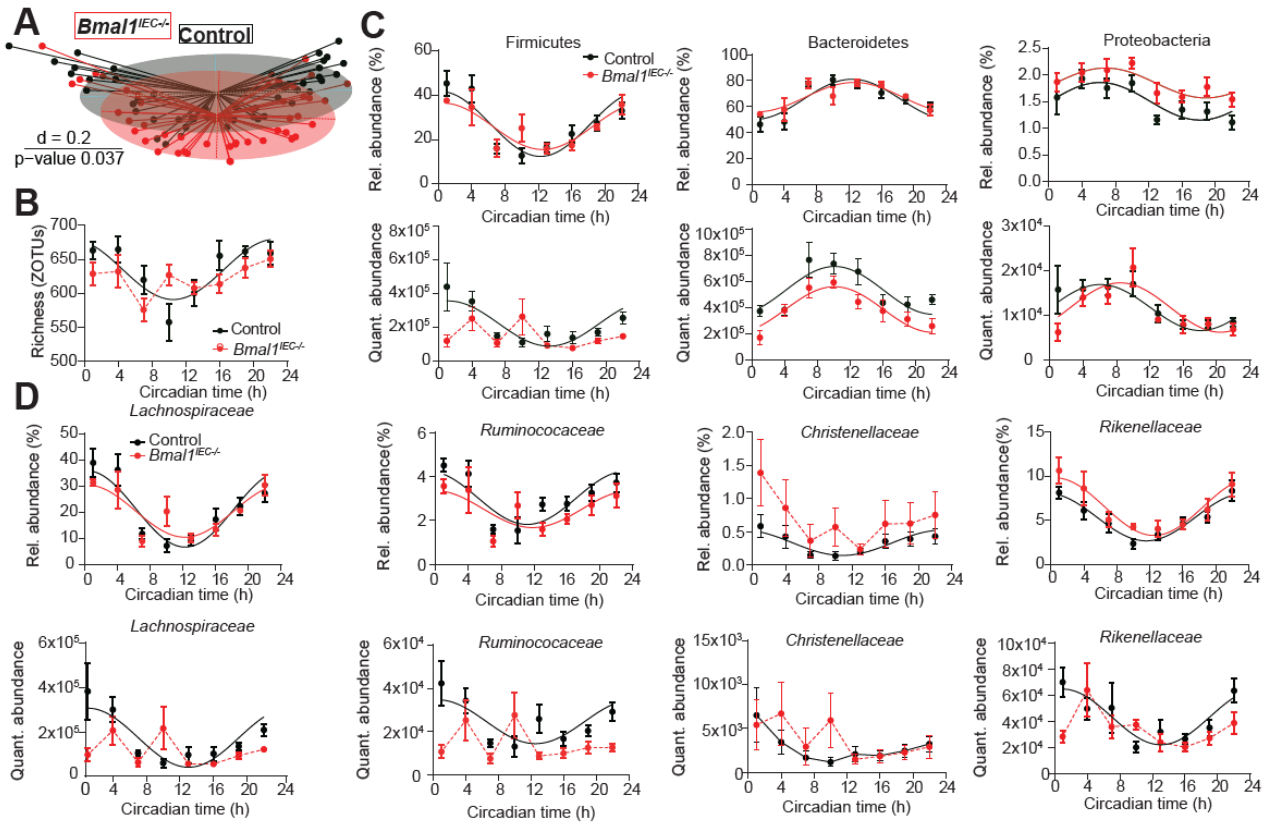

Figure 10: The gut clock drives microbial rhythmicity

A) MDS plot of beta diversity based on G. UniFrac distances of the fecal microbiota composition, stratified by genotype. (B-D) Circadian profile of microbial alpha diversity (B) and the major phyla (C) and families (D) in relative and quantitative abundance. Bmal1$^{IEC-/-}$ mice are represented by red, while the controls are represented by black. N = 5-6 mice/genotype/time point. Cosine-wave regression was used to assess rhythmicity. Solid lines indicate significant rhythms (p-value ≤ 0.05), while dashed lines indicate arrhythmicity. Data are illustrated as mean ± SEM.

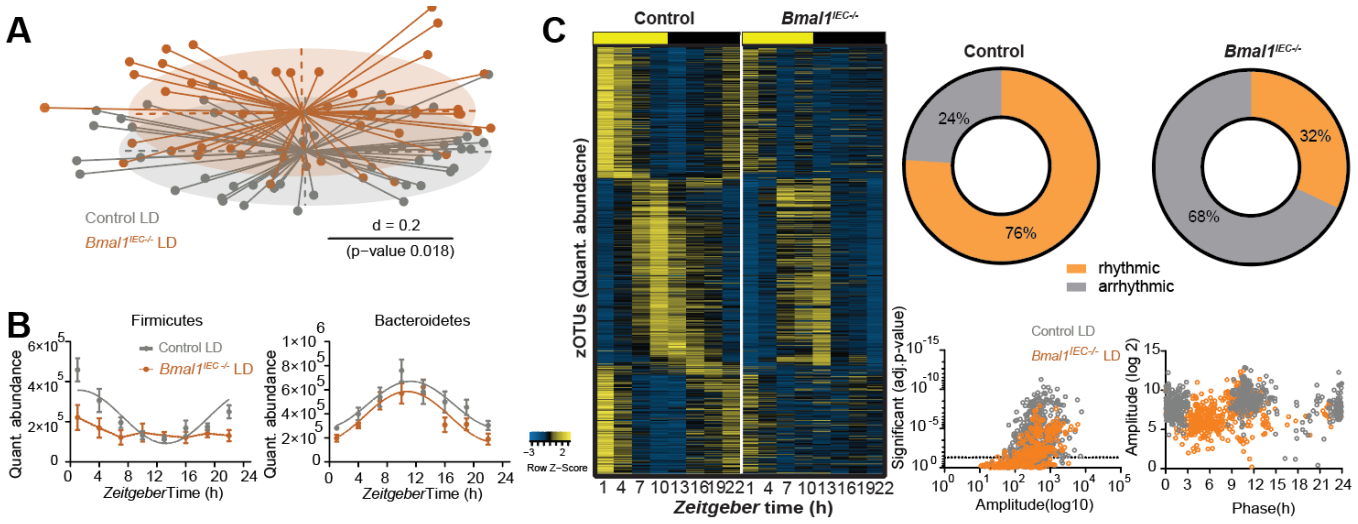

Figure 11: Robust role of the gut clock in controlling microbial rhythmicity in LD condition

(A) MDS plot of beta diversity based on G. UniFrac distances of the fecal microbiota composition stratified by genotype. (B) Circadian profile of quantitative abundance of major phyla. (C) Heatmap illustrates 580 zOTUs' quantitative abundance (relative abundance mean > 0.1% and prevalence > 10%). zOTUs are ordered based on the phase of zOTUs in the ad libitum group; data are normalized based on the peak of each individual zOTU. Pie charts illustrate the percentage of rhythmic and arrhythmic zOTUs in both genotypes. Significant adj. p-value, amplitude (calculated by JTK_CYCLE) and phase distribution (calculated by cosine regression) of all zOTUs in both genotypes. Dashed lines represent JTK_CYCLE adj. p-value = 0.05. Bmal1$^{IEC-/-}$ mice in LD are represented by orange, while the controls in LD are represented by grey. N = 5-6 mice/genotype/time point. Cosine-wave regression was used to assess rhythmicity. Solid lines indicate significant rhythms (p-value ≤ 0.05), while dashed lines indicate arrhythmicity. Data are illustrated as mean ± SEM.

Moreover, we observed disrupted zOTU oscillations upon the loss of the gut clock, as illustrated by relative and quantitative analyses of heatmaps (Figure 11C, Figure 12A-B). In both analyses, more than 60% of the zOTUs oscillate rhythmically in the controls (Figure 11C, Figure 12A-B). Importantly, the loss of the gut clock abolishes two-thirds of rhythmic zOTU circadian oscillations, independent of light conditions (Figure 11C, Figure 12A-B). According to both relative and quantitative analyses, the gut clock controls those zOTUs that predominantly belong to the families *Ruminococcaceae* and *Lachnospiraceae* (Figure 12 C-D, Figure 13A). Moreover, taxa belonging to *Ruminococcus*, *Lactobacillus*, *Odoribacter*, *Anaerotignum*, and *Alistipes* differ in their abundance and rhythmicity in *bmal1*$^{IEC-/-}$ mice, according to DODR analysis (Thaben and Westermark 2016) (Figure 12C).

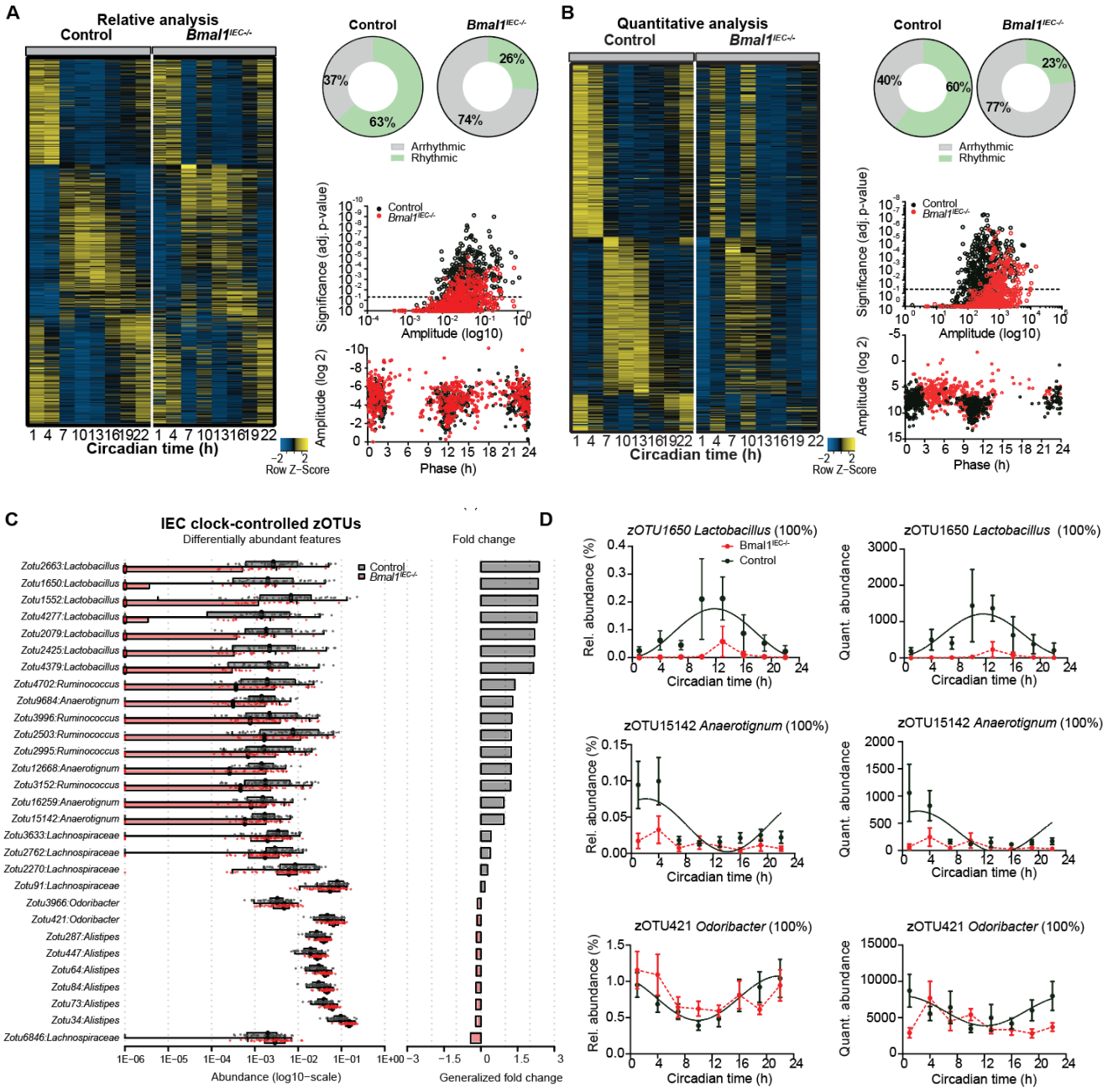

Figure 12: The gut clock controls the majority of zOTUs' rhythmicity according to relative and quantitative analyses

(A-B) Heatmap illustrates 580 zOTUs in relative (A) and quantitative (B) abundance (relative abundance mean > 0.1% and prevalence > 10%). zOTUs are ordered based on the phase of zOTUs in the control group, data are normalized based on the peak of each individual zOTU. Pie charts illustrate the percentage of rhythmic and arrhythmic zOTUs in both genotypes. Significant adj. p-value, amplitude (calculated by JTK_CYCLE) and phase distribution (calculated by cosine regression) of all zOTUs in both genotype. Dashed lines represent JTK_CYCLE adj. p-value = 0.05. (C) Bar charts show the significant (adj. p-value ≤ 0.05) abundance differences of zOTUs that lost their rhythmicity in bmal1$^{SCNfl/-}$ mice. (D) Circadian profile of zOTUs relative and quantitative abundance. Bmal1$^{IEC-/-}$ mice are represented by red, while the controls are represented by black. N = 5-6 mice/genotype/time point. Cosine-wave regression was used to assess rhythmicity. Solid lines indicate significant rhythms (p-value ≤ 0.05), while dashed lines indicate arrhythmicity. Data are illustrated as mean ± SEM.

Although the gut clock controls the majority of rhythmic zOTUs (Figure 13A.), rhythms persisted in around 20% of zOTUs in *bmal1*$^{IEC-/-}$ mice such as *Pseudoflavonifractor* and *Lactobacillus animalis* (Figure 13B).

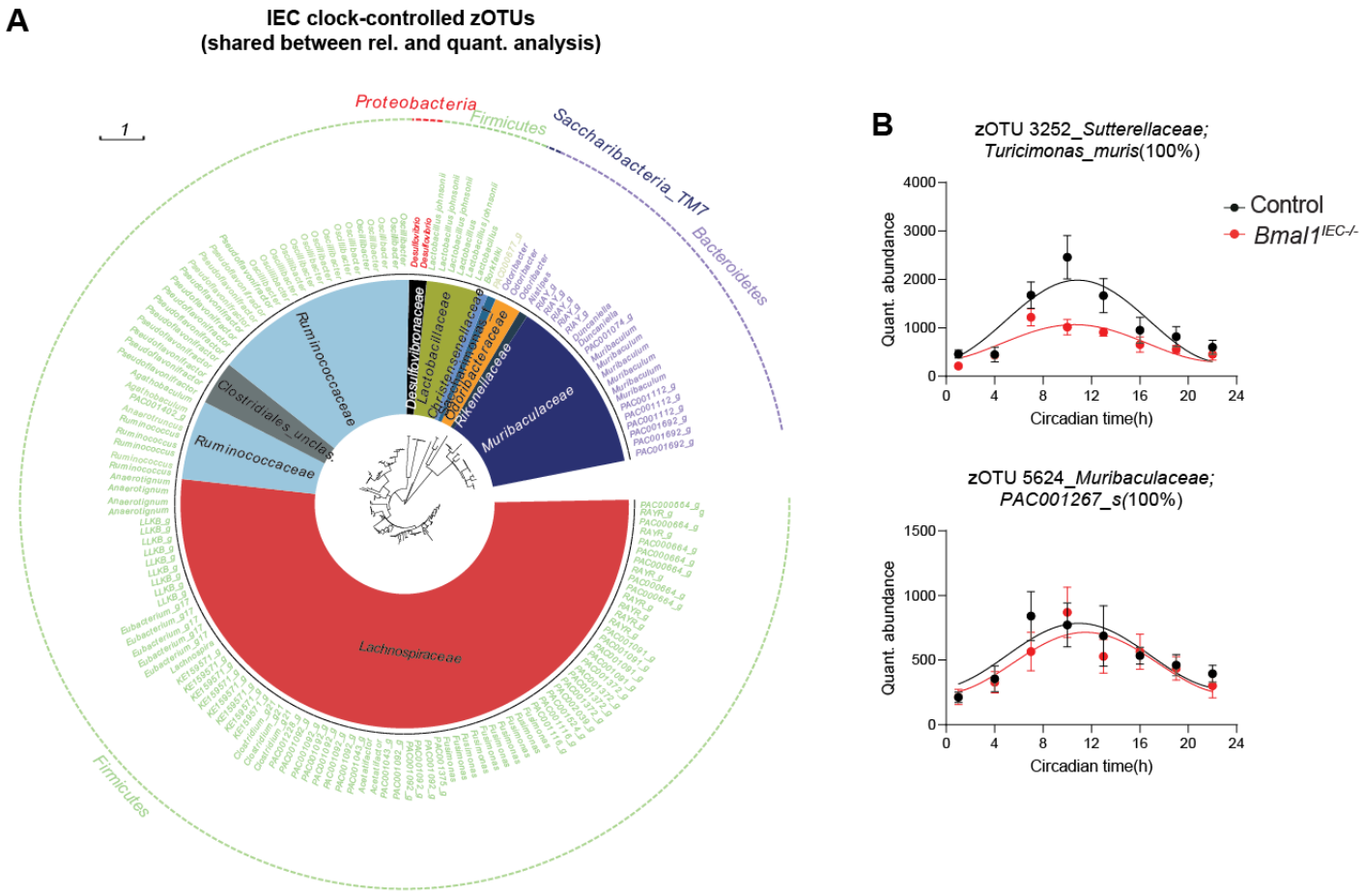

Figure 13: Gut clock-controlled zOTUs

(A) Taxonomic tree of the zOTUs that lost rhythmicity in bmal1$^{IEC-l/-}$ *mice, shared between relative and quantitative analyses. Taxonomic ranking is indicated as the phylum level (outer dashed ring), family level (inner circle), and genus level (middle names). Every zOTU is represented by a single branch. (B) Circadian profile of zOTUs' quantitative abundance. Bmal1*$^{IEC-/-}$ *mice are represented by red, while the controls are represented by black. N = 5-6 mice/genotype/time point. Cosine-wave regression was used to assess rhythmicity. Solid lines indicate significant rhythms (p-value ≤ 0.05), while dashed lines indicate arrhythmicity. Data are illustrated as mean ± SEM.*

To test whether these remaining microbial rhythms are driven by *bmal1*$^{IEC-/-}$ mice rhythmic food intake, we analyzed fecal samples collected during the second day of DD of starved *bmal1*$^{IEC-/-}$ mice (Figure 8A). While the absence of rhythmic food intake -or starvation- alters

microbiota composition (Figure 14A), in both feeding conditions, the effects on major phyla were indistinguishable (Figure 14B). Furthermore, starvation slightly affects zOTUs' rhythmicity in *bmal1*$^{IEC-/-}$ mice, as few taxa lost rhythmicity upon starvation in these mice (e.g., taxa belonging to *Muribaculaceae* and *Turicimonas muris*) (Figure 14C-E).

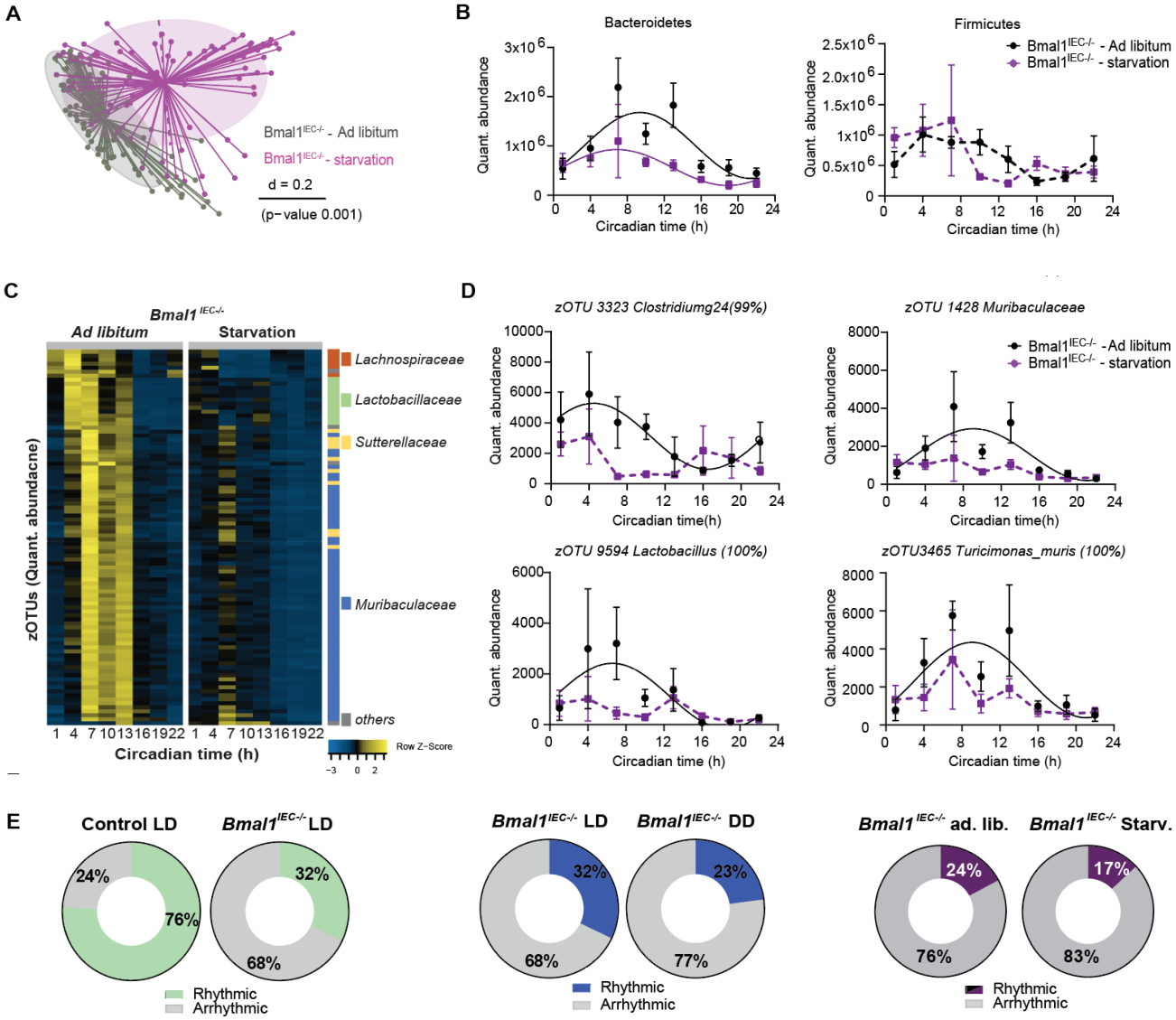

Figure 14: Starvation slightly induces zOTU arrhythmicity in bmal1$^{IEC-/-}$ mice

(A) MDS plot of beta diversity based on G. UniFrac distances of the fecal microbiota composition stratified by feeding conditions. (B) Circadian profile of quantitative abundance of the major phyla. (C) Heatmap illustrates the quantitative abundance of the zOTUs that lost rhythmicity upon starving bmal1 $^{IEC-/-}$ mice. zOTUs are ordered based on the phase of zOTUs in the ad libitum group; data are normalized based on the peak of each individual zOTU. (D) Circadian profile of zOTUs quantitative abundance. (E) Pie charts represent the percentage of rhythmic and arrhythmic zOTUs in different experiments. Bmal1$^{IEC-/-}$ mice in starvation and ad libitum feeding conditions are represented by purple and black, respectively. N = 5-6 mice/genotype/time point for WT and bmal1$^{IEC-/-}$ mice in LD and DD. For the starvation experiment, six mice were used per group to collect 43-44 samples over eight time points from bmal1$^{IEC-/-}$ mice in ad libitum and starvation conditions. Cosine-wave regression was used to assess rhythmicity. Solid lines indicate significant rhythms (p-value ≤ 0.05), while dashed lines indicate arrhythmicity. Data are illustrated as mean ± SEM.

Next, we addressed the functional relevance of gut clock-controlled zOTUs. PICRUST 2.0 (Langille, Zaneveld et al. 2013) analysis shows changes in abundance and loss of microbial pathway rhythmicity in *bmal1*$^{IEC-/-}$ mice (Figure 15 A-B). The gut clock drives the oscillations of microbial pathways involved in SCFA fermentation, vitamin biosynthesis, and the metabolism of amino acids, fatty acids, and sugar. Altogether, based on fecal microbiota rhythmicity analysis in *bmal1*$^{IEC-/-}$ mice and their controls, it can be stated that the gut clock represents the dominant driver of microbial rhythmicity and its rhythmic functionalities.

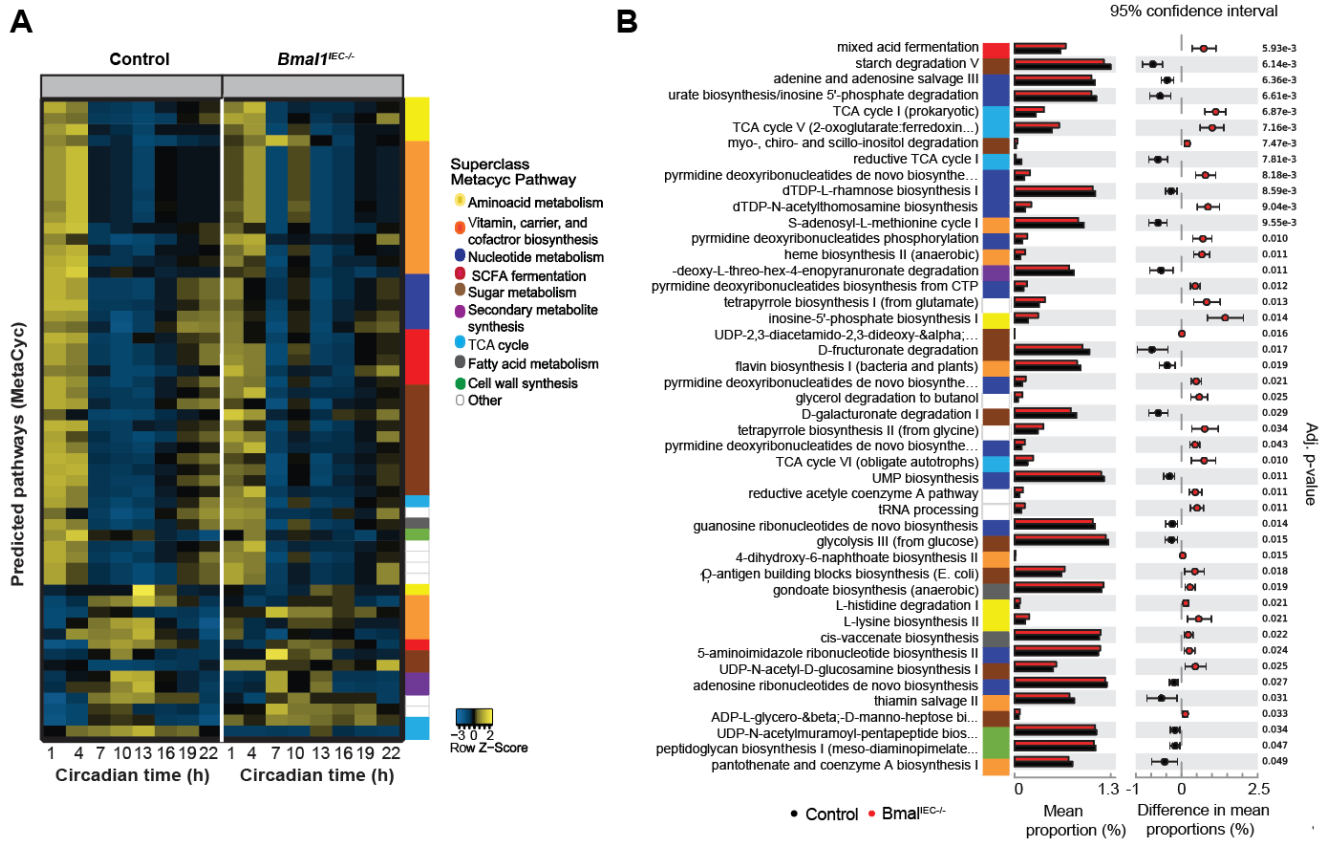

Figure 15: Lack of the intestinal clock disrupts microbial pathways

(A) Heatmap illustrates predicted microbial MetaCyc pathways of zOTUs that lost rhythmicity in bmal1$^{IEC-/-}$ *mice. Pathways are ordered based on the phase of the control group and normalized to each pathway's peak abundance. (B) Abundance differences between genotypes of predicted microbial MetaCyc pathways of zOTUs that lost rhythmicity in bmal1*$^{IEC-/-}$ *mice. To detect abundance differences, White's non-parametric two-sided t-test was used and then adjusting for multiple testing was performed using Benjamini Hochberg dales discovery rate. Bmal1* $^{IEC-/-}$ *mice are represented by red, while the controls are represented by black. N = 6 mice/genotype/time point.*

4.4. Genetic or environmental disruption of the central clock induces gut clock desynchronization

Microbial dysbiosis has been associated with various metabolic diseases (Metwaly, Reitmeier et al. 2022). Moreover, a recent report has linked arrhythmic microbiota to obesity and development of type 2 diabetes (Reitmeier, Kiessling et al. 2020). On the other hand, various metabolic abnormalities are induced by circadian disruption through jet lag and shift work (Woller and Gonze 2021). For example, chronic jet lag promotes weight gain in mice (Thaiss, Zeevi et al. 2014, Voigt, Forsyth et al. 2014). Despite the impact of circadian disruption in term of altering the gut microbiota (Thaiss, Zeevi et al. 2014, Voigt, Forsyth et al. 2014), little is known about the relationship between microbial rhythmicity and circadian disruption in promoting metabolic disease. In the following sections, we provide mechanistic insights on the host-microbe interaction during circadian disruption and its impact on host metabolic balance.

Central clock-disrupted mice (*bmal1*$^{SCNfl/-}$) possess rhythmic food intake in LD cycle, with slightly reduced amplitude (Figure 16A). However, upon being released in DD, *bmal1*$^{SCNfl/-}$ mice lost their rhythmic food intake behavior (Figure 16B). These results accord with a previous report showing rhythmic locomotor activity of *bmal1*$^{SCNfl/-}$ mice in LD cycle, which is lost completely in DD (Husse, Leliavski et al. 2014).

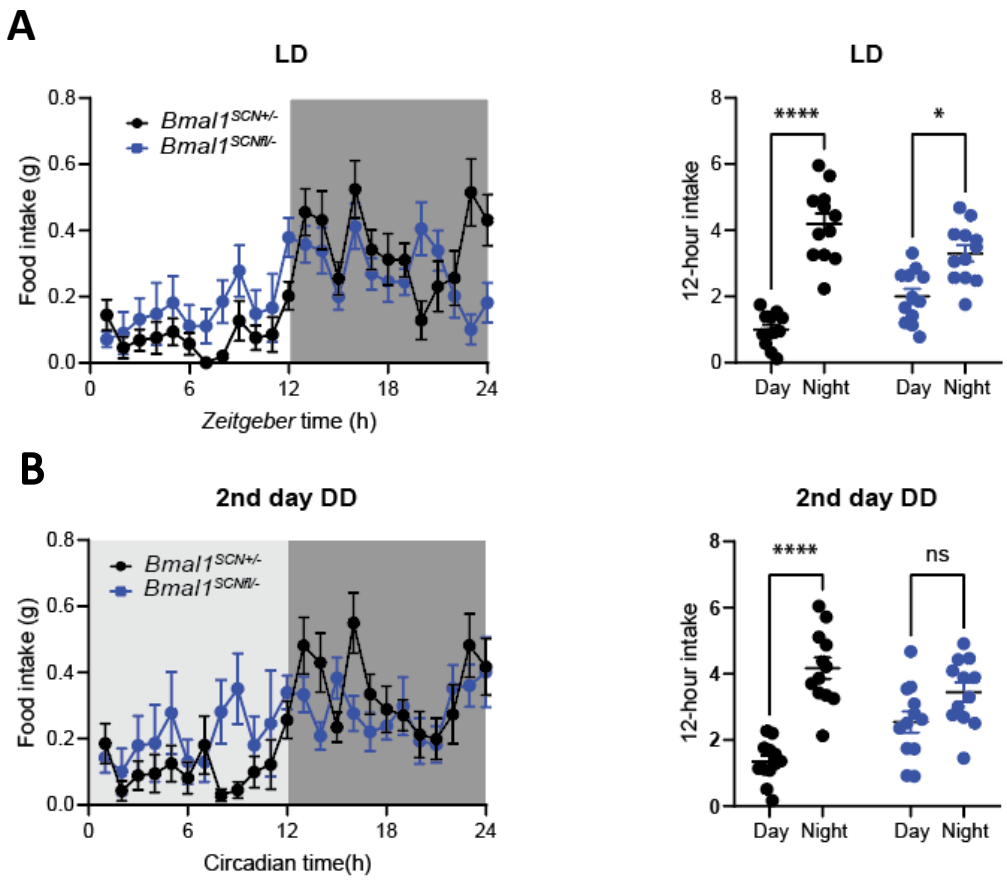

Figure 16: Arrhythmic food intake of bmal1$^{SCNfl/-}$ mice in DD
*(A-B) Food intake behavior of bmal1$^{SCNfl/-}$ mice and their controls in LD (A) and on the second day in DD (B). Bmal1$^{SCNfl/-}$ mice are represented by blue, while the controls are represented by black. N = 12 mice/group/light condition. To assess the day-night and group differences, 2 Way-ANOVA was used. * = p-value ≤ 0.05, **** = p-value ≤ 0.0001. Data are illustrated as mean ± SEM.*

A recent report has shown that the peripheral clocks are gradually desynchronized in *bmal1$^{SCNfl/}$* mice in DD (e.g., in the liver, adrenal, heart, kidney, white adipose tissue, and pancreas) (Husse, Leliavski et al. 2014, Kolbe, Husse et al. 2016). Due to global circadian desynchronization, *bmal1$^{SCNfl/-}$* mice develop altered glucose metabolism and obesity (Kolbe, Leinweber et al. 2019). Metabolic balance is partially regulated by gastrointestinal functions, which in turn are controlled by the circadian system (Segers and Depoortere 2021). To test the functionality of the gut clock in *bmal1$^{SCNfl/-}$* mice, we measured clock-gene expression in the proximal colon, cecum, and jejunum on the second day of DD (Figure 17, Table4).

The core clock genes *rev-erbα*, *per2*, and *bmal1* oscillated rhythmically in the jejunum of *bmal1*$^{SCNfl/-}$ mice and their controls (Figure 17A, Table4). However, all examined clock genes were phase-advanced in the jejunum (*rev-erbα:* 5.7h, *per2*: 3.6h, *bmal1*: 2.7h). Moreover, we discovered a loss of *cry1* rhythmicity and a reduction in *rev-erbα* baseline in the jejunum. *Dbp* did not reach a significant p-value according to cosine regression rhythmicity analysis; nevertheless, a significant time effect was found in both genotypes (p-value = 0.01) according to two-way ANOVA analysis. In the cecum, all examined clock genes lost rhythmicity, although two-way ANOVA showed a time difference in both genotypes (Figure 17B, Table 4) (two-way ANOVA time: *bmal1* p-value = 0.006, *per2* p-value = 0.002, *rev-erbα* p-value = 0.0009, *dbp* p-value = 0.03, *cry1* p-value = 0.003). In the proximal colon, both genotypes had comparable rhythmicity of *cry1*, *per2*, and *bmal1* expression (Figure 17C, Table 4). However, *dbp* lost its rhythmic expression and *rev-erbα* expressed with a lower amplitude. In summary, in *bmal1*$^{SCNfl/-}$ mice, the clock in the jejunum free-runs with dampened amplitude, the cecal clock slowly loses its functionality, and the colon clock is still functional with reduced amplitude. Thus, our data demonstrate a profound intestinal clock disruption in the absence of central clock functionalities, which manifests directly upon releasing the mice in DD.

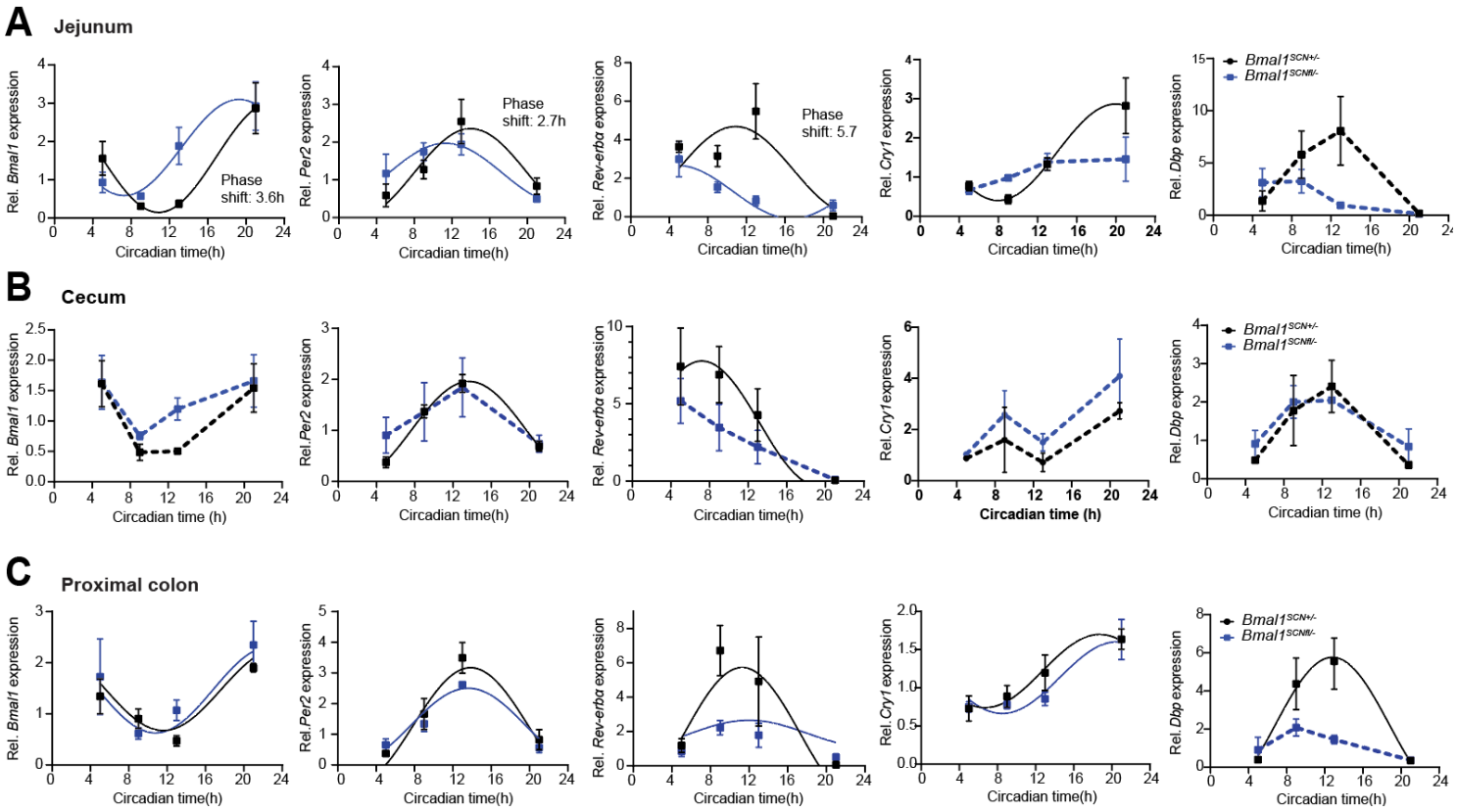

Figure 17: Disrupted-gut clock in bmal1$^{SCNfl/-}$ mice in DD

Relative clock-gene expression in the jejunum (A), cecum (B) and proximal colon (C) of bmal1$^{SCNfl/-}$ mice and their controls. Bmal1$^{SCNfl/-}$ mice are represented by blue, while the controls are represented by black. N = 3-4 mice/genotype/time point. Cosine-wave regression was used to assess rhythmicity. Solid lines indicate significant rhythms (p-value ≤ 0.05), while dashed lines indicate arrhythmicity. Significant phase shifts (p-value ≤ 0.05) are indicated by the number of hours of the phase shift. Data are illustrated as mean ± SEM.

Table 4: Clock-gene rhythmicity of bmal1$^{SCNfl/-}$ mice gastrointestinal tract

Gastrointestinal tissue	Gene	Group	Rhythmicity (P. value)	Phase shift (P. value)	Amplitude difference (P. value)	Baseline difference (P. value)
Jejunum	*Bmal*	*Bmal1$^{SCN+/-}$* *Bmal1$^{SCNfl/-}$*	0.004 0.01	0.02 Phase shift=3.6	0.64	0.42
	Per2	*Bmal1$^{SCN+/-}$* *Bmal1$^{SCNfl/-}$*	0.02 0.01	0.04 Phase shift=2.7	0.28	0.83
	Rev-erbα	*Bmal1$^{SCN+/-}$* *Bmal1$^{SCNfl/-}$*	0.03 0.04	0.03 Phase shift=5.7	0.28	0.04
	Cry1	*Bmal1$^{SCN+/-}$* *Bmal1$^{SCNfl/-}$*	0.009 0.42	0.33	0.07	0.11
	Dbp	*Bmal1$^{SCN+/-}$* *Bmal1$^{SCNfl/-}$*	0.056 0.06	0.08	0.08	0.14
Cecum	*Bmal*	*Bmal1$^{SCN+/-}$* *Bmal1$^{SCNfl/-}$*	0.06 0.33	0.53	0.34	0.3
	Per2	*Bmal1$^{SCN+/-}$* *Bmal1$^{SCNfl/-}$*	0.00006 0.31	0.54	0.37	0.59
	Rev-erbα	*Bmal1$^{SCN+/-}$* *Bmal1$^{SCNfl/-}$*	0.02 0.08	0.59	0.29	0.12
	Cry1	*Bmal1$^{SCN+/-}$* *Bmal1$^{SCNfl/-}$*	0.37 0.52	0.76	0.74	0.15
	Dbp	*Bmal1$^{SCN+/-}$* *Bmal1$^{SCNfl/-}$*	0.056 0.1	0.78	0.34	0.45
Proximal colon	*Bmal*	*Bmal1$^{SCN+/-}$* *Bmal1$^{SCNfl/-}$*	0.01 0.04	0.53	0.67	0.22
	Per2	*Bmal1$^{SCN+/-}$* *Bmal1$^{SCNfl/-}$*	0.004 0.001	0.56	0.13	0.25
	Rev-erbα	*Bmal1$^{SCN+/-}$*	0.03	0.98	0.02	0.07

		Bmal1$^{SCNfl/-}$	0.03			
	Cry1	*Bmal1*$^{SCN+/-}$ *Bmal1*$^{SCNfl/-}$	0.01 0.01	0.27	0.94	0.47
	Dbp	*Bmal1*$^{SCN+/-}$ *Bmal1*$^{SCNfl/-}$	0.008 0.07	0.39	0.002	0.04

4.5. Dysfunctional central clock disrupts microbial rhythmicity

The intestinal clock regulates microbial circadian oscillations (see Figures 10-13). Therefore, gut clock disruption in *bmal1*$^{SCNfl/-}$ mice might affect microbial rhythms and, consequently, its rhythmic functionalities. To test this, we collected fecal samples from *bmal1*$^{SCNfl/-}$ mice on the second day in DD. 16S rRNA analysis showed alteration in the gut microbiota in *bmal1*$^{SCNfl/-}$ mice (Figure 18A). Moreover, the observed rhythmicity in microbial diversity in the control mice was completely disrupted in the *bmal1*$^{SCNfl/-}$ mice (Figure 18B). Although relative abundance analysis showed similar rhythmicity patterns for Firmicutes and Bacteroidetes, quantitative analysis revealed a loss of circadian rhythmicity in both major phyla in *bmal1*$^{SCNfl/-}$ mice (Figure 18C). Moreover, families such as *Lactobacillaceae* and *Clostridiales* lost rhythmicity in *bmal1*$^{SCNfl/-}$ mice, independent of the analysis (Figure 18D).

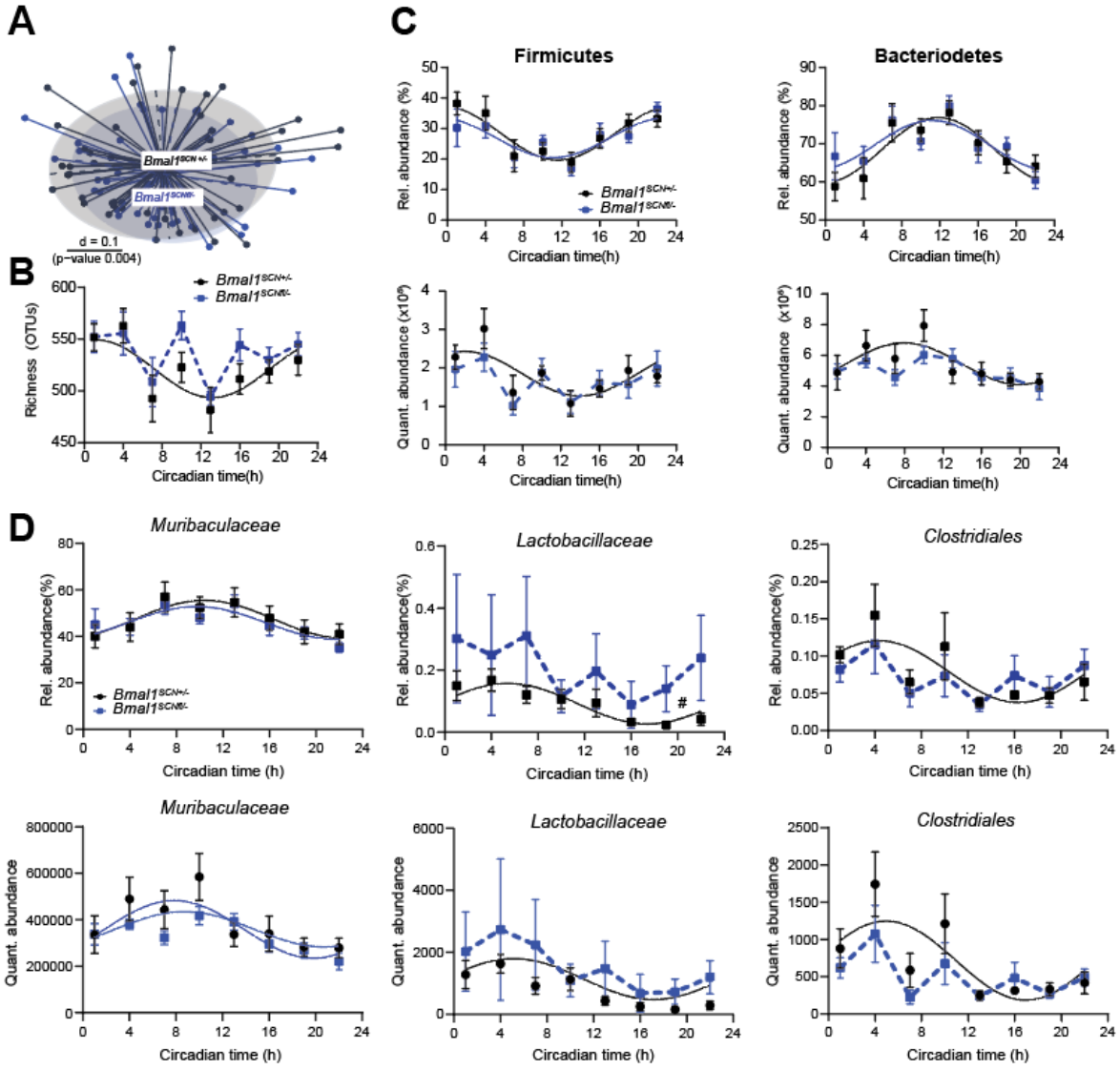

Figure 18: Loss of the central clock disrupts microbial rhythmicity

(A) MDS plot of beta diversity based on G. UniFrac distances of the fecal microbiota composition, stratified by genotype. (B-D) Circadian profile of microbial alpha diversity (B), the major phyla (C), and families (D) in relative and quantitative abundance. Bmal1$^{SCNfl/-}$ mice are represented by blue, while the controls are represented by black. N = 6 mice/genotype/time point. Cosine-wave regression was used to assess rhythmicity. Solid lines indicate significant rhythms (p-value ≤ 0.05), while dashed lines indicate arrhythmicity. Data are illustrated as mean ± SEM.

Then, we analyzed microbial rhythmicity at the zOTU level. After removing low abundance taxa, heatmaps showed loss of zOTU oscillations in *bmal1*$^{SCNfl/-}$ mice in both quantitative and relative analyses (Figure 19A, Figure 20A). In fact, three-quarters of rhythmic zOTUs became arrhythmic in the absence of a functional central clock in DD. The majority of zOTUs that lost rhythmicity in *bmal1*$^{SCNfl/-}$ mice belong to the mucus forager families *Muribaculaceae* and

Ruminococcaceae (Figure 19B, Figure 20B), families involved in production of SCFAs and bile acids (Biddle, Stewart et al. 2013, Gerard 2013). In particular, SCFA-producing taxa such as *Agathobaculum* and *Faecalibaculum* became arrhythmic in *bmal1*$^{SCNfl/-}$ mice (Figure 19C, Figure 20C). Notably, some taxa not only lost their rhythmicity but also differed in their abundances such as *Faecalibaculum Alloprevotella,* and *Muribaculaceae* (Figure 19D). In summary, the loss of the central clock disrupts microbial rhythmicity.

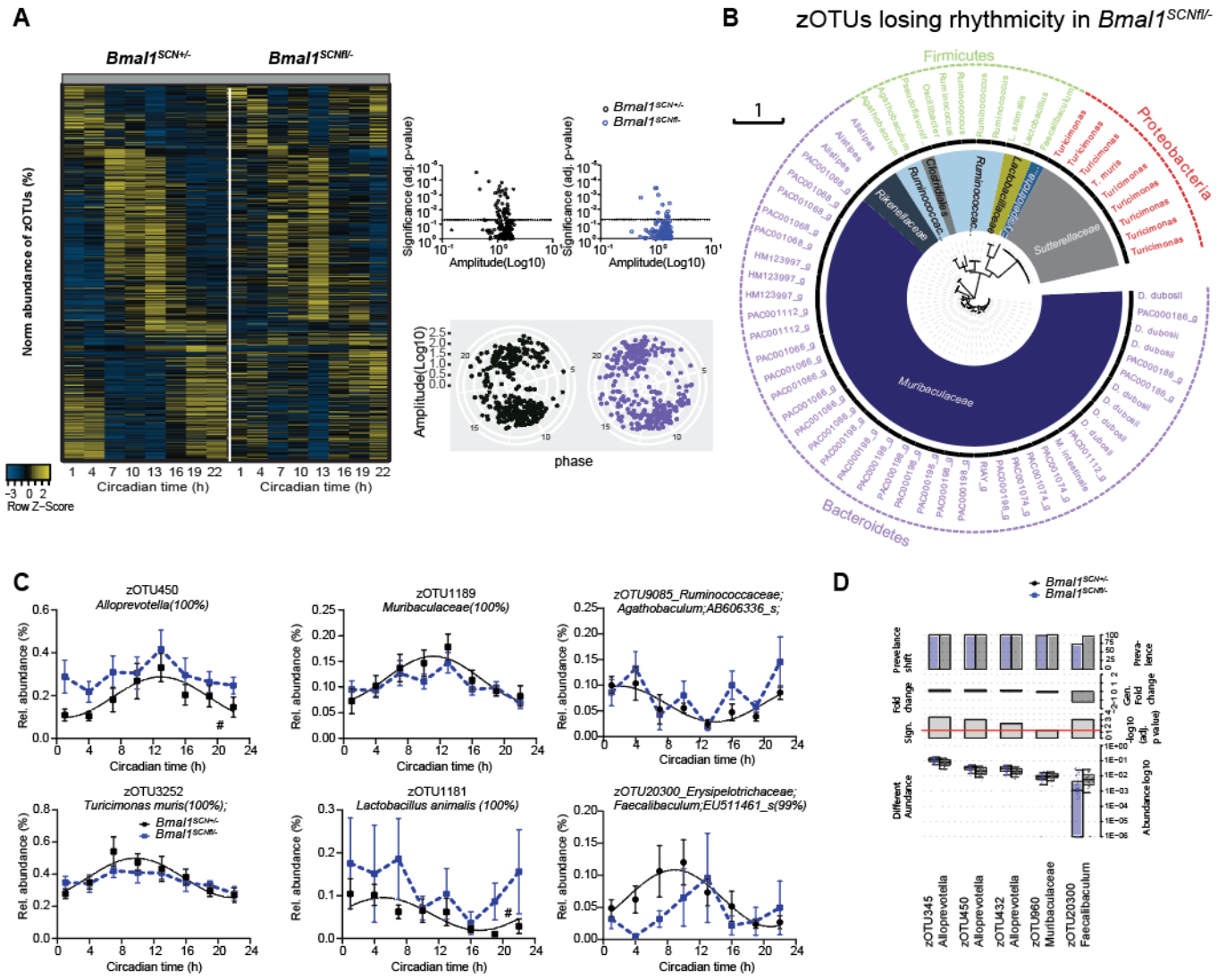

Figure 19: Loss of zOTU rhythmicity in bmal1$^{SCNfl/-}$ mice in DD based on relative analysis

(A) Heatmap illustrates 412 zOTUs' relative abundance (relative abundance mean > 0.1% and prevalence > 10%). zOTUs are ordered based on the phase of zOTUs in the control group; data are normalized based on the peak of each individual zOTU. Significant adj. p-value, amplitude (calculated by JTK_CYCLE) and phase distribution (calculated by cosine regression) of all zOTUs in both genotypes. Dashed lines represent JTK_CYCLE adj. p-value = 0.05. (B) Taxonomic tree of the zOTUs that lost rhythmicity in bmal1$^{SCNfl/-}$ mice in DD based on relative analysis. Taxonomic ranking is indicated as the phylum level (outer dashed ring), family level (inner circle), and genus level (middle names). Every zOTU is represented by a single branch. (C) Circadian profile of zOTUs' relative abundance in both genotypes. Bar charts show the significant (adj. p-value ≤0.05) abundance differences of zOTUs that lost their rhythmicity in bmal1$^{SCNfl/-}$ mice. Bmal1$^{SCNfl/-}$ mice are represented by blue, while the controls are represented by black. N = 6 mice/genotype/time point. Cosine-wave regression was used to assess rhythmicity. Solid lines indicate significant rhythms (p-value ≤ 0.05), while dashed lines indicate arrhythmicity. Data are illustrated as mean ± SEM.

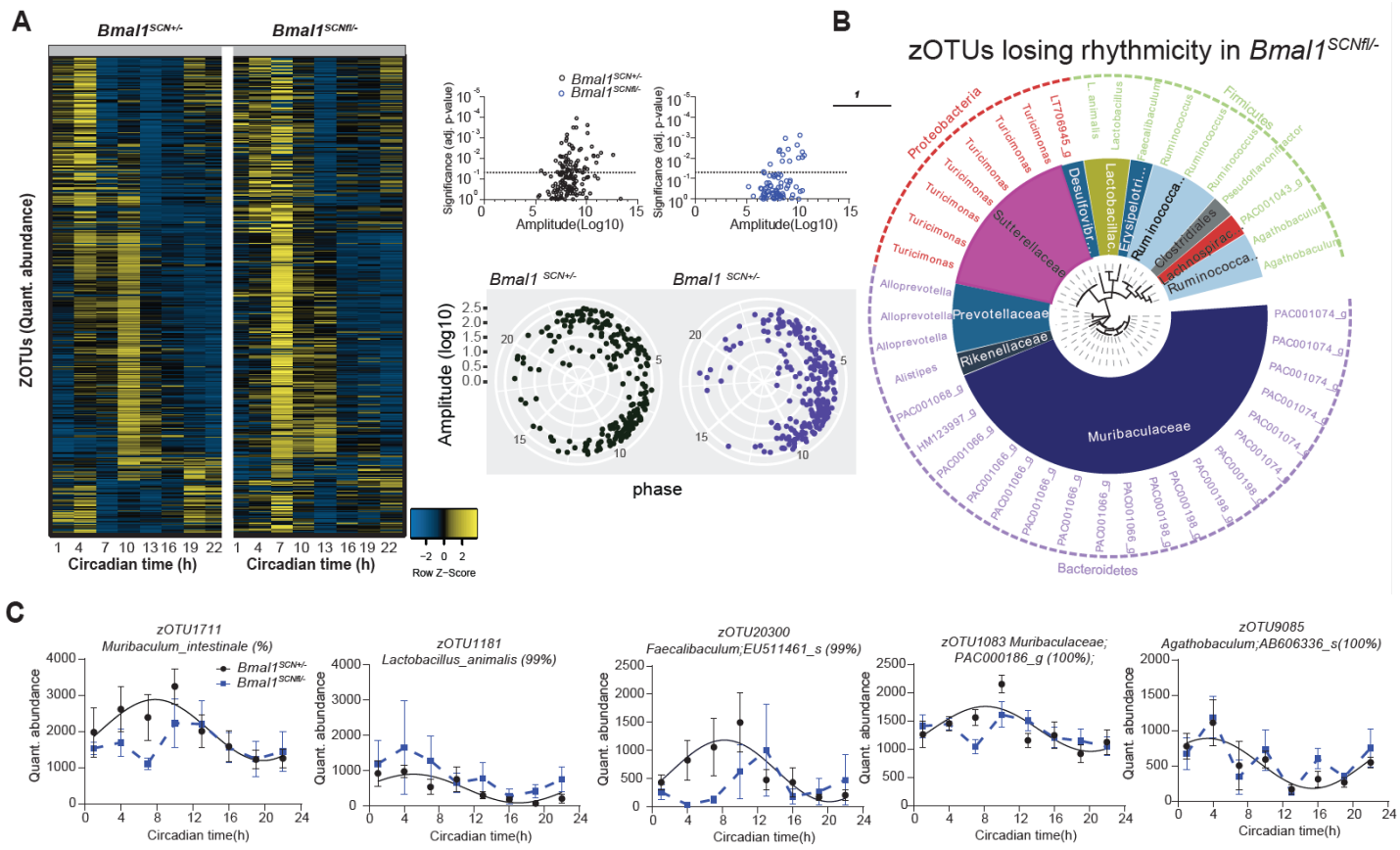

Figure 20: Loss of zOTU rhythmicity in bmal1$^{SCNfl/-}$ mice in DD based on quantitative analysis

(A) Heatmap illustrates 412 zOTUs' quantitative abundance (relative abundance mean > 0.1% and prevalence > 10%). zOTUs are ordered based on the phase of zOTUs in the control group, data are normalized based on the peak of each individual zOTU. Significant adj. p-value, amplitude (calculated by JTK_CYCLE) and phase distribution (calculated by cosine regression) of all zOTUs in both genotypes. Dashed lines represent JTK_CYCLE adj. p-value = 0.05. (B) Taxonomic tree of the zOTUs that lost rhythmicity in bmal1$^{SCNfl/-}$ mice in DD based on quantitative analysis. Taxonomic ranking is indicated as the phylum level (outer dashed ring), family level (inner circle), and genus level (middle names). Every zOTU is represented by a single branch. (C) Circadian profile of zOTUs quantitative abundance in both genotypes. Bmal1$^{SCNfl/-}$ mice are represented by blue, while the controls are represented by black. N = 6 mice/genotype/time point. Cosine-wave regression was used to assess rhythmicity. Solid lines indicate significant rhythms (p-value ≤ 0.05), while dashed lines indicate arrhythmicity. Data are illustrated as mean ± SEM.

4.6. Arrhythmic microbial functions in central clock-disrupted mice

To address the functional relevance of microbial rhythmicity, we used PICRUST 2.0 analysis to assess the functionalities of the central clock-controlled zOTUs (Langille, Zaneveld et al. 2013). Interestingly, microbial pathways relating to SCFA fermentation, fatty acid metabolism, and sugar metabolism lost rhythmicity and differed in abundance in *bmal1$^{SCNfl/-}$* mice (Figure 21 A-B). These results accord with the metabolic alteration found in these mice (Kolbe, Leinweber et al. 2019).

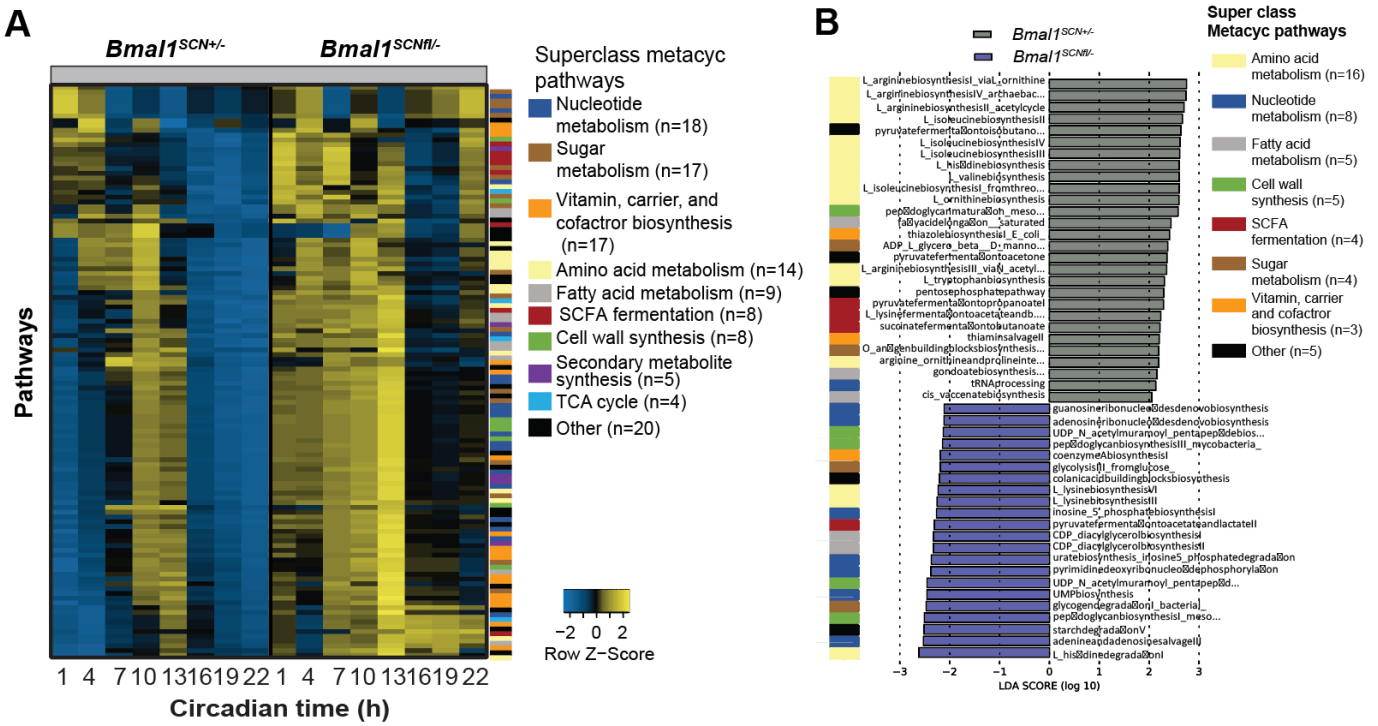

Figure 21: Lack of central clock disrupts microbial pathways
(A) Heatmap illustrates predicted microbial MetaCyc pathways of zOTUs that lost rhythmicity in bmal1$^{SCNfl/-}$ mice. Pathways are ordered based on the phase of the control group and are normalized to each pathway's peak abundance. (B) LDA score for MetaCyc pathways differed between bmal1$^{SCNfl/-}$ mice and their controls. Bmal1$^{SCNfl/-}$ mice are represented by blue, while the controls are represented by black. N = 6 mice/genotype/time point.

Furthermore, we found altered bacterial products such as SCFAs and bile acids in the fecal samples of *bmal1*$^{SCNfl/-}$ mice, according to targeted metabolite analysis (Figure 22-25). For example, *bmal1*$^{SCNfl/-}$ mice have lower levels of propionic acid (Figure 22), essential for lipid metabolism (Lin, Frassetto et al. 2012). Although total SCFA concentrations were normal in *bmal1*$^{SCNfl/-}$ mice, branched-chain fatty acids were reduced, e.g., 2-methylbutyric acid, isobutyric acid and, isovaleric acid (Figure 22).

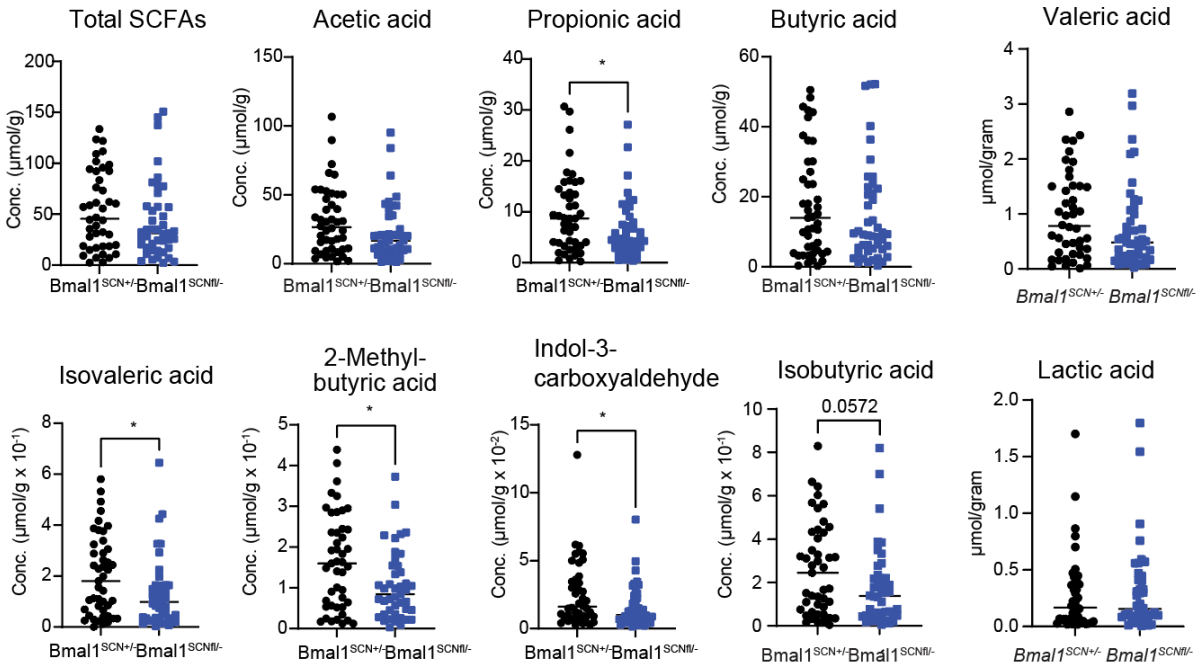

Figure 22: Slight alteration of SCFA concentration in bmal1$^{SCNfl/-}$ mice
*Fecal SCFA concentration in bmal1$^{SCNfl/-}$ mice and their controls. Bmal1$^{SCNfl/-}$ mice are represented by blue, while the controls are represented by black. N = 48 mice/genotype. Group differences were calculated based on Mann Whitney U test. Significance * = p-value ≤ 0.05*

Moreover, the absence of a functional central clock abolished rhythmicity in the accumulative abundance of SCFAs and other microbial products, including propionic acid, lactic acid, and acetic acid (Figure 23). Notably, some SCFAs oscillated rhythmically in both genotypes, including valeric acid and butyric acid (Figure 23).

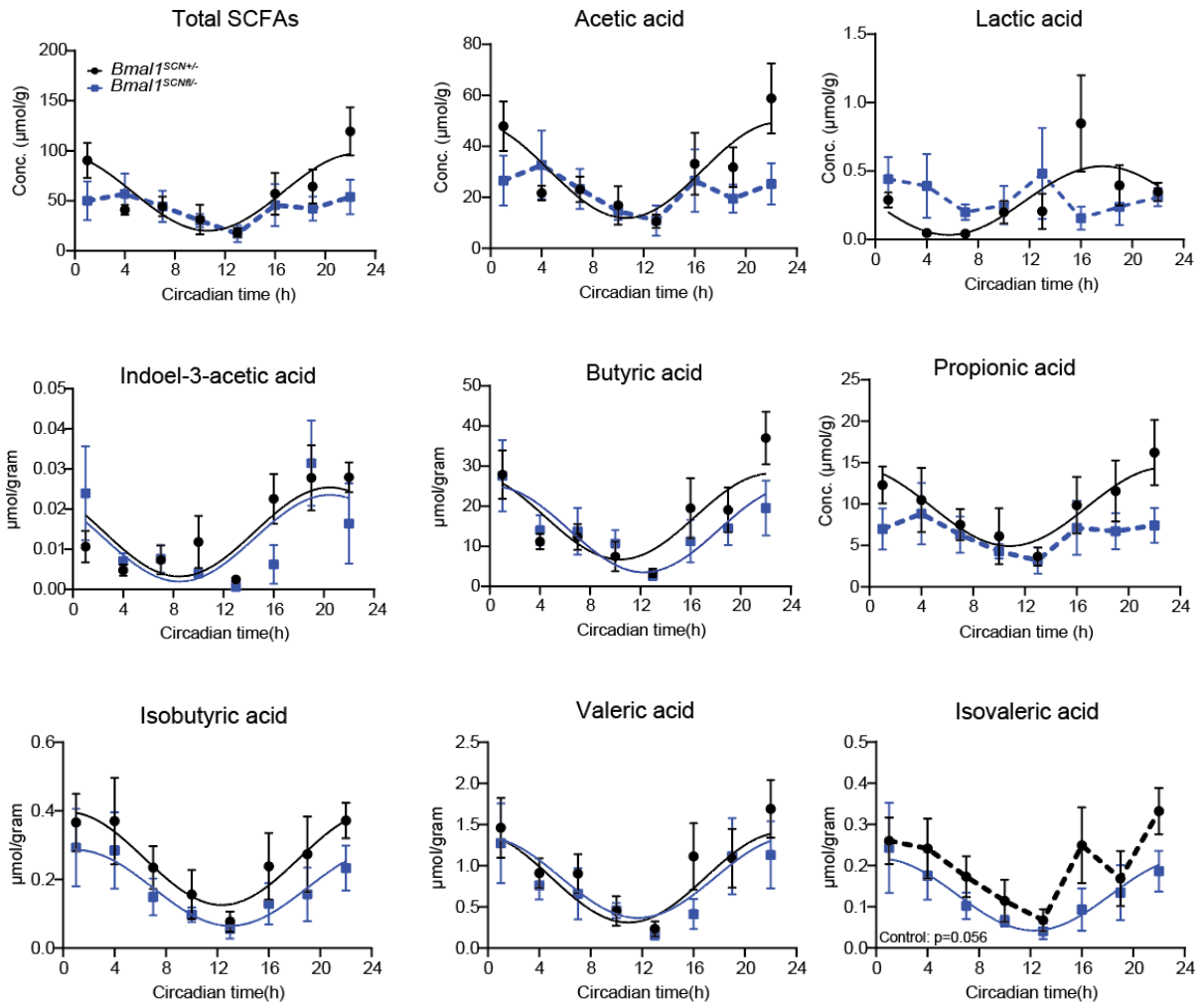

Figure 23: Disrupted SCFA rhythmicity in bmal1$^{SCNfl/-}$ mice

Circadian profile of fecal SCFAs in bmal1$^{SCNfl/-}$ mice and their controls. Bmal1$^{SCNfl/-}$ mice are represented by blue, while the controls are represented by black. N = 6 mice/time point/genotype. Cosine-wave regression was used to assess rhythmicity. Solid lines indicate significant rhythms (p-value ≤ 0.05), while dashed lines indicate arrhythmicity. Data are illustrated as mean ± SEM.

Additionally, the absence of a functional central clock alters bile acid concentration. For example, the concentration of 6-ketolithocholic acid is reduced, while tauro-a-muricholic acid and b-muricholic acid concentrations are increased in *bmal1$^{SCNfl/-}$* mice (Figure 24).

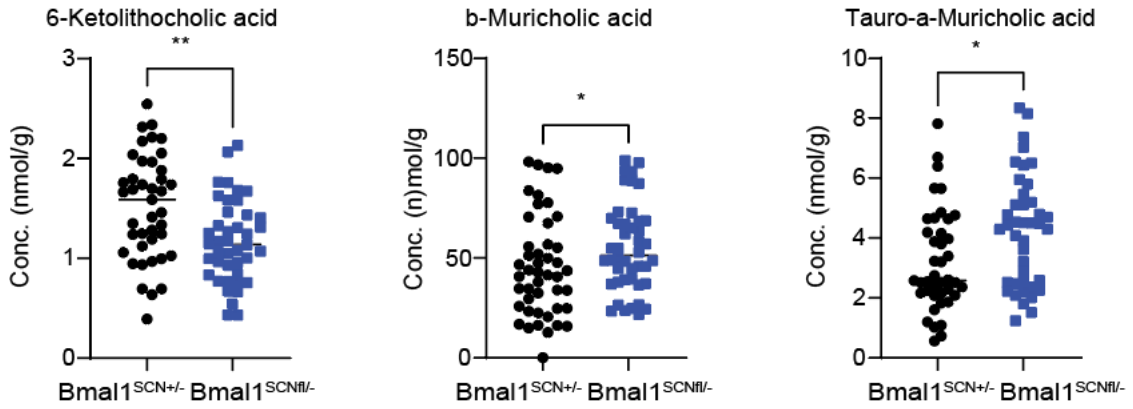

Figure 24: Slight alteration of bile acid concentrations in bmal1$^{SCNfl/-}$ mice

*Fecal bile acid concentration in bmal1$^{SCNfl/-}$ mice and their controls. Bmal1$^{SCNfl/-}$ mice are represented by blue, while the controls are represented by black. N = 48 mice/genotype. Group differences are calculated based on Mann Whitney U test. Significance * = p-value ≤ 0.05, ** = p-value ≤ 0.01*

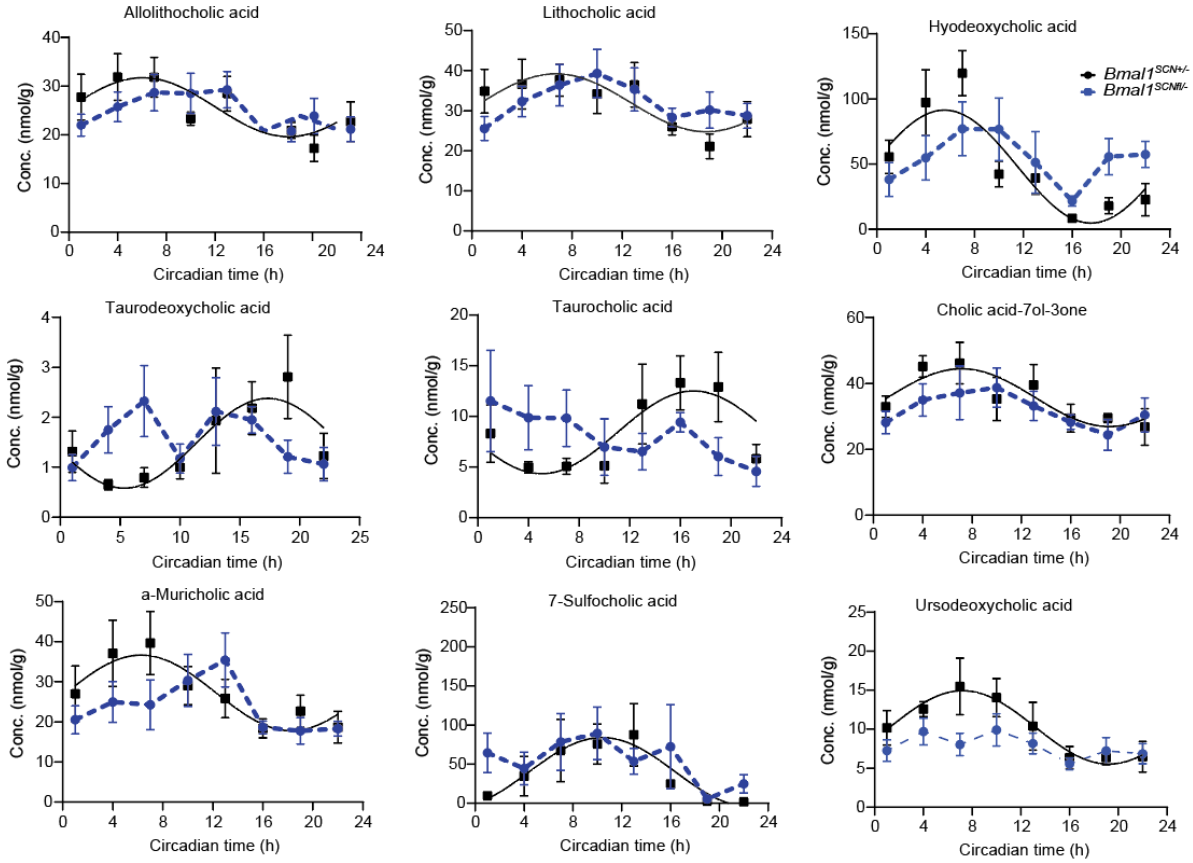

Figure 25: Disrupted bile acid rhythmicity in bmal1$^{SCNfl/-}$ mice

Circadian profile of fecal bile acids in bmal1$^{SCNfl/-}$ mice and their controls. Bmal1$^{SCNfl/-}$ mice are represented by blue, while the controls are represented by black. N = 6 mice/time point/genotype. Cosine-wave regression was used to assess rhythmicity. Solid lines indicate significant rhythms (p-value ≤ 0.05), while dashed lines indicate arrhythmicity. Data are illustrated as mean ± SEM.

Although other measured bile acids showed similar concentrations in both genotypes (Suppl. Figure 2), their rhythms were disrupted in *bmal1*$^{SCNfl/-}$ mice. Examples include allolithocholic acid, taurocholic acid, ursodeoxycholic acid, and 7-sulfocholic acid (Figure 25), suggesting altered cholesterol and fat metabolisms (Dawson and Karpen 2015).

Altogether, the central clock is essential for synchronizing the intestinal clock. A disrupted intestinal clock might be the reason for arrhythmic gut microbiota in *bmal1*$^{SCNfl/-}$ mice. Loss of microbial rhythmicity abolishes its rhythmic functional output, including levels of bile acids and SCFAs, in *bmal1*$^{SCNfl/-}$ mice.

4.7. Simulated shift work (SSW) disrupts peripheral clocks

Shift work and frequent jet lag promote metabolic diseases and weight gain (Parsons, Moffitt et al. 2015, Qiao, Beibei et al. 2020), as also seen in *bmal1*$^{SCNfl/-}$ mice (Kolbe, Leinweber et al. 2019). These frequent environmental shifts disrupt the circadian system by inducing inter- and intra-clock desynchronization (Kiessling, Eichele et al. 2010). To investigate whether environmental circadian disruption promotes gut clock desynchronization, similar to *bmal1*$^{SCNfl/-}$ mice, we placed wild-type mice in SSW conditions (Figure 26A). Although mice in SSW have total activity that is comparable to the controls, their activity gradually adjusts to the new LD cycle in SSW, losing the day-night difference (Figure 26B-C).

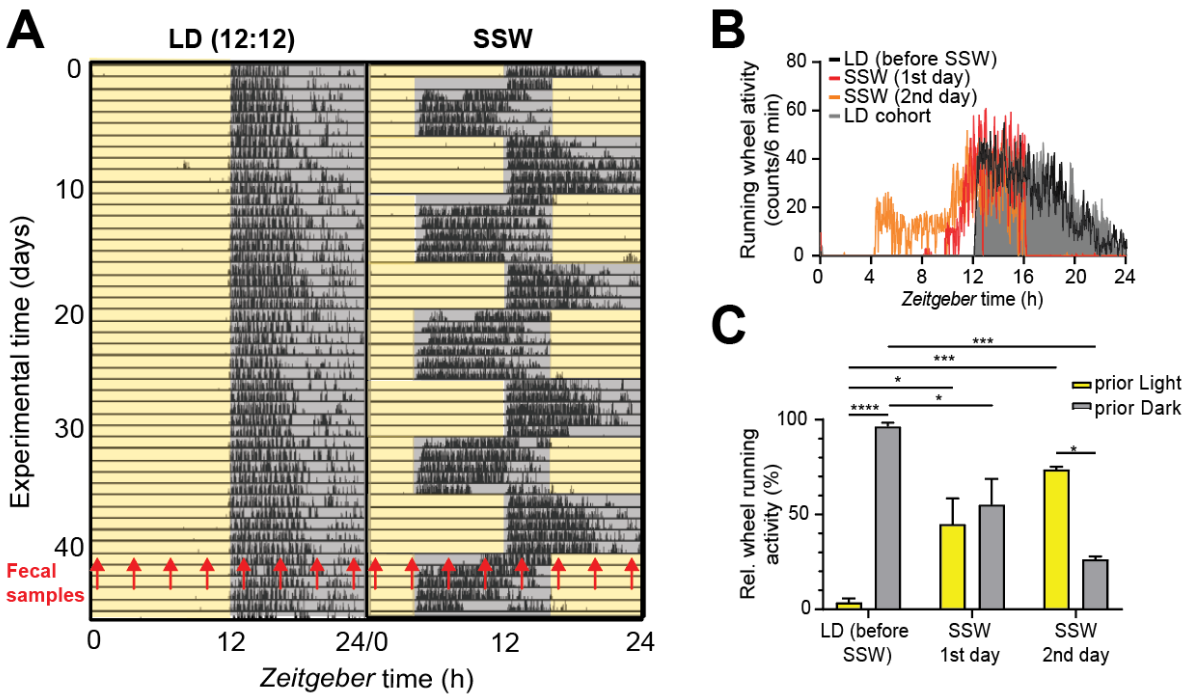

Figure 26: SSW disrupts rhythmic activity behavior

*(A) Representative actogram of activity behavior of SSW mice and their LD controls. Each row represents one day and tick marks illustrate running wheel activity. Yellow shading represents light, while gray shading represents darkness. Red arrows point to the time of fecal sample collection. (B) Diurnal profile of SSW and LD mice total running wheel activity. (C) Running wheel activity summary in day and night of SSW and LD mice. N = 4-5 mice/light condition. The change of activity was assessed by two-way ANOVA. Significance * = p-value ≤ 0.05, *** = p-value ≤ 0.001, **** = p-value ≤ 0.0001. Data are illustrated as mean ± SEM.*

In accordance with previous reports (Thaiss, Zeevi et al. 2014, Desmet, Thijs et al. 2021), SSW induced body weight gain, although food intake was comparable to that of the controls (Figure 27 A-B). A previous report has correlated metabolic syndrome with intestinal permeability, thereby influencing nutrient uptake (Teixeira, Souza et al. 2012). While SSW slightly enhanced colon permeability at ZT 13, no significant difference between light conditions was detected. Moreover, mice in LD and SSW had similar energy assimilation (Figure 27C-D).

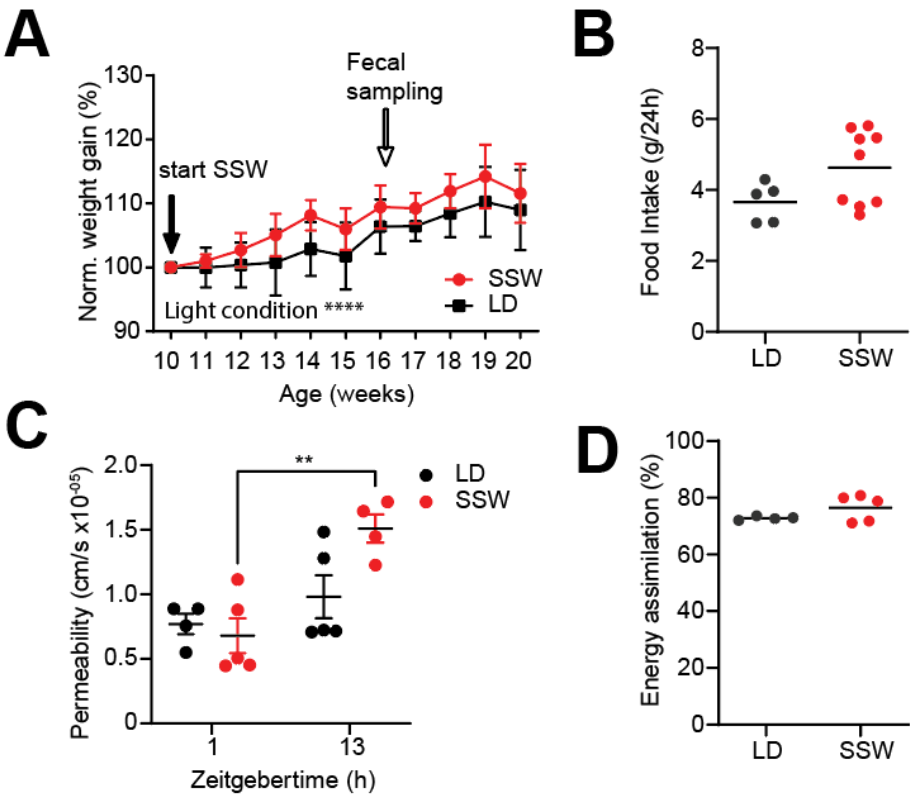

Figure 27: SSW induces weight gain

*(A) Normalized body weight over 10 weeks for mice in SSW and LD light condition. (B-D) Food intake (B), gut permeability (C), and energy assimilation (D) of mice in SSW and LD conditions. Red represents mice in SSW, while black represents mice in LD. N = 4-5 mice/time point/light condition. The change in body weight and gut permeability were assessed by two-way ANOVA. Food intake and energy assimilation differences were assessed by Mann Whitney U test. Significance ** = p-value ≤ 0.01, **** = p-value ≤ 0.0001. Data are illustrated as mean ± SEM.*

To test the effect of SSW on the gut clock, we measured clock-gene expression in the proximal colon, cecum, and jejunum at ZT 1 and ZT 13. In accordance with a previous report showing different resetting speeds of peripheral clocks in case of chronic jet lag (Kiessling, Eichele et al. 2010), SSW induced tissue- and gene-specific alterations in the examined peripheral clocks (Figure 28). For example, although *per2* and *bmal1* in the proximal colon, jejunum, and liver showed daytime differences in both light conditions, *rev-erbα, dbp*, and *cry1* responded to SSW in a tissue-specific manner (Figure 28 A, C-D). For instance, *rev-erbα* is reduced dramatically at ZT 13 in the colon in SSW while losing its daytime difference in the liver (Figure 28 C-D). By contrast, SSW abolished *bmal1* daytime differences and enhanced *cry1* expression at ZT 13 in the cecum without affecting *rev-erbα, dbp*, and *per2* expression (Figure 28B). Moreover,

clock genes maintained daytime-dependent expression (except c*ry1*) in the proximal colon of mice under SSW, although *rev-erbα, dbp,* and *bmal1* were suppressed at ZT 13 (Figure 28C). Altogether, our results further confirm that SSW induces tissue- and gene-specific clock disruption. Consequently, SSW induces inter- and intra-gut clock disruptions.

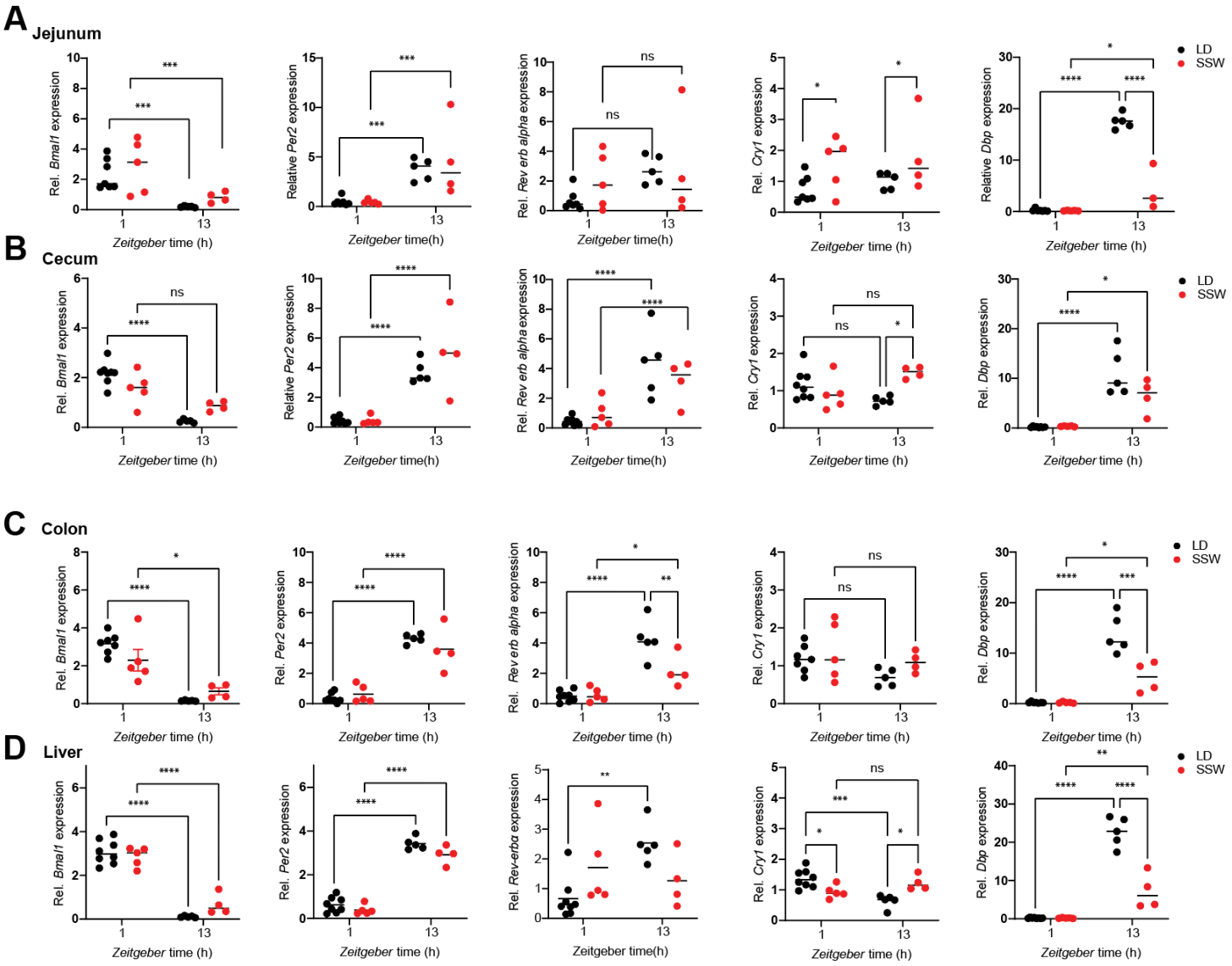

Figure 28: SSW disrupts gut and liver clock genes time difference

*Relative clock-gene expression in the jejunum (A), cecum (B), proximal colon (C) and liver (D) of mice in SSW and LD. Red represents mice in SSW, while black represents mice in LD. N = 4-5 mice/time point/light condition. Time and group differences were assessed by two-way ANOVA. Significance * = p-value ≤ 0.05, ** = p-value ≤ 0.01, *** = p-value ≤ 0.001, **** = p-value ≤ 0.0001.*

4.8. Arrhythmic microbial composition and function under SSW

Environmental light conditions affect the gut microbiota (Thaiss, Zeevi et al. 2014, Voigt, Forsyth et al. 2014, Deaver, Eum et al. 2018, Li, Wang et al. 2021). To test the impact of SSW on microbial composition and rhythmicity, we collected fecal samples over the day from mice

in SSW and LD (Figure 26A). Indeed, exposing mice to SSW altered the microbial composition significantly (Figure 29A).

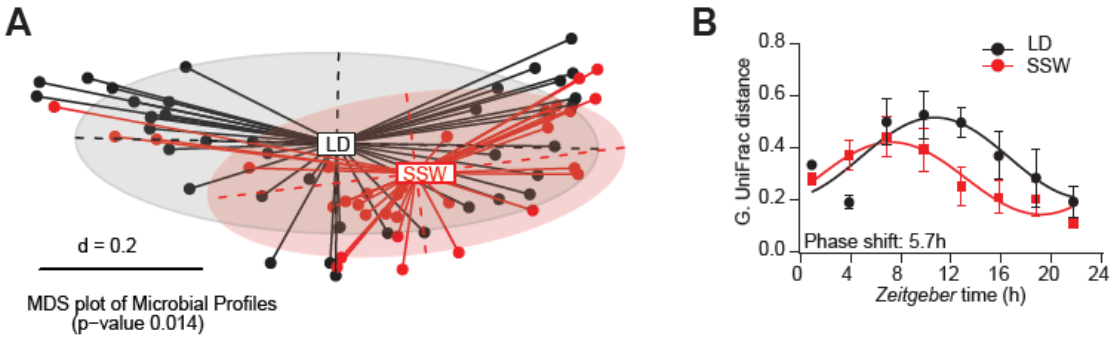

Figure 29: SSW alters microbial composition
(A) MDS plot of beta diversity based on G. UniFrac distances of the fecal microbiota composition stratified by light condition. (B) Diurnal profile of G. UniFrac distances calculated to the controls' ZT 1. Red represents mice in SSW, while black represents mice in LD. N = 4-5 mice/time point/light condition. Solid lines indicate significant rhythms (p-value ≤ 0.05), while dashed lines indicate arrhythmicity. Significant phase shifts (p-value ≤ 0.05) are indicated by the number of hours of the phase shift. Data are illustrated as mean ± SEM.

In terms of the impact of SSW on microbial rhythmicity, it shifted the phase of the rhythmic G. UniFrac distances as well as major phyla and families to align with the advanced rhythmic behavior (Figure 29B, Figure 30A, Figure 31A, Figure 32A). Moreover, quantitative analysis reveals a loss of Bacteroidetes rhythmicity in the SSW condition (Figure 30B).

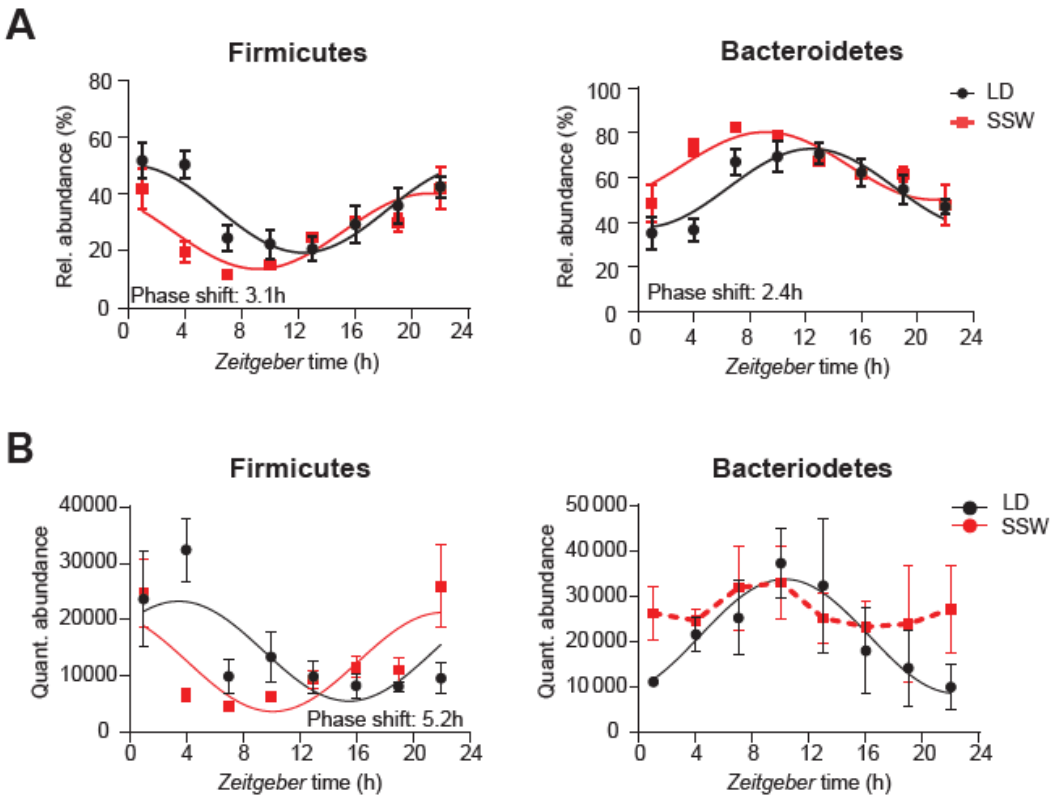

Figure 30: SSW disrupts major phyla rhythmicity
(A-B) Diurnal profile of major phyla in relative (A) and quantitative (B) analysis. Red represents mice in SSW, while black represents mice in LD. N = 4-5 mice/time point/light condition. Solid lines indicate significant rhythms (p-value ≤ 0.05), while dashed lines indicate arrhythmicity. Significant phase shifts (p-value ≤ 0.05) are indicated by the number of hours of the phase shift. Data are illustrated as mean ± SEM.

Next, we addressed the impact of SSW at the level of zOTUs. SSW advanced the phase of rhythmic zOTUs, as illustrated by quantitative and relative abundance heatmaps (Figure 31B, Figure 32B). Furthermore, SSW disrupted almost half of the rhythmic zOTUs oscillating in LD (Figure 31C, Figure 32C, Figure 33A, Figure 34A), including *Odoribacter*, *Lactobacillus*, and *Ruminococcus*. Quantitative and relative analyses show that taxa belonging to *Ruminococcus*, *Eubacterium*, and *Bacteroides* lost rhythmicity in SSW (Figure 33A-B, Figure 34A-B).

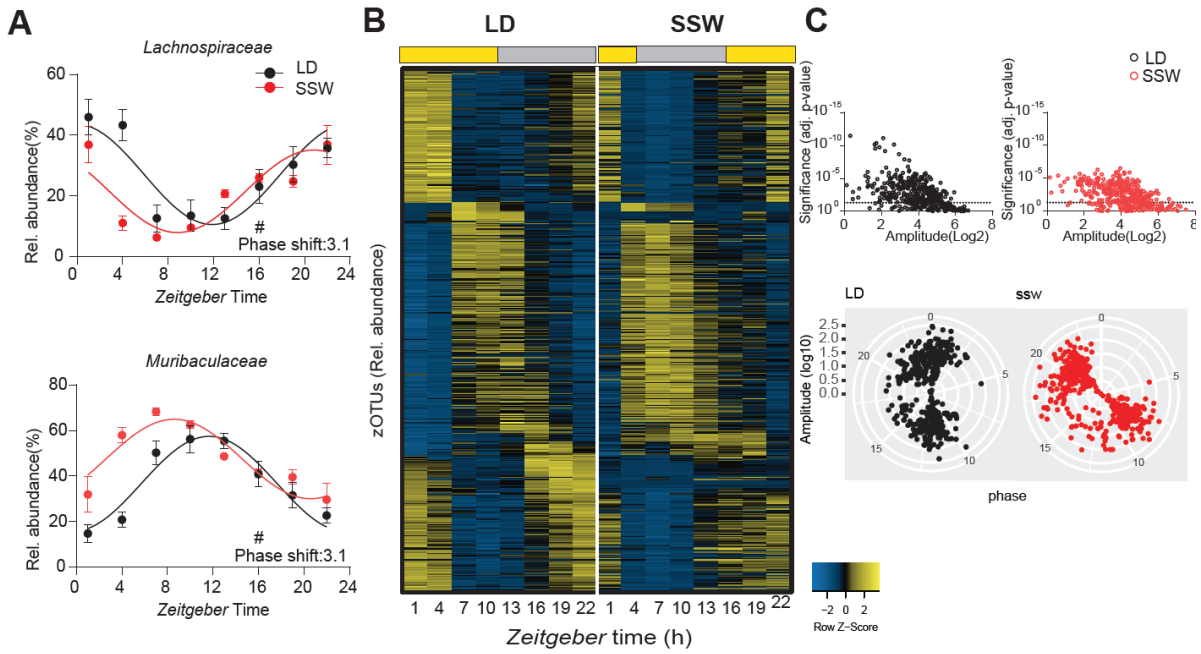

Figure 31: Altered microbial rhythmicity in SSW according to relative analysis

(A) Diurnal profile of families' relative abundance for mice in SSW and LD. (B) Heatmap illustrates the relative abundance of 473 zOTUs' relative abundance (relative abundance mean > 0.1% and prevalence > 10%). zOTUs are ordered based on the phase of zOTUs in the control group, and data are normalized based on the peak of each individual zOTU. (C) Significant adj. p-value, amplitude (calculated by JTK_CYCLE) and phase distribution (calculated by cosine regression) of all zOTUs in both light conditions. Dashed lines represent JTK_CYCLE adj. p-value = 0.05. Red represents mice in SSW, while black represents mice in LD. N = 4-5 mice/time point/light condition. Solid lines indicate significant rhythms (p-value ≤ 0.05), while dashed lines indicate arrhythmicity. Significant phase shifts (p-value ≤ 0.05) are indicated by the number of hours of the phase shift. Data are illustrated as mean ± SEM.

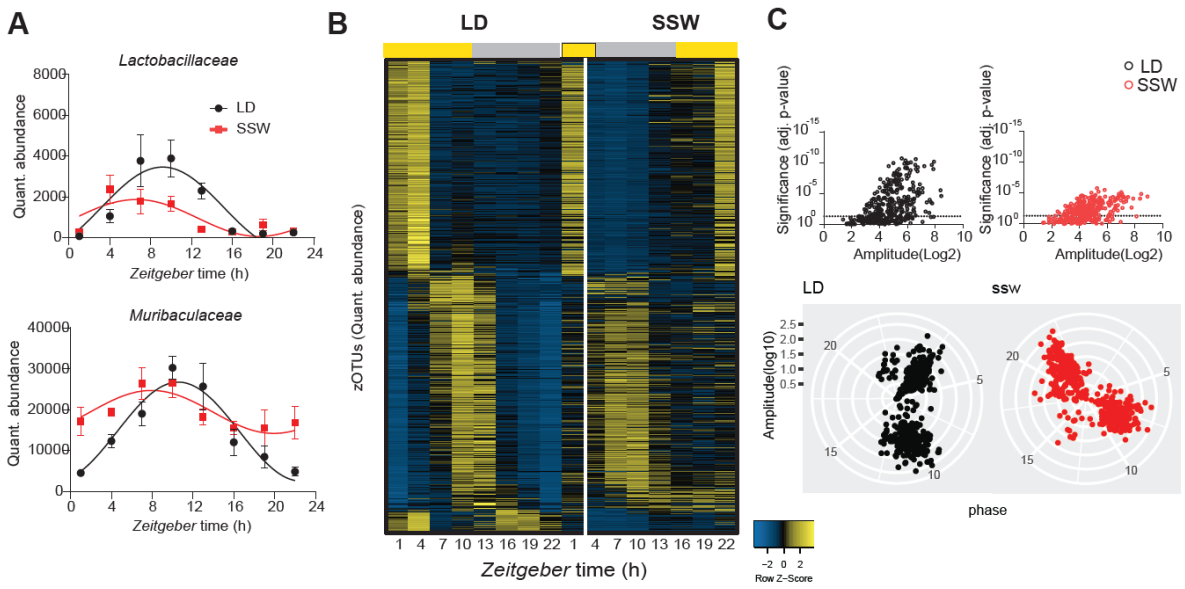

Figure 32: Altered microbial rhythmicity in SSW according to quantitative analysis
(A) Diurnal profile of families' quantitative abundance for mice in SSW and LD conditions. (B) Heatmap illustrates 473 zOTUs' quantitative abundance (relative abundance mean > 0.1% and prevalence > 10%). zOTUs are ordered based on the phase of zOTUs in the control group, and data are normalized based on the peak of each individual zOTU. (C) Significant adj. p-value, amplitude (calculated by JTK_CYCLE) and phase distribution (calculated by cosine regression) of all zOTUs in both light conditions. Dashed lines represent JTK_CYCLE adj. p-value = 0.05. Red represents mice in SSW, while black represents mice in LD. N = 4-5 mice/time point/light condition. Solid lines indicate significant rhythms (p-value ≤ 0.05), while dashed lines indicate arrhythmicity. Data are illustrated as mean ± SEM.

Interestingly, taxa that remained rhythmic in SSW have a 3.7-6.4-hour advanced phase (Figure 31B-C, Figure 32B-C). These include the genera *Oscillibacter*, *Roseburia*, *Alistipes*, and *Duncaniella*, as well as taxa belonging to the family *Lachnospiraceae*. Notably, SSW altered the average abundance of taxa belonging to the genera *Lactobacillus* and to the families *Ruminococcaceae* and *Muribaculaceae* (Figure 33 B-C, Figure 34 B-C), which accords with previous data from mice maintained under conditions of sleep deprivation or chronic jetlag (Thaiss, Zeevi et al. 2014, Voigt, Forsyth et al. 2014, Deaver, Eum et al. 2018, Bowers, Vargas et al. 2020).

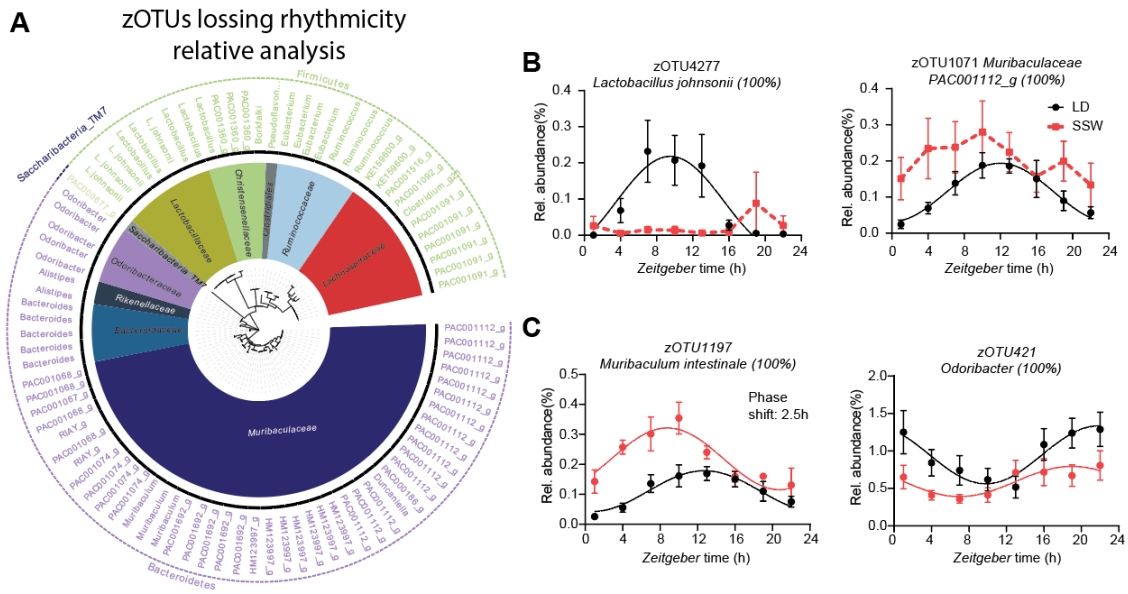

Figure 33: SSW-controlled zOTUs according to relative analysis

(A) Taxonomic tree of the zOTUs that lost rhythmicity in SSW based on relative analysis. Taxonomic ranking is indicated as the phylum level (outer dashed ring), family level (inner circle), and genus level (middle names). Every zOTU is represented by a single branch. (B-C) Diurnal profile of zOTUs' relative abundance in both light conditions. Red represents mice in SSW, while black represents mice in LD. N = 4-5 mice/time point/light condition. Solid lines indicate significant rhythms (p-value ≤ 0.05), while dashed lines indicate arrhythmicity. Significant phase shifts (p-value ≤ 0.05) are indicated by the number of hours of the phase shift. Data are illustrated as mean ± SEM.

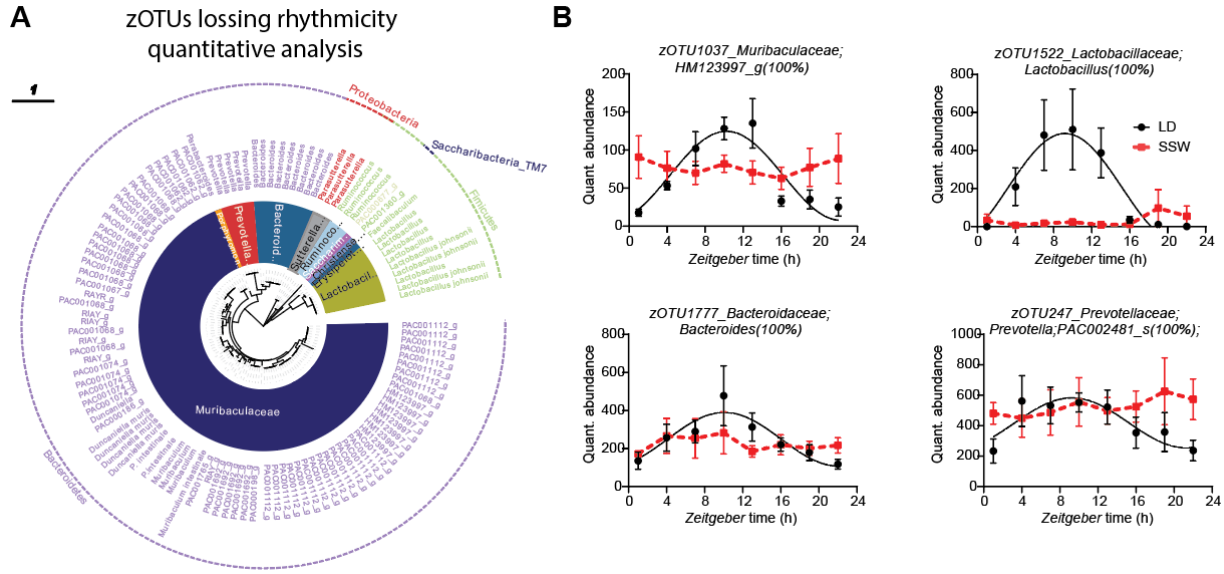

Figure 34: SSW-controlled zOTUs according to quantitative analysis

(A) Taxonomic tree of the zOTUs that lost rhythmicity in SSW based on quantitative analysis. Taxonomic ranking is indicated as the phylum level (outer dashed ring), family level (inner circle), and genus level (middle names). Every zOTU is represented by a single branch. (B) Diurnal profile of zOTUs' quantitative abundance in both light conditions. Red represents mice in SSW, while black represents mice in LD. N = 4-5 mice/time point/light condition. Solid lines indicate significant rhythms (p-value ≤ 0.05), while dashed lines indicate arrhythmicity. Data are illustrated as mean ± SEM.

Since both SSW and central clock disruption induced gut clock desynchronization, we tested whether they induced comparable disturbances of microbial rhythmicity. However, the microbiota compositions of both experiments were not comparable due to different animal housing facilities (Supplementary Figure 3). These results accord with frequent reports showing the impact of housing conditions on the gut microbiota (Parker, Albeke et al. 2018).

Next, we assessed microbiota functionality using PICRUST 2.0 analysis for zOTUs that lost rhythmicity in SSW. Microbial pathways were then compared to the results obtained from central clock-controlled zOTUs (Figure 21). Interestingly, both environmental and genetic circadian disruption altered the abundance and abolished the rhythmicity of microbial pathways related to metabolism of sugar, fatty acids, and amino acids as well as SCFA fermentation (Figure 21 A-B, Figure 35A-B, Figure 36). These results suggest a functional link between the gut clock and circadian microbiota functionalities.

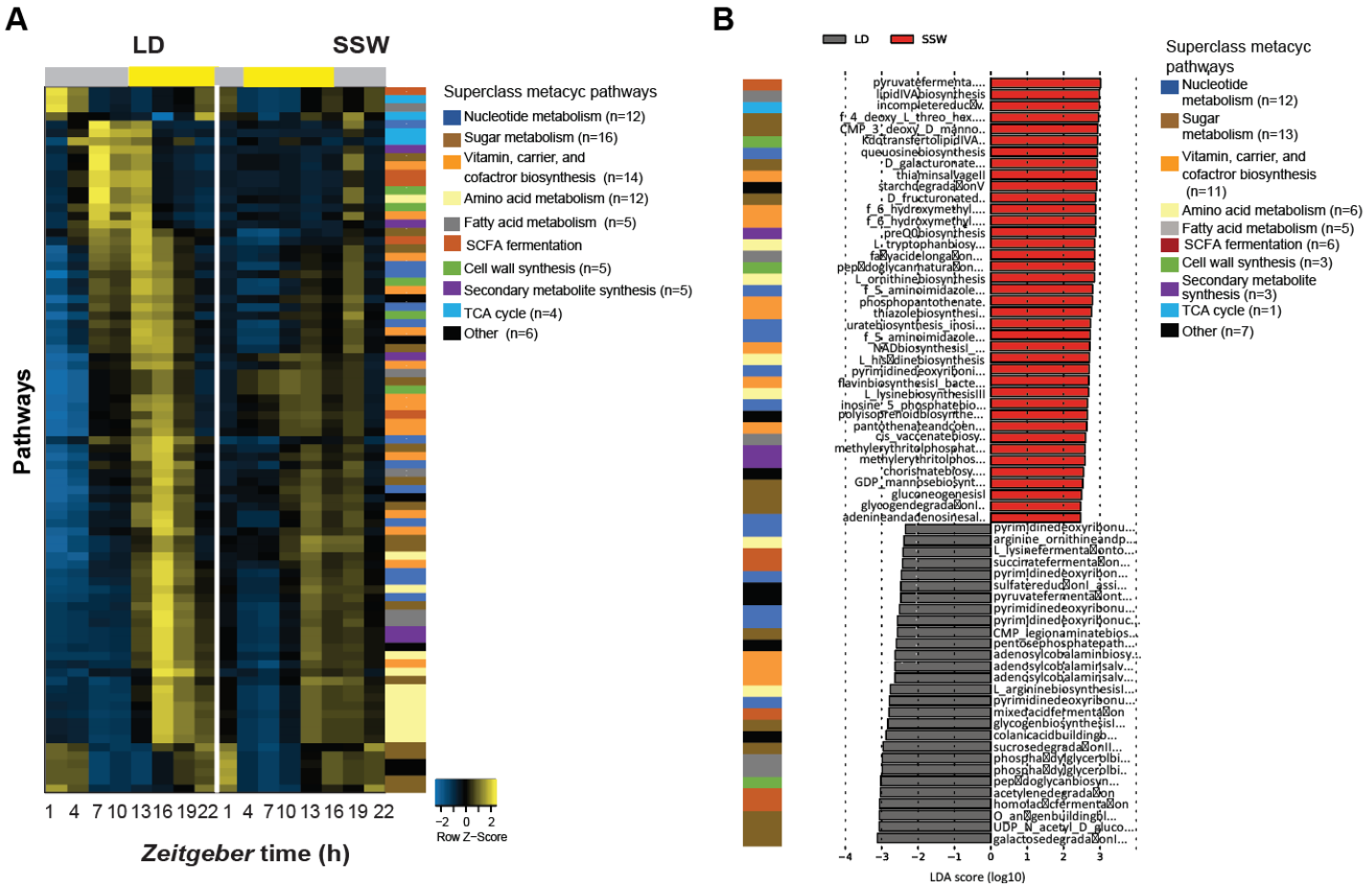

Figure 35: SSW disrupts microbial pathways

(A) Heatmap illustrates predicted microbial MetaCyc pathways of zOTUs that lost rhythmicity in SSW. Pathways are ordered based on the phase of the control group and normalized to each pathway's peak abundance. (B) LDA score of MetaCyc pathways differs between mice in SSW and their LD controls. Mice in SSW are represented by red, while the LD controls are represented by black. N = 4-5 mice/genotype/time point.

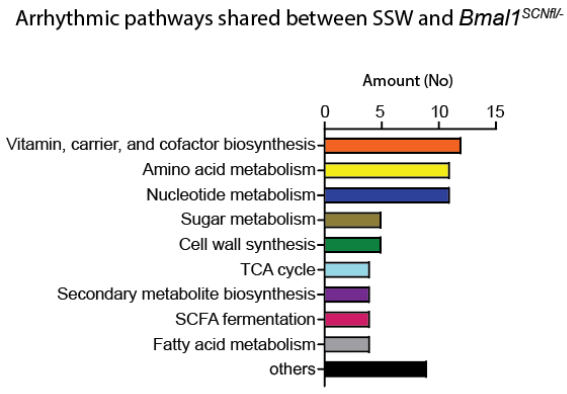

Figure 36: Genetic and environmental circadian disruption induce similar disruption in microbial pathways

Bar charts represent the number of shared microbial pathways that lost rhythmicity in SSW and bmal1$^{SCNfl/-}$ mice. N = 36-48 mice/group

4.9. Arrhythmic microbiota alters host homeostasis

To directly test the physiological relevance of SSW-induced microbial alteration, we colonized germ-free wild-type mice with cecal microbiota from mice exposed to SSW and their LD controls (Figure 37A). SSW-associated microbiota induced a significant increase in body weight in comparison to LD-associated microbiota (Figure 37B), which accords with previous data from germ-free mice colonized with the fecal microbiota of chronic jet-lagged mice (Thaiss, Zeevi et al. 2014).

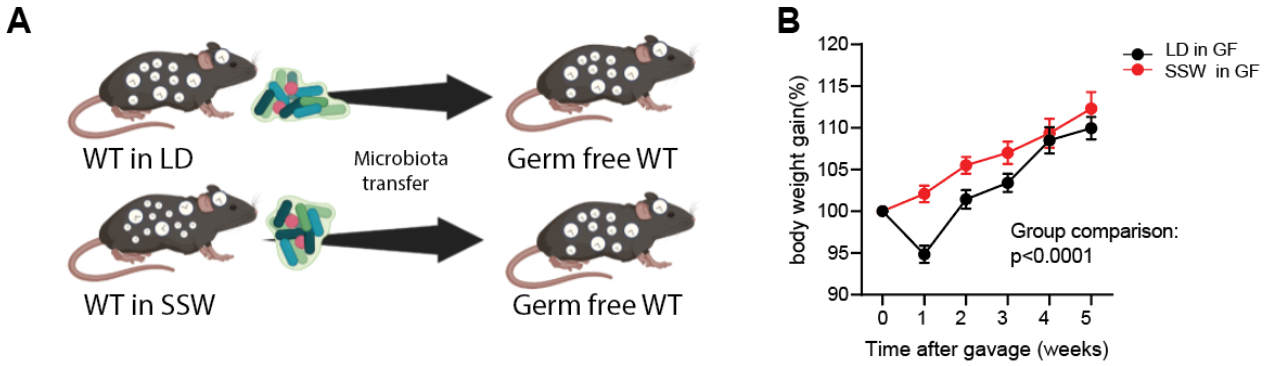

Figure 37: SSW microbiota induces weight gain
(A) Schematic illustration of cecal microbiota transplantation from donor mice under SSW and LD conditions (n = 4-5) to germ-free wild-type mice. (B) Normalized body weight over six weeks of recipient mice. Changes in body weight were assessed using two-way ANOVA. Red represents germ free (GF) mice receiving SSW microbiota, while black represents GF mice receiving LD microbiota. N = 12 mice/recipient group. Data are illustrated as mean ± SEM.

Interestingly, after six weeks of colonization, both SSW and LD recipients had similar body weights and similar weights for most organs, indicating temporary effects of arrhythmic microbiota on a rhythmic host (Suppl. Figure 4A). Notably, SSW-associated microbiota increased cecum weight and slightly increased plasma glucose, while no effect was observed in plasma triglycerides (Suppl. Figure 4B).

Previous reports showed that the gut microbiota and its derived products such as SCFAs and bile acids impact intestinal clock-gene expression (Leone, Gibbons et al. 2015, Tahara, Yamazaki et al. 2018). Therefore, we measured the expression of intestinal clock genes in SSW and LD recipients as well as in germ-free controls. Indeed, after six weeks of colonization, SSW-associated microbiota altered intestinal clock-gene expression (Figure 38). Although most examined clock genes in the proximal colon showed daytime-dependent expression in SSW and LD recipient groups, SSW-associated microbiota suppressed *per2* expression at ZT 13 and abolished *rev-erbα* daytime-dependent expression (Figure 38C). Similarly, *per2, dbp,* and *cry1* expression in the jejunum and *per2, dbp,* and *rev-erbα* expression in the cecum are suppressed at ZT 13 as a result of receiving SSW-associated microbiota (Figure 38A-B). Notably, mice receiving SSW-associated microbiota followed a similar trend of dampened time differences in intestinal clock-gene expression, as seen in germ-free control. These results point to the importance of microbial rhythmicity for intestinal clock functionalities and, consequently, gastrointestinal physiology.

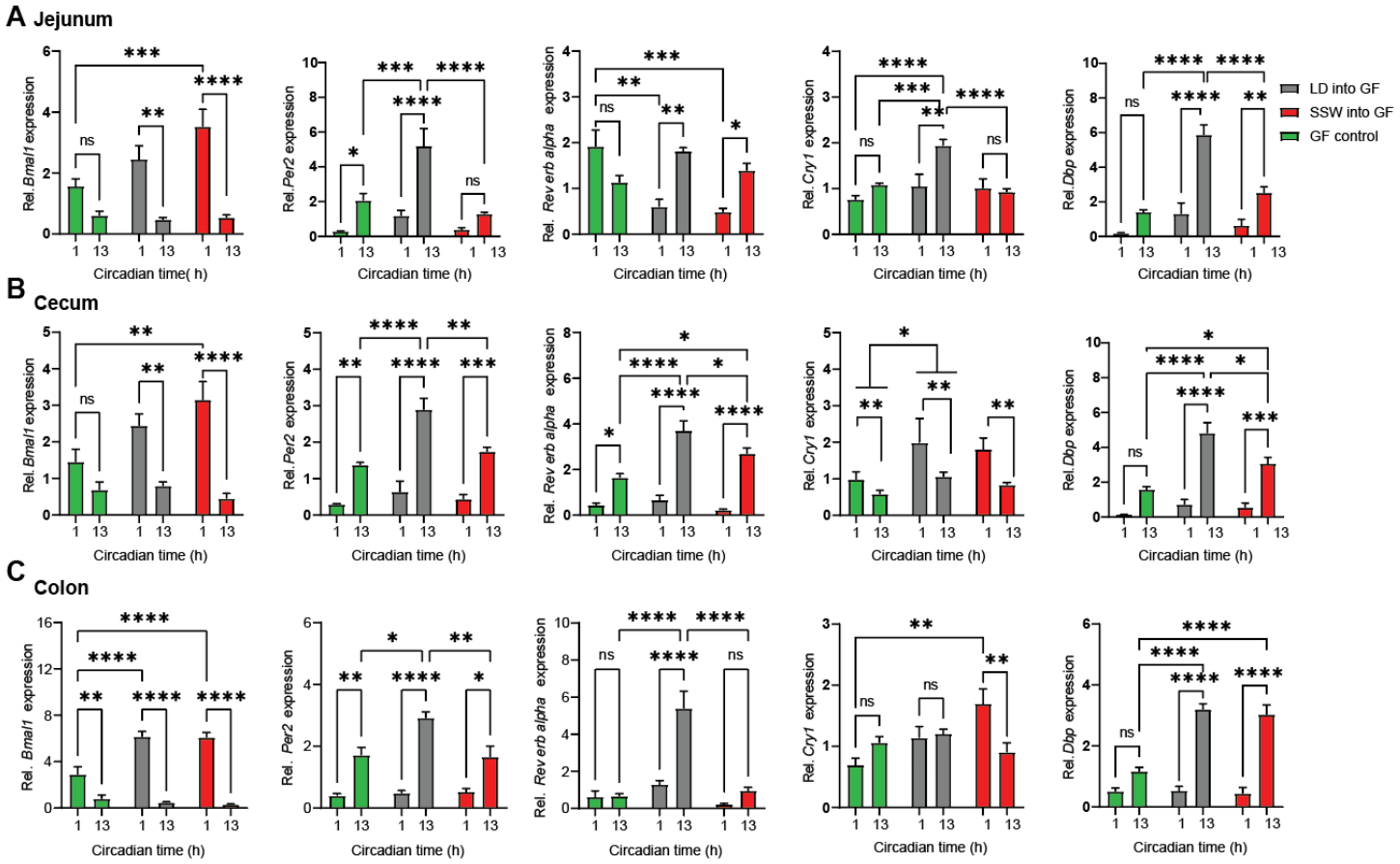

Figure 38: SSW-associated microbiota alters the gut clock

*Relative clock-gene expression in the jejunum(A), cecum(B), and proximal colon (C) of mice receiving SSW and LD microbiota and their germ free (GF) controls. Red represents GF mice receiving SSW-associated microbiota, while black represents GF mice receiving LD-associated microbiota and green color represents GF control. N = 5-6 mice/time point/group. Time and group differences were assessed by two-way ANOVA. Significance * = p-value ≤ 0.05, ** = p-value ≤ 0.01, *** = p-value ≤ 0.001, **** = p-value ≤ 0.0001. Data are illustrated as mean ± SEM.*

Next, we investigated the impact of SSW-associated microbiota on CCGs, especially genes related to fat and glucose metabolism such as *sglt1*, *glut2*, *fabp2*, *ifabp*, and *ppary* (Duszka, Picard et al. 2016, Lau, Marques et al. 2016, Lackey, Chen et al. 2020). We found suppressed expression in the jejunum of *sglt1* and *glut2*, glucose uptake regulators (Gouyon, Caillaud et al. 2003, Lehmann and Hornby 2016), as well as *fabp2*, important for lipid uptake (Lau, Marques et al. 2016) (Figure 39). Moreover, SSW-associated microbiota enhanced *ifabp* and *ppary* expression in the colon, important regulators for lipid and glucose metabolism (Figure 39) (Duszka, Picard et al. 2016, Oh, Visvalingam et al. 2019). In summary, our results

demonstrate the importance of gut clock–microbial rhythmicity crosstalk for host metabolic homeostasis.

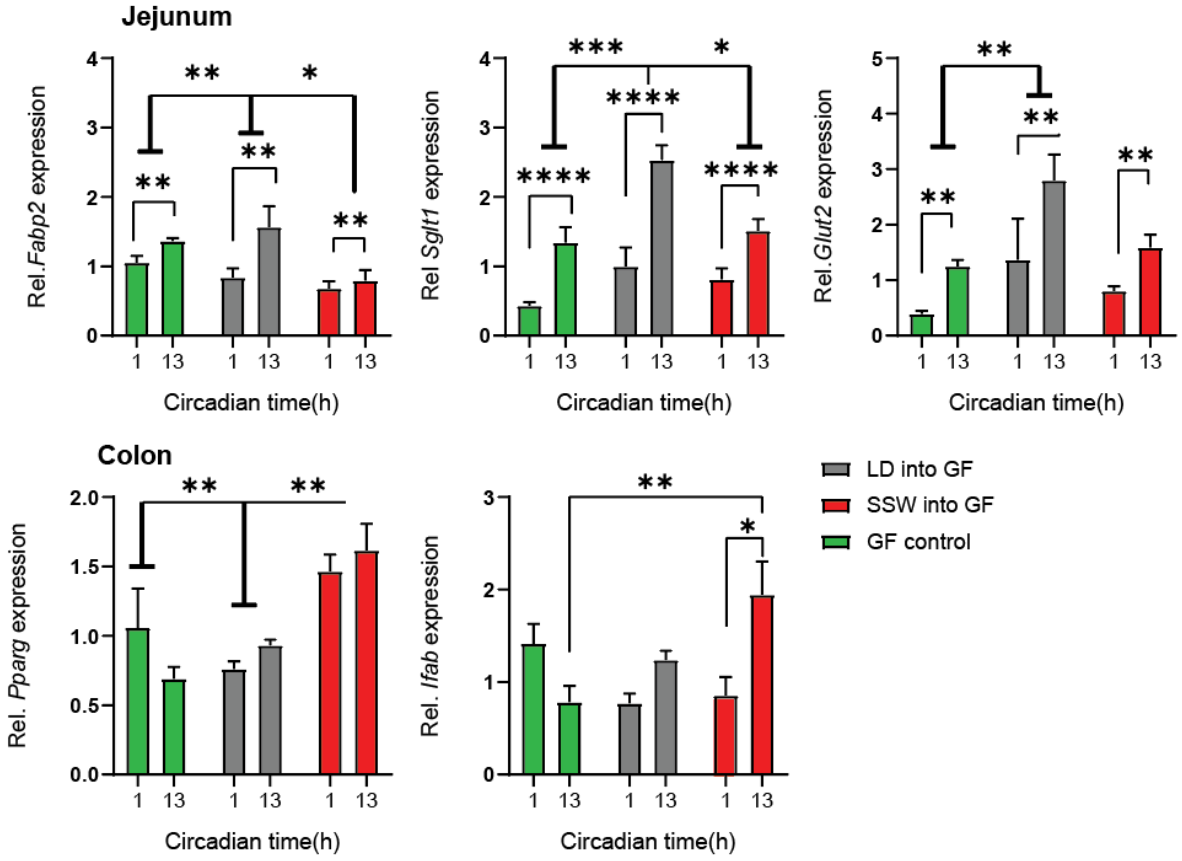

Figure 39: SSW alters intestinal metabolic genes expression

*Relative metabolic genes expression in the jejunum(A) and proximal colon (B) of mice receiving SSW and LD microbiota and their germ free (GF) controls. Red represents GF mice receiving SSW-associated microbiota, while black represents GF mice receiving LD-associated microbiota and green represents GF controls. N = 5-6 mice/time point/group. Time and group differences were assessed by two-way ANOVA. Significance * = p-value ≤ 0.05, ** = p-value ≤ 0.01, *** = p-value ≤ 0.001, **** = p-value ≤ 0.0001. Data are illustrated as mean ± SEM.*

5. Discussion

In the present work, we have investigated the factors driving microbial rhythmicity. Moreover, we provide mechanistic insights into the role of the gut microbiota during circadian disruption. First, we studied the impact of environmental factors on taxa rhythmicity. Although light and food represent the main *Zeitgebers* for the central and peripheral clocks, respectively, the withdrawal of these timing cues are found to slightly impact microbial rhythms, indicating their circadian nature. Second, using an intestinal-specific clock-deficient mouse model, we have pinpointed the intestinal clock as the primary driver of microbial rhythms. Next, we observed intestinal clock disruption in both genetic and environmental circadian disruption mouse models. A desynchronized intestinal clock disturbed rhythmic microbial composition and function. But what is the role of microbial rhythmicity? Germ-free transfer experiments reveal that circadian disruption-associated microbiota alters metabolic homeostasis and disrupts the intestinal clock. Therefore, our results demonstrate a bidirectional relationship between the host intestinal clock and microbial rhythms affecting host metabolic homeostasis.

5.1. Robust circadian rhythms despite environmental changes

The gut microbiota follows a diurnal rhythm in humans and mice (Thaiss, Zeevi et al. 2014, Zarrinpar, Chaix et al. 2014, Leone, Gibbons et al. 2015, Liang, Bushman et al. 2015, Reitmeier, Kiessling et al. 2020). Here, we demonstrate that most taxa oscillate not only diurnally but also in the absence of environmental timing cues such as light and food. Therefore, our results reveal for the first time the circadian nature of fecal microbial rhythmicity. These findings are in contrast to previous data showing attenuated cecal and ileal microbial rhythmicity in mice kept in darkness (Wu, Tang et al. 2018). Our results instead demonstrate robust circadian oscillations of the fecal microbiota in DD.

These different results might be explained by the use of different mouse lines, the alteration in microbial composition between animal facilities, and the variation of microbial niches across the gastrointestinal tract (Parker, Albeke et al. 2018, Anders, Moustafa et al. 2021). Furthermore, previous research frequently suggests the prominent role of feeding time on microbial rhythmicity (Thaiss, Zeevi et al. 2014, Zarrinpar, Chaix et al. 2014, Leone, Gibbons et al. 2015). By contrast, our data illustrate the robust microbial rhythmicity of dominant taxa in starvation conditions. These results accord with a previous report showing microbial oscillations in mice continually fed parenteral nutrition intravenously (Leone, Gibbons et al. 2015). Therefore, rhythmic food intake is not the driver of microbial oscillations.

Previous reports indicate rather a small percentage of rhythmic fecal microbiota in comparison with the high percentage found in our results (Thaiss, Zeevi et al. 2014, Leone, Gibbons et al. 2015). Our comparison analysis points to the different taxa classification methods as one of the main reasons for this discrepancy. However, other methodological differences might impact study comparability: for example, sampling intervals (our data: 3h/day, (Thaiss, Zeevi et al. 2014): 4h/day, (Wu, Tang et al. 2018): 6h/day), as well as amplicon sequencing of the 16S rRNA target region (our data: V3-V4, (Thaiss, Zeevi et al. 2014): V1-V2, (Wu, Tang et al. 2018): V4, (Voigt, Forsyth et al. 2014): V1-V3, (Deaver, Eum et al. 2018): Meta-transcriptome). In summary, the gut microbiota follows a circadian rhythm. The persistence of microbial rhythmicity under constant environmental conditions suggests host or bacterial circadian mechanisms driving microbial circadian oscillations.

5.2. The gut clock is the dominant driver of microbial rhythmicity

The host circadian system plays a role in microbial rhythmicity. For example, tissue-wide loss of *per1/2* or *bmal1* in mice abolishes taxa rhythmicity, e.g., *Lachnospiraceae, Lactobacillaceae,* and *Odoribacteraceae* (Thaiss, Zeevi et al. 2014, Liang, Bushman et al.

2015). Yet it is unclear which of a host's clocks drive microbial rhythms. Our results demonstrate a similar loss of microbial oscillations using an intestinal-specific loss of *bmal1*, pinpointing the gut clock as the driver of these rhythms. In fact, the lack of a functional intestinal clock disrupts microbial rhythms dramatically. For example, two-thirds of rhythmic taxa in our study became arrhythmic in the absence of a functional intestinal clock. This dominant role of the gut clock in driving taxa rhythmicity is further confirmed by the data obtained from experiments in normal LD conditions, and using relative and quantitative analysis.

It is notable that, despite the wide use of relative abundance in analyzing microbial composition, this might exaggerate microbial oscillations due to the masking effect of highly abundant taxa (Liang, Bushman et al. 2015). Indeed, relative and quantitative analyses did not yield identical results, highlighting the importance of both analyses for interpreting circadian microbiota composition. Notably, some of the few rhythmic taxa in *bmal1*$^{IEC-/-}$ mice lost their rhythmicity upon starvation. Some of these bacteria have previously been reported to be affected by food availability (Thaiss, Zeevi et al. 2014, Zarrinpar, Chaix et al. 2014). Importantly, although *bmal1*$^{IEC-/-}$ mice eat rhythmically, the loss of the intestinal clock abolished microbial rhythms. These data further prove the importance of the intestinal clock as the driver of microbial rhythms, in comparison with the modulatory effect of environmental factors (Figure 40).

This leads us to the question how the intestinal clock regulates microbial rhythms. Previous studies show rhythmic oscillations in various intestinal functions that impact host-microbe interaction, including microbial patterns of recognition, immune functions, nuclear receptors, aryl hydrocarbon receptors, mucus secretion, and antimicrobial peptide production (Mukherji, Kobiita et al. 2013, Kuang, Wang et al. 2019, Frazier, Kambal et al. 2020). Interestingly, the gut clock drives the rhythmic expression of genes involved in microbe-host crosstalk such as

ang4, *tlr2*, *muc2*, *hdac3*, and *nfil3* (Heddes, Altaha et al. 2021). For example, we found loss of *hdac3* and *tlr2* rhythmicity in *bmal1*$^{IEC-/-}$ mice; deletion of these genes disrupts microbial composition and intestinal homeostasis (Caricilli, Picardi et al. 2011, Alenghat, Osborne et al. 2013). Moreover, *muc2*, another gut-clock-controlled gene, alters gut microbiota: directly by providing mucin glycans to metabolize (Wu, Hashimoto-Hill et al. 2020), and indirectly through bacterial cross-feeding (Schroeder 2019). Although the gut clock controls several genes that affect microbiota composition, further research is required to fully understand the gut clock mechanism for driving microbial oscillations.

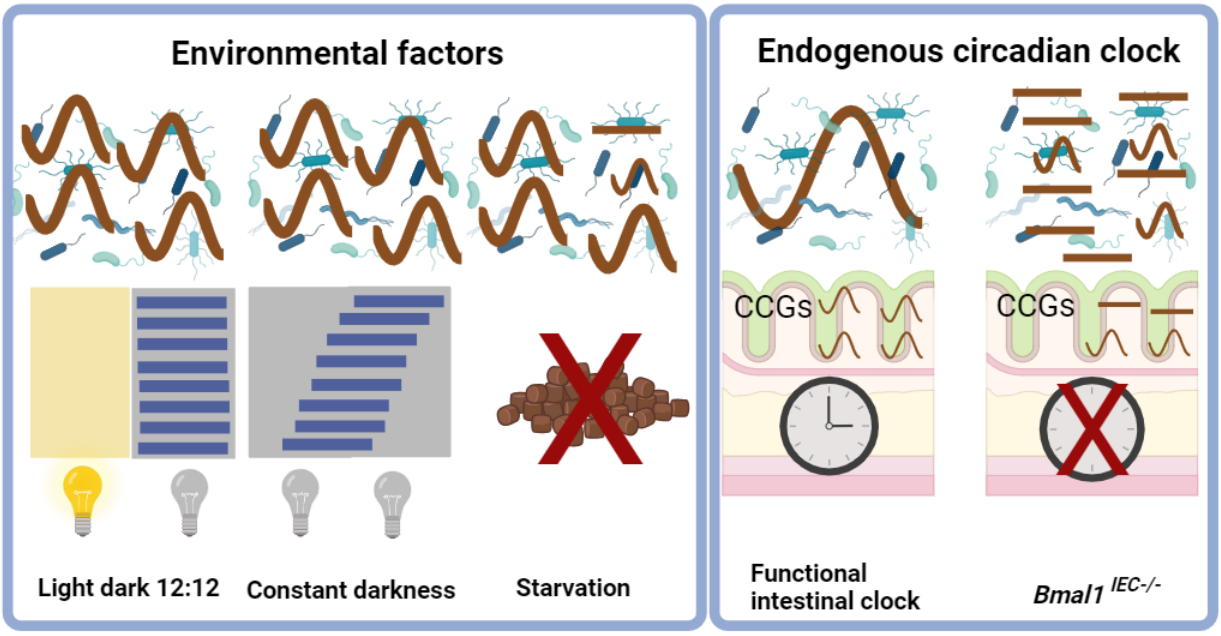

Figure 40: The gut clock drives microbial rhythmicity, in comparison with the modulatory effects of light and food.
Here, we summarize the impact of environmental factors and the intestinal clock on microbial rhythmicity. A cosine wave represents rhythmic oscillations, whereas a straight line represents arrhythmic fluctuation. The blue line represents activity. Yellow and grey shading illustrate light and dark phases, respectively.

5.3. Microbial rhythms are essential for host homeostasis

The gut microbiota is essential for host homeostasis (Turnbaugh, Ley et al. 2006, Coleman, Lobner et al. 2018, Lloyd-Price, Arze et al. 2019, Reitmeier, Kiessling et al. 2020). Our results

show that the gut clock controls rhythmic SCFA-fermenting taxa such as *Odoribacteraceae*, *Lachnospiraceae*, and *Ruminococcaceae*, lactate acid-producing taxa such as *Lactobacillaceae*, and mucus foragers, *Lachnospiraceae*, *Muribaculaceae*, and *Rickenellaceae* (Carr, Chill et al. 2002, Biddle, Stewart et al. 2013, Tailford, Crost et al. 2015). Moreover, we found that the gut clock regulates the rhythmicity of bile acid-converting taxa, including *Ruminococcus* and *Lactobacillus* (Gerard 2013). Consequently, the gut clock is likely to influence microbial functions. Indeed, the loss of the gut clock alters the abundance and abolishes the rhythmicity of microbial pathways related to the metabolism of amino acids, fatty acids and sugar, the biosynthesis of vitamins and the fermentation of SCFAs. Interestingly, many gut clock-controlled pathways lose rhythmicity in obesity and diabetes, pointing to the functional relevance of microbial rhythmicity (Thaiss, Zeevi et al. 2014, Beli, Prabakaran et al. 2019, Reitmeier, Kiessling et al. 2020). In fact, a recent report links arrhythmic microbiota to obesity and the development of type 2 diabetes (Reitmeier, Kiessling et al. 2020). Moreover, germ-free transfer experiments demonstrate the importance of rhythmic microbiota for host metabolic and intestinal homeostasis (Heddes, Altaha et al. 2022). Although microbial rhythms are indispensable for the host's homeostasis, further research should address the role of microbial rhythmicity in various microbiota-associated diseases.

5.4. Environmental and genetic circadian disruption alter intestinal clock functionalities

Microbial dysbiosis and circadian disruption promote various metabolic diseases (Thaiss, Zeevi et al. 2014, Voigt, Forsyth et al. 2014, Metwaly, Reitmeier et al. 2022). Yet little is known about the link between circadian disruption and the gut microbiota in metabolic abnormalities. Using genetic and environmental circadian disruption models, we can shed light on the role of the gut microbiota in metabolic abnormalities during circadian disruption.

The lack of the central clock desynchronizes peripheral clocks such as those in the liver, heart, pancreas, and epididymal white adipose tissue (eWAT) (Husse, Leliavski et al. 2014, Kolbe, Leinweber et al. 2019). According to our results, the absence of the central clock further disrupts the intestinal clock. Moreover, we also observed a disrupted intestinal clock in wild-type mice in SSW conditions. This accord with a previous report showing altered colonic clock-gene expression in mice exposed to chronic jet lag (Thaiss, Zeevi et al. 2014).

Notably, distinct sections of the gastrointestinal circadian system respond differently to circadian disruption. These results might be explained by the clock genes' temporal phase gradient through the gut craniocaudal axis (Polidarova, Sotak et al. 2009). Although both environmental and genetic models of circadian disruption possess an altered intestinal clock, differences in intestinal clock-gene expression patterns between models are noted. This discrepancy may be a result of different food intake behaviors between models. Our results show arrhythmic food intake in *bmal1*$^{SCNfl/-}$ mice in DD, whereas SSW shifts food intake behavior without impacting its rhythmicity (Zhong, Li et al. 2019). Importantly, intestinal clock disruption is common in environmental and genetic circadian disruptions.

5.5. Arrhythmic gut microbiota and circadian disruption

The gut clock drives the majority of microbial rhythms. Consequently, the lack of a functional intestinal clock may, upon circadian disruption, alter microbial rhythmicity. Indeed, our results demonstrate the loss of rhythmic microbiota in both environmental and genetic circadian disruption models. Similar to intestinal clock-deficient mice, many taxa lose their rhythmicity in mice undergoing SSW as well as in *bmal1*$^{SCNfl/-}$ mice. These include taxa belonging to the families *Muribaculaceae, Ruminococcaceae,* and *Rikenellaceae,* and the genera *Alistipes* and *Lactobacillus*. Notably, genetic disruption of the central clock has a more pronounced effect

on microbial rhythmicity than SSW. For example, losing central clock functionalities disrupts the rhythmicity of major phyla and families.

Despite the loss of substantial microbial rhythms in SSW, the phylum Bacteroidetes and a reasonable number of bacteria remain rhythmic, but with an altered phase. This discrepancy between models could be explained by the difference in food-intake behavior. In fact, feeding time controls the phase of some taxa belonging to *Lactobacillus, Alistipes,* and *Bacteroides* (Thaiss, Zeevi et al. 2014, Heddes, Altaha et al. 2021). Moreover, our data from mice under starvation conditions show that rhythmic food intake drives the rhythm of some bacterial taxa. Therefore, some taxa oscillate rhythmicity with an altered phase in SSW, which is likely the result of advanced rhythmic food intake behaviors. Nevertheless, SSW abolishes the rhythmicity of many taxa, similar to the genetic loss of the central and intestinal clocks. Therefore, an altered gut clock during environmental and genetic circadian disruption is likely responsible for microbial arrhythmicity.

5.6. Arrhythmic gut microbiota promotes metabolic abnormalities

A recent report links arrhythmic microbiota to obesity and type 2 diabetes development in humans (Reitmeier, Kiessling et al. 2020), suggesting a causative role of microbial rhythmicity in metabolic diseases. Indeed, germ-free transfer experiments provide direct evidence of the role of microbial rhythmicity in metabolic health. For example, fecal microbiota transferred from human donors experiencing jet lag have been shown to promote an obesity-associated phenotype in germ-free recipient mice (Ridaura, Faith et al. 2013, Thaiss, Zeevi et al. 2014, Voigt, Forsyth et al. 2014). Moreover, in another study, the transfer of arrhythmic microbiota from *bmal1*$^{IEC-/-}$ mice disrupted germ-free recipients' intestinal homeostasis (Heddes, Altaha et al. 2022). In accordance with these studies, we found that microbiota transferred from mice undergoing SSW induced weight gain in germ-free recipients. These results accord with the

previous reports showing an increase in body weight after receiving fecal microbiota from mice undergoing jet lag (Thaiss, Zeevi et al. 2014). Overall, microbial rhythmicity is a critical factor for host metabolic homeostasis.

5.7. Circadian disruption alters gastrointestinal homeostasis

Gastrointestinal metabolism is strongly affected by the gut microbiota and its derived products such as SCFAs and bile acids (Rios-Covian, Ruas-Madiedo et al. 2016, Just, Mondot et al. 2018). Our results demonstrate the loss of rhythmic microbial functionalities during environmental and genetic circadian disruption, especially pathways related to SCFA fermentation as well as the metabolism of fatty acids, amino acids, and sugar. Moreover, targeted metabolite analyses confirm the loss of SCFAs' and bile acids' rhythmicity upon genetic circadian disruption in *bmal1*$^{SCNfl/-}$ mice. For example, circadian disruption resulted in arrhythmic propionic acid and acetic acid. Both SCFAs are crucial for fat and glucose metabolism, in addition to their role in preventing insulin resistance and diet-induced obesity (Lin, Frassetto et al. 2012). Moreover, circadian disruption altered taurine-conjugated bile acids and secondary bile acid abundance and rhythmicity, disturbing glucose and lipid homeostasis (Dawson and Karpen 2015).

What are the consequences of losing bacterial metabolite rhythmicity following circadian disruption? Considering the essential role of SCFAs and bile acids in sugar and fatty acid metabolism as well as host metabolism (Nieuwdorp, Gilijamse et al. 2014, Wahlström, Sayin et al. 2016), their loss of rhythmicity might disrupt host metabolic homeostasis. In fact, both genetic and environmental circadian disruptions lead to the development of obesity-related phenotypes (Thaiss, Zeevi et al. 2014, Kolbe, Leinweber et al. 2019). For example, *bmal1*$^{SCNfl/-}$ mice show a significant increase in body weight and impaired glucose metabolism following multiple weeks in DD (Kolbe, Leinweber et al. 2019). Interestingly, we found a loss of

microbial rhythms and subsequent functionalities involved in lipid and glucose metabolism in *bmal1*$^{SCNfl/-}$ mice following their second day in DD, preceding the onset of the obesity phenotype in these mice. Therefore, loss of microbial rhythmicity might be an early event that promotes the development of obesity, potentially through losing bacterial byproduct rhythmicity (Kolbe, Leinweber et al. 2019).

5.8. Arrhythmic gut microbiota disrupts intestinal clock functionalities

How does microbial arrhythmicity disturb the host's metabolic homeostasis? Our results show that SSW-associated microbiota promotes weight gain, slightly induces plasma glucose levels, and directly impacts the host's intestinal clock functions. In particular, intestinal clock disruption in SSW donors is also evident in germ-free recipients. For example, both donor and recipient mice have suppressed *rev-erbα* expression in the colon and *dbp* expression in the jejunum, indicating a microbial role in transferring the circadian phenotype.

The intestinal clock controls various functions by regulating tissue-specific CCGs such as *muc2, tlr2, hdac3,* and *nfil3* (Zhang, Lahens et al. 2014, Kawai, Kinoshita et al. 2019, Chen, Yu et al. 2021, Martchenko, Martchenko et al. 2021, Heddes, Altaha et al. 2022). Accordingly, we found that disrupted intestinal clocks in recipient mice altered clock control genes involved in fat and glucose metabolism such as *glut2, ppary, sglt1, ifabp,* and *fabp2*. (Gouyon, Caillaud et al. 2003, Duszka, Picard et al. 2016). Our results suggest a bidirectional relationship between microbial rhythms and the intestinal clock in controlling tissue homeostasis. Indeed, bacterial byproducts such as SCFAs and bile acids directly affect intestinal clock rhythmicity and host metabolic response (Govindarajan, MacSharry et al. 2016, Tahara, Yamazaki et al. 2018, Segers, Desmet et al. 2019, Desmet, Thijs et al. 2021).

In summary, circadian disruption desynchronizes the intestinal clock, abolishing microbial rhythmicity. The arrhythmic microbiota further disrupts the host's intestinal clock and

metabolic homeostasis. Together, our data provide for the first time mechanistic insights into the microbial-dependent metabolic phenotype observed in circadian disruption (Figure 41).

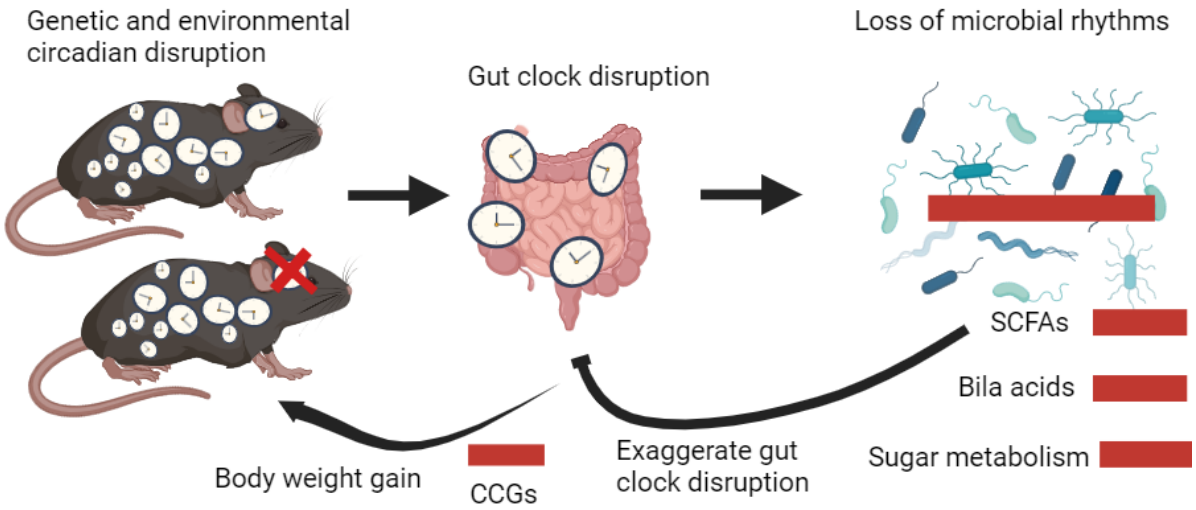

Figure 41: Bidirectional relationship between the intestinal clock and rhythmic microbiota

Closing remarks

In this work, we explore the origin of gut microbiota oscillations. In line with current literature, our data showed diurnal oscillations of the gut microbiota. Importantly, we also provide the first evidence of the circadian origin of these oscillations, identifying environmental signals as mere modulators of microbial rhythms. Moreover, we demonstrate that the intestinal clock drives the majority of microbial rhythms. Although the lack of the intestinal clock abolishes such rhythms, some taxa (~30%) manage to sustain their rhythmicity, which might result from rhythmic food intake, and the LD cycle. Indeed, environmental signals, rhythmic food intake and the LD cycle, control the rhythmicity of some microbial taxa. Notably, a few taxa (~15%) oscillate despite the absence of the aforementioned factors (gut clock, rhythmic food intake, and the LD cycle). Therefore, future research should investigate other factors that may impact microbial rhythmicity such as microbial intrinsic factors and other peripheral clocks.

In this dissertation, we also shed light on the impact of circadian disruption on the intestinal clock and microbiota rhythmicity. We show that genetic and environmental circadian disruptions desynchronize peripheral clocks, especially the intestinal clock. Moreover, we have observed a loss of microbial rhythmicity in both models, thereby reinforcing the role of the intestinal clock in driving microbial rhythms. Although circadian disruption mouse models possess different microbial ecosystems, both share a similar loss of rhythmic microbial functionalities.

Finally, the microbial colonization experiment reveals a bidirectional relationship between the intestinal clock and oscillating taxa, and demonstrates its importance for the host's metabolic health. Several future directions for research could follow from our findings. For example, it would be useful to explore the role of microbial rhythmicity on microbiota-dependent disease development. Future studies could also target the peripheral clocks, including the intestinal

clock, to prevent circadian disruption-induced metabolic abnormalities, e.g., by restricting feeding. In summary, we highlight the relevance of investigating the role of the intestinal clock in driving microbial rhythmicity for host metabolic homeostasis and disease development.

Reference

Akashi, M. and T. Takumi (2005). "The orphan nuclear receptor RORalpha regulates circadian transcription of the mammalian core-clock Bmal1." Nat Struct Mol Biol **12**(5): 441-448.

AL-Taha, B. M., J. Wadi and A. A. Shehabi (2018). "Probiotics: Past, Present and Future Challenges." The International Arabic Journal of Antimicrobial Agents **8**(1).

Alenghat, T., L. C. Osborne, S. A. Saenz, D. Kobuley, C. G. Ziegler, S. E. Mullican, I. Choi, S. Grunberg, R. Sinha, M. Wynosky-Dolfi, A. Snyder, P. R. Giacomin, K. L. Joyce, T. B. Hoang, M. Bewtra, I. E. Brodsky, G. F. Sonnenberg, F. D. Bushman, K. J. Won, M. A. Lazar and D. Artis (2013). "Histone deacetylase 3 coordinates commensal-bacteria-dependent intestinal homeostasis." Nature **504**(7478): 153-157.

Anders, J. L., M. A. M. Moustafa, W. M. A. Mohamed, T. Hayakawa, R. Nakao and I. Koizumi (2021). "Comparing the gut microbiome along the gastrointestinal tract of three sympatric species of wild rodents." Sci Rep **11**(1): 19929.

Aschoff, J. (1960). "Exogenous and endogenous components in circadian rhythms." Cold Spring Harb Symp Quant Biol **25**: 11-28.

Babicki, S., D. Arndt, A. Marcu, Y. Liang, J. R. Grant, A. Maciejewski and D. S. Wishart (2016). "Heatmapper: web-enabled heat mapping for all." Nucleic Acids Res **44**(W1): W147-153.

Beli, E., S. Prabakaran, P. Krishnan, C. Evans-Molina and M. B. Grant (2019). "Loss of Diurnal Oscillatory Rhythms in Gut Microbiota Correlates with Changes in Circulating Metabolites in Type 2 Diabetic db/db Mice." Nutrients **11**(10).

Biddle, A., L. Stewart, J. Blanchard and S. Leschine (2013). "Untangling the Genetic Basis of Fibrolytic Specialization by Lachnospiraceae and Ruminococcaceae in Diverse Gut Communities." Diversity **5**(3): 627-640.

Bisanz, J. E., V. Upadhyay, J. A. Turnbaugh, K. Ly and P. J. Turnbaugh (2019). "Meta-Analysis Reveals Reproducible Gut Microbiome Alterations in Response to a High-Fat Diet." Cell Host Microbe **26**(2): 265-272 e264.

Bowers, S. J., F. Vargas, A. Gonzalez, S. He, P. Jiang, P. C. Dorrestein, R. Knight, K. P. Wright, Jr., C. A. Lowry, M. Fleshner, M. H. Vitaterna and F. W. Turek (2020). "Repeated sleep disruption in mice leads to persistent shifts in the fecal microbiome and metabolome." PLoS One **15**(2): e0229001.

Browne, H. P., Y. Shao and T. D. Lawley (2022). "Mother-infant transmission of human microbiota." Curr Opin Microbiol **69**: 102173.

Bunger, M. K., L. D. Wilsbacher, S. M. Moran, C. Clendenin, L. A. Radcliffe, J. B. Hogenesch, M. C. Simon, J. S. Takahashi and C. A. Bradfield (2000). "Mop3 is an essential component of the master circadian pacemaker in mammals." Cell **103**(7): 1009-1017.

Caricilli, A. M., P. K. Picardi, L. L. de Abreu, M. Ueno, P. O. Prada, E. R. Ropelle, S. M. Hirabara, A. Castoldi, P. Vieira, N. O. Camara, R. Curi, J. B. Carvalheira and M. J. Saad (2011). "Gut microbiota is a key modulator of insulin resistance in TLR 2 knockout mice." PLoS Biol **9**(12): e1001212.

Carr, F. J., D. Chill and N. Maida (2002). "The lactic acid bacteria: a literature survey." Crit Rev Microbiol **28**(4): 281-370.

Cash, H. L., C. V. Whitham, C. L. Behrendt and L. V. Hooper (2006). "Symbiotic bacteria direct expression of an intestinal bactericidal lectin." Science **313**(5790): 1126-1130.

Castanon-Cervantes, O., M. Wu, J. C. Ehlen, K. Paul, K. L. Gamble, R. L. Johnson, R. C. Besing, M. Menaker, A. T. Gewirtz and A. J. Davidson (2010). "Dysregulation of inflammatory responses by chronic circadian disruption." J Immunol **185**(10): 5796-5805.

Chen, X., F. Yu, X. Guo, C. Su, S. S. Li and B. Wu (2021). "Clock gene Bmal1 controls diurnal rhythms in expression and activity of intestinal carboxylesterase 1." J Pharm Pharmacol **73**(1): 52-59.

Claesson, M. J., S. Cusack, O. O'Sullivan, R. Greene-Diniz, H. de Weerd, E. Flannery, J. R. Marchesi, D. Falush, T. Dinan, G. Fitzgerald, C. Stanton, D. van Sinderen, M. O'Connor, N. Harnedy, K. O'Connor, C. Henry, D. O'Mahony, A. P. Fitzgerald, F. Shanahan, C. Twomey, C. Hill, R. P. Ross and P. W. O'Toole (2011). "Composition, variability, and temporal stability of the intestinal microbiota of the elderly." Proc Natl Acad Sci U S A **108 Suppl 1**(Suppl 1): 4586-4591.

Clarke, L. L. (2009). "A guide to Ussing chamber studies of mouse intestine." Am J Physiol Gastrointest Liver Physiol **296**(6): G1151-1166.

Clausen, M. R. and P. B. Mortensen (1995). "Kinetic studies on colonocyte metabolism of short chain fatty acids and glucose in ulcerative colitis." Gut **37**(5): 684-689.

Codoner-Franch, P. and M. Gombert (2018). "Circadian rhythms in the pathogenesis of gastrointestinal diseases." World J Gastroenterol **24**(38): 4297-4303.

Coleman, O. I. and D. Haller (2017). "Bacterial Signaling at the Intestinal Epithelial Interface in Inflammation and Cancer." Front Immunol **8**: 1927.

Coleman, O. I., E. M. Lobner, S. Bierwirth, A. Sorbie, N. Waldschmitt, E. Rath, E. Berger, I. Lagkouvardos, T. Clavel, K. D. McCoy, A. Weber, M. Heikenwalder, K. P. Janssen and D. Haller (2018). "Activated ATF6 Induces Intestinal Dysbiosis and Innate Immune Response to Promote Colorectal Tumorigenesis." Gastroenterology **155**(5): 1539-1552 e1512.

Cummings, J. H., E. R. Beatty, S. M. Kingman, S. A. Bingham and H. N. Englyst (1996). "Digestion and physiological properties of resistant starch in the human large bowel." Br J Nutr **75**(5): 733-747.

Cummings, J. H., E. W. Pomare, W. J. Branch, C. P. Naylor and G. T. Macfarlane (1987). "Short chain fatty acids in human large intestine, portal, hepatic and venous blood." Gut **28**(10): 1221-1227.

Damiola, F., N. Le Minh, N. Preitner, B. Kornmann, F. Fleury-Olela and U. Schibler (2000). "Restricted feeding uncouples circadian oscillators in peripheral tissues from the central pacemaker in the suprachiasmatic nucleus." Genes Dev **14**(23): 2950-2961.

Davidson, A. J., M. T. Sellix, J. Daniel, S. Yamazaki, M. Menaker and G. D. Block (2006). "Chronic jet-lag increases mortality in aged mice." Curr Biol **16**(21): R914-916.

Dawson, P. A. and S. J. Karpen (2015). "Intestinal transport and metabolism of bile acids." J Lipid Res **56**(6): 1085-1099.

de la Cuesta-Zuluaga, J., N. T. Mueller, R. Alvarez-Quintero, E. P. Velasquez-Mejia, J. A. Sierra, V. Corrales-Agudelo, J. A. Carmona, J. M. Abad and J. S. Escobar (2018). "Higher Fecal Short-Chain Fatty Acid Levels Are Associated with Gut Microbiome Dysbiosis, Obesity, Hypertension and Cardiometabolic Disease Risk Factors." Nutrients **11**(1).

De Vadder, F., P. Kovatcheva-Datchary, D. Goncalves, J. Vinera, C. Zitoun, A. Duchampt, F. Backhed and G. Mithieux (2014). "Microbiota-generated metabolites promote metabolic benefits via gut-brain neural circuits." Cell **156**(1-2): 84-96.

Deaver, J. A., S. Y. Eum and M. Toborek (2018). "Circadian Disruption Changes Gut Microbiome Taxa and Functional Gene Composition." Front Microbiol **9**: 737.

den Besten, G., K. Lange, R. Havinga, T. H. van Dijk, A. Gerding, K. van Eunen, M. Muller, A. K. Groen, G. J. Hooiveld, B. M. Bakker and D. J. Reijngoud (2013). "Gut-derived short-chain fatty acids are vividly assimilated into host carbohydrates and lipids." Am J Physiol Gastrointest Liver Physiol **305**(12): G900-910.

den Besten, G., K. van Eunen, A. K. Groen, K. Venema, D. J. Reijngoud and B. M. Bakker (2013). "The role of short-chain fatty acids in the interplay between diet, gut microbiota, and host energy metabolism." J Lipid Res **54**(9): 2325-2340.

Desmet, L., T. Thijs, A. Segers, K. Verbeke and I. Depoortere (2021). "Chronodisruption by chronic jetlag impacts metabolic and gastrointestinal homeostasis in male mice." Acta Physiol (Oxf) **233**(4): e13703.

Dibner, C., U. Schibler and U. Albrecht (2010). "The mammalian circadian timing system: organization and coordination of central and peripheral clocks." Annu Rev Physiol **72**: 517-549.

Duguay, D. and N. Cermakian (2009). "The crosstalk between physiology and circadian clock proteins." Chronobiol Int **26**(8): 1479-1513.

Dunlap, J. C. (1999). "Molecular bases for circadian clocks." Cell **96**(2): 271-290.

Duszka, K., A. Picard, S. Ellero-Simatos, J. Chen, M. Defernez, E. Paramalingam, A. Pigram, L. Vanoaica, C. Canlet, P. Parini, A. Narbad, H. Guillou, B. Thorens and W. Wahli (2016). "Intestinal PPARgamma signalling is required for sympathetic nervous system activation in response to caloric restriction." Sci Rep **6**: 36937.

Edgar, R. C. (2010). "Search and clustering orders of magnitude faster than BLAST." Bioinformatics **26**(19): 2460-2461.

Edgar, R. C. (2016). "UNOISE2: improved error-correction for Illumina 16S and ITS amplicon sequencing." bioRxiv: 081257.

Edgar, R. C., B. J. Haas, J. C. Clemente, C. Quince and R. Knight (2011). "UCHIME improves sensitivity and speed of chimera detection." Bioinformatics **27**(16): 2194-2200.

Fan, Y. and O. Pedersen (2021). "Gut microbiota in human metabolic health and disease." Nat Rev Microbiol **19**(1): 55-71.

Forman, R. A., M. L. deSchoolmeester, R. J. Hurst, S. H. Wright, A. D. Pemberton and K. J. Else (2012). "The goblet cell is the cellular source of the anti-microbial angiogenin 4 in the large intestine post Trichuris muris infection." PLoS One **7**(9): e42248.

Frazier, K., A. Kambal, E. A. Zale, J. F. Pierre, N. Hubert, S. Miyoshi, J. Miyoshi, D. Ringus, D. Harris and K. Yang (2020). "High fat diet disrupts diurnal interactions between REG3g and small intestinal gut microbes resulting in metabolic dysfunction." bioRxiv.

Fulde, M., F. Sommer, B. Chassaing, K. van Vorst, A. Dupont, M. Hensel, M. Basic, R. Klopfleisch, P. Rosenstiel, A. Bleich, F. Backhed, A. T. Gewirtz and M. W. Hornef (2018). "Neonatal selection by Toll-like receptor 5 influences long-term gut microbiota composition." Nature **560**(7719): 489-493.

Gensollen, T., S. S. Iyer, D. L. Kasper and R. S. Blumberg (2016). "How colonization by microbiota in early life shapes the immune system." Science **352**(6285): 539-544.

Gerard, P. (2013). "Metabolism of cholesterol and bile acids by the gut microbiota." Pathogens **3**(1): 14-24.

Godon, J. J., E. Zumstein, P. Dabert, F. Habouzit and R. Moletta (1997). "Molecular microbial diversity of an anaerobic digestor as determined by small-subunit rDNA sequence analysis." Appl Environ Microbiol **63**(7): 2802-2813.

Gordon, H. A., E. Bruckner-Kardoss, T. E. Staley, M. Wagner and B. S. Wostmann (1966). "CHARACTERISTICS OF THE GERMFREE RAT." Cells Tissues Organs **64**(1-3): 367-389.

Gouyon, F., L. Caillaud, V. Carriere, C. Klein, V. Dalet, D. Citadelle, G. L. Kellett, B. Thorens, A. Leturque and E. Brot-Laroche (2003). "Simple-sugar meals target GLUT2 at enterocyte apical membranes to improve sugar absorption: a study in GLUT2-null mice." J Physiol **552**(Pt 3): 823-832.

Govindarajan, K., J. MacSharry, P. G. Casey, F. Shanahan, S. A. Joyce and C. G. Gahan (2016). "Unconjugated Bile Acids Influence Expression of Circadian Genes: A Potential Mechanism for Microbe-Host Crosstalk." PLoS One **11**(12): e0167319.

Green, D. J. and R. Gillette (1982). "Circadian rhythm of firing rate recorded from single cells in the rat suprachiasmatic brain slice." Brain Res **245**(1): 198-200.

Guarner, F. and J. R. Malagelada (2003). "Gut flora in health and disease." Lancet **361**(9356): 512-519.

Gustafsson, B. E., T. Midtvedt and K. Strandberg (1970). "Effects of microbial contamination on the cecum enlargement of germfree rats." Scand J Gastroenterol **5**(4): 309-314.

Han, J., K. Lin, C. Sequeira and C. H. Borchers (2015). "An isotope-labeled chemical derivatization method for the quantitation of short-chain fatty acids in human feces by liquid chromatography-tandem mass spectrometry." Anal Chim Acta **854**: 86-94.

Hardbower, D. M., M. Asim, T. Murray-Stewart, R. A. Casero, Jr., T. Verriere, N. D. Lewis, R. Chaturvedi, M. B. Piazuelo and K. T. Wilson (2016). "Arginase 2 deletion leads to enhanced M1 macrophage

activation and upregulated polyamine metabolism in response to Helicobacter pylori infection." Amino Acids **48**(10): 2375-2388.

Heddes, M., B. Altaha, Y. Niu, S. Reitmeier, K. Kleigrewe, D. Haller and S. Kiessling (2021). "The intestinal circadian clock drives microbial rhythmicity to maintain gastrointestinal homeostasis." bioRxiv: 2021.2010.2018.464061.

Heddes, M., B. Altaha, Y. Niu, S. Reitmeier, K. Kleigrewe, D. Haller and S. Kiessling (2022). "The intestinal clock drives the microbiome to maintain gastrointestinal homeostasis." Nature Communications **13**(1): 6068.

Hoogerwerf, W. A. (2010). "Role of clock genes in gastrointestinal motility." Am J Physiol Gastrointest Liver Physiol **299**(3): G549-555.

Horowitz, R. E., H. Bauer, F. Paronetto, G. D. Abrams, K. C. Watkins and H. Popper (1964). "The Response of the Lymphatic Tissue to Bacterial Antigen. Studies in Germfree Mice." Am J Pathol **44**: 747-761.

Hughes, M. E., J. B. Hogenesch and K. Kornacker (2010). "JTK_CYCLE: an efficient nonparametric algorithm for detecting rhythmic components in genome-scale data sets." J Biol Rhythms **25**(5): 372-380.

Husse, J., A. Leliavski, A. H. Tsang, H. Oster and G. Eichele (2014). "The light-dark cycle controls peripheral rhythmicity in mice with a genetically ablated suprachiasmatic nucleus clock." FASEB J **28**(11): 4950-4960.

Husse, J., X. Zhou, A. Shostak, H. Oster and G. Eichele (2011). "Synaptotagmin10-Cre, a driver to disrupt clock genes in the SCN." J Biol Rhythms **26**(5): 379-389.

Inagaki, T., A. Moschetta, Y.-K. Lee, L. Peng, G. Zhao, M. Downes, R. T. Yu, J. M. Shelton, J. A. Richardson, J. J. Repa, D. J. Mangelsdorf and S. A. Kliewer (2006). "Regulation of antibacterial defense in the small intestine by the nuclear bile acid receptor." Proceedings of the National Academy of Sciences **103**(10): 3920-3925.

Jud, C., I. Schmutz, G. Hampp, H. Oster and U. Albrecht (2005). "A guideline for analyzing circadian wheel-running behavior in rodents under different lighting conditions." Biol Proced Online **7**: 101-116.

Just, S., S. Mondot, J. Ecker, K. Wegner, E. Rath, L. Gau, T. Streidl, G. Hery-Arnaud, S. Schmidt, T. R. Lesker, V. Bieth, A. Dunkel, T. Strowig, T. Hofmann, D. Haller, G. Liebisch, P. Gerard, S. Rohn, P. Lepage and T. Clavel (2018). "The gut microbiota drives the impact of bile acids and fat source in diet on mouse metabolism." Microbiome **6**(1): 134.

Kaczmarczyk, O., A. Dabek-Drobny, M. Wozniakiewicz, P. Pasko, J. Dobrowolska-Iwanek, A. Wozniakiewicz, A. Targosz, A. Ptak-Belowska, A. Piatek-Guziewicz, K. Wcislo, P. Zagrodzki and M. Zwolinska-Wcislo (2022). "Association between fecal levels of Short-Chain Fatty Acids and serum Pro- and Anti-Inflammatory Cytokines in patients with Inflammatory Bowel Disease." Folia Med Cracov **62**(1): 43-55.

Kawai, M., S. Kinoshita, M. Yamazaki, K. Yamamoto, C. J. Rosen, S. Shimba, K. Ozono and T. Michigami (2019). "Intestinal clock system regulates skeletal homeostasis." JCI Insight **4**(5).

Kennedy, E. A., K. Y. King and M. T. Baldridge (2018). "Mouse Microbiota Models: Comparing Germ-Free Mice and Antibiotics Treatment as Tools for Modifying Gut Bacteria." Front Physiol **9**: 1534.

Keubler, L. M., M. Buettner, C. Hager and A. Bleich (2015). "A Multihit Model: Colitis Lessons from the Interleukin-10-deficient Mouse." Inflamm Bowel Dis **21**(8): 1967-1975.

Kiessling, S., G. Dubeau-Laramee, H. Ohm, N. Labrecque, M. Olivier and N. Cermakian (2017). "The circadian clock in immune cells controls the magnitude of Leishmania parasite infection." Sci Rep **7**(1): 10892.

Kiessling, S., G. Eichele and H. Oster (2010). "Adrenal glucocorticoids have a key role in circadian resynchronization in a mouse model of jet lag." J Clin Invest **120**(7): 2600-2609.

Ko, F. C., S. B. Jochum, B. M. Wilson, A. Adra, N. Patel, S. Wilber, M. Shaikh, C. Forsyth, A. Keshavarzian, G. R. Swanson and D. Rick Sumner (2021). "Colon epithelial cell-specific Bmal1 deletion impairs bone formation in mice." bioRxiv: 2021.2008.2002.454190.

Kolbe, I., J. Husse, G. Salinas, T. Lingner, M. Astiz and H. Oster (2016). "The SCN Clock Governs Circadian Transcription Rhythms in Murine Epididymal White Adipose Tissue." J Biol Rhythms **31**(6): 577-587.

Kolbe, I., B. Leinweber, M. Brandenburger and H. Oster (2019). "Circadian clock network desynchrony promotes weight gain and alters glucose homeostasis in mice." Mol Metab **30**: 140-151.

Kuang, Z., Y. Wang, Y. Li, C. Ye, K. A. Ruhn, C. L. Behrendt, E. N. Olson and L. V. Hooper (2019). "The intestinal microbiota programs diurnal rhythms in host metabolism through histone deacetylase 3." Science **365**(6460): 1428-1434.

Kumar, S., G. Stecher, M. Li, C. Knyaz and K. Tamura (2018). "MEGA X: Molecular Evolutionary Genetics Analysis across Computing Platforms." Mol Biol Evol **35**(6): 1547-1549.

Lackey, A. I., T. Chen, Y. X. Zhou, N. M. Bottasso Arias, J. M. Doran, S. M. Zacharisen, A. M. Gajda, W. O. Jonsson, B. Corsico, T. G. Anthony, L. B. Joseph and J. Storch (2020). "Mechanisms underlying reduced weight gain in intestinal fatty acid-binding protein (IFABP) null mice." Am J Physiol Gastrointest Liver Physiol **318**(3): G518-G530.

Lagkouvardos, I., S. Fischer, N. Kumar and T. Clavel (2017). "Rhea: a transparent and modular R pipeline for microbial profiling based on 16S rRNA gene amplicons." PeerJ **5**: e2836.

Lambert, G., M. J. Amar, G. Guo, H. B. Brewer, Jr., F. J. Gonzalez and C. J. Sinal (2003). "The farnesoid X-receptor is an essential regulator of cholesterol homeostasis." J Biol Chem **278**(4): 2563-2570.

Langille, M. G., J. Zaneveld, J. G. Caporaso, D. McDonald, D. Knights, J. A. Reyes, J. C. Clemente, D. E. Burkepile, R. L. Vega Thurber, R. Knight, R. G. Beiko and C. Huttenhower (2013). "Predictive functional profiling of microbial communities using 16S rRNA marker gene sequences." Nat Biotechnol **31**(9): 814-821.

Lau, E., C. Marques, D. Pestana, M. Santoalha, D. Carvalho, P. Freitas and C. Calhau (2016). "The role of I-FABP as a biomarker of intestinal barrier dysfunction driven by gut microbiota changes in obesity." Nutr Metab (Lond) **13**: 31.

Lehmann, A. and P. J. Hornby (2016). "Intestinal SGLT1 in metabolic health and disease." Am J Physiol Gastrointest Liver Physiol **310**(11): G887-898.

Leone, V., S. M. Gibbons, K. Martinez, A. L. Hutchison, E. Y. Huang, C. M. Cham, J. F. Pierre, A. F. Heneghan, A. Nadimpalli, N. Hubert, E. Zale, Y. Wang, Y. Huang, B. Theriault, A. R. Dinner, M. W. Musch, K. A. Kudsk, B. J. Prendergast, J. A. Gilbert and E. B. Chang (2015). "Effects of diurnal variation of gut microbes and high-fat feeding on host circadian clock function and metabolism." Cell Host Microbe **17**(5): 681-689.

Li, F., C. Jiang, K. W. Krausz, Y. Li, I. Albert, H. Hao, K. M. Fabre, J. B. Mitchell, A. D. Patterson and F. J. Gonzalez (2013). "Microbiome remodelling leads to inhibition of intestinal farnesoid X receptor signalling and decreased obesity." Nat Commun **4**: 2384.

Li, Q., B. Wang, H. Y. Qiu, X. J. Yan, L. Cheng, Q. Q. Wang and S. L. Chen (2021). "Chronic Jet Lag Exacerbates Jejunal and Colonic Microenvironment in Mice." Front Cell Infect Microbiol **11**: 648175.

Li, Z., A. Chalazonitis, Y. Y. Huang, J. J. Mann, K. G. Margolis, Q. M. Yang, D. O. Kim, F. Cote, J. Mallet and M. D. Gershon (2011). "Essential roles of enteric neuronal serotonin in gastrointestinal motility and the development/survival of enteric dopaminergic neurons." J Neurosci **31**(24): 8998-9009.

Liang, X., F. D. Bushman and G. A. FitzGerald (2015). "Rhythmicity of the intestinal microbiota is regulated by gender and the host circadian clock." Proc Natl Acad Sci U S A **112**(33): 10479-10484.

Lin, H. V., A. Frassetto, E. J. Kowalik, Jr., A. R. Nawrocki, M. M. Lu, J. R. Kosinski, J. A. Hubert, D. Szeto, X. Yao, G. Forrest and D. J. Marsh (2012). "Butyrate and propionate protect against diet-induced obesity and regulate gut hormones via free fatty acid receptor 3-independent mechanisms." PLoS One **7**(4): e35240.

Liu, A. C., H. G. Tran, E. E. Zhang, A. A. Priest, D. K. Welsh and S. A. Kay (2008). "Redundant function of REV-ERBalpha and beta and non-essential role for Bmal1 cycling in transcriptional regulation of intracellular circadian rhythms." PLoS Genet **4**(2): e1000023.

Lloyd-Price, J., C. Arze, A. N. Ananthakrishnan, M. Schirmer, J. Avila-Pacheco, T. W. Poon, E. Andrews, N. J. Ajami, K. S. Bonham, C. J. Brislawn, D. Casero, H. Courtney, A. Gonzalez, T. G. Graeber, A. B. Hall, K. Lake, C. J. Landers, H. Mallick, D. R. Plichta, M. Prasad, G. Rahnavard, J. Sauk, D. Shungin, Y. Vazquez-Baeza, R. A. White, 3rd, I. Investigators, J. Braun, L. A. Denson, J. K. Jansson, R. Knight, S. Kugathasan, D. P. B. McGovern, J. F. Petrosino, T. S. Stappenbeck, H. S. Winter, C. B. Clish, E. A. Franzosa, H. Vlamakis, R. J. Xavier and C. Huttenhower (2019). "Multi-omics of the gut microbial ecosystem in inflammatory bowel diseases." Nature **569**(7758): 655-662.

Lozupone, C. A., J. Stombaugh, A. Gonzalez, G. Ackermann, D. Wendel, Y. Vazquez-Baeza, J. K. Jansson, J. I. Gordon and R. Knight (2013). "Meta-analyses of studies of the human microbiota." Genome Res **23**(10): 1704-1714.

Ma, K., P. K. Saha, L. Chan and D. D. Moore (2006). "Farnesoid X receptor is essential for normal glucose homeostasis." J Clin Invest **116**(4): 1102-1109.

Macfarlane, G. T., J. H. Cummings and C. Allison (1986). "Protein degradation by human intestinal bacteria." J Gen Microbiol **132**(6): 1647-1656.

Manella, G., E. Sabath, R. Aviram, V. Dandavate, S. Ezagouri, M. Golik, Y. Adamovich and G. Asher (2021). "The liver-clock coordinates rhythmicity of peripheral tissues in response to feeding." Nat Metab **3**(6): 829-842.

Martchenko, S. E., A. Martchenko, A. D. Biancolin, A. Waller and P. L. Brubaker (2021). "L-cell Arntl is required for rhythmic glucagon-like peptide-1 secretion and maintenance of intestinal homeostasis." Mol Metab **54**: 101340.

Masana, M. I., I. C. Sumaya, M. Becker-Andre and M. L. Dubocovich (2007). "Behavioral characterization and modulation of circadian rhythms by light and melatonin in C3H/HeN mice homozygous for the RORbeta knockout." Am J Physiol Regul Integr Comp Physiol **292**(6): R2357-2367.

Matsumoto, S., H. Setoyama and Y. Umesaki (1992). "Differential induction of major histocompatibility complex molecules on mouse intestine by bacterial colonization." Gastroenterology **103**(6): 1777-1782.

Metwaly, A., S. Reitmeier and D. Haller (2022). "Microbiome risk profiles as biomarkers for inflammatory and metabolic disorders." Nat Rev Gastroenterol Hepatol **19**(6): 383-397.

Moore, S. R., J. Pruszka, J. Vallance, E. Aihara, T. Matsuura, M. H. Montrose, N. F. Shroyer and C. I. Hong (2014). "Robust circadian rhythms in organoid cultures from PERIOD2::LUCIFERASE mouse small intestine." Dis Model Mech **7**(9): 1123-1130.

Mukherji, A., A. Kobiita, T. Ye and P. Chambon (2013). "Homeostasis in intestinal epithelium is orchestrated by the circadian clock and microbiota cues transduced by TLRs." Cell **153**(4): 812-827.

Muller, V. M., T. Zietek, F. Rohm, J. Fiamoncini, I. Lagkouvardos, D. Haller, T. Clavel and H. Daniel (2016). "Gut barrier impairment by high-fat diet in mice depends on housing conditions." Mol Nutr Food Res **60**(4): 897-908.

Natividad, J. M. and E. F. Verdu (2013). "Modulation of intestinal barrier by intestinal microbiota: pathological and therapeutic implications." Pharmacol Res **69**(1): 42-51.

Nieuwdorp, M., P. W. Gilijamse, N. Pai and L. M. Kaplan (2014). "Role of the microbiome in energy regulation and metabolism." Gastroenterology **146**(6): 1525-1533.

Nilsson, N. E., K. Kotarsky, C. Owman and B. Olde (2003). "Identification of a free fatty acid receptor, FFA2R, expressed on leukocytes and activated by short-chain fatty acids." Biochem Biophys Res Commun **303**(4): 1047-1052.

Nishida, A., R. Inoue, O. Inatomi, S. Bamba, Y. Naito and A. Andoh (2018). "Gut microbiota in the pathogenesis of inflammatory bowel disease." Clin J Gastroenterol **11**(1): 1-10.

Oh, H. Y. P., V. Visvalingam and W. Wahli (2019). "The PPAR-microbiota-metabolic organ trilogy to fine-tune physiology." FASEB J **33**(9): 9706-9730.

Oike, H., M. Sakurai, K. Ippoushi and M. Kobori (2015). "Time-fixed feeding prevents obesity induced by chronic advances of light/dark cycles in mouse models of jet-lag/shift work." Biochem Biophys Res Commun **465**(3): 556-561.

Pacha, J. and A. Sumova (2013). "Circadian regulation of epithelial functions in the intestine." Acta Physiol (Oxf) **208**(1): 11-24.

Parkar, S. G., A. Kalsbeek and J. F. Cheeseman (2019). "Potential Role for the Gut Microbiota in Modulating Host Circadian Rhythms and Metabolic Health." Microorganisms **7**(2).

Parker, K. D., S. E. Albeke, J. P. Gigley, A. M. Goldstein and N. L. Ward (2018). "Microbiome Composition in Both Wild-Type and Disease Model Mice Is Heavily Influenced by Mouse Facility." Front Microbiol **9**: 1598.

Parséus, A., N. Sommer, F. Sommer, R. Caesar, A. Molinaro, M. Ståhlman, T. U. Greiner, R. Perkins and F. Bäckhed (2017). "Microbiota-induced obesity requires farnesoid X receptor." Gut **66**(3): 429-437.

Parsons, M. J., T. E. Moffitt, A. M. Gregory, S. Goldman-Mellor, P. M. Nolan, R. Poulton and A. Caspi (2015). "Social jetlag, obesity and metabolic disorder: investigation in a cohort study." Int J Obes (Lond) **39**(5): 842-848.

Partch, C. L., C. B. Green and J. S. Takahashi (2014). "Molecular architecture of the mammalian circadian clock." Trends Cell Biol **24**(2): 90-99.

Pelikan, A., H. Herzel, A. Kramer and B. Ananthasubramaniam (2021). "Venn diagram analysis overestimates the extent of circadian rhythm reprogramming." FEBS J.

Penny, H. A., R. G. Domingues, M. Z. Krauss, F. Melo-Gonzalez, M. A. E. Lawson, S. Dickson, J. Parkinson, M. Hurry, C. Purse, E. Jegham, C. Godinho-Silva, M. Rendas, H. Veiga-Fernandes, D. A. Bechtold, R. K. Grencis, K. M. Toellner, A. Waisman, J. R. Swann, J. E. Gibbs and M. R. Hepworth (2022). "Rhythmicity of intestinal IgA responses confers oscillatory commensal microbiota mutualism." Sci Immunol **7**(75): eabk2541.

Peplonska, B., A. Bukowska and W. Sobala (2015). "Association of Rotating Night Shift Work with BMI and Abdominal Obesity among Nurses and Midwives." PLoS One **10**(7): e0133761.

Peterson, L. W. and D. Artis (2014). "Intestinal epithelial cells: regulators of barrier function and immune homeostasis." Nat Rev Immunol **14**(3): 141-153.

Polidarova, L., M. Sotak, M. Sladek, J. Pacha and A. Sumova (2009). "Temporal gradient in the clock gene and cell-cycle checkpoint kinase Wee1 expression along the gut." Chronobiol Int **26**(4): 607-620.

Preitner, N., F. Damiola, L. Lopez-Molina, J. Zakany, D. Duboule, U. Albrecht and U. Schibler (2002). "The orphan nuclear receptor REV-ERBalpha controls circadian transcription within the positive limb of the mammalian circadian oscillator." Cell **110**(2): 251-260.

Qiao, H., Z. Beibei, T. Chong, Z. Tieying, G. Yuzhi, M. Jing and P. M. Davidson (2020). "Both frequency and duration of rotating night shifts are associated with metabolic parameters: a cross-sectional study." Sleep Med **71**: 89-96.

Reiter, S., A. Dunkel, A. Metwaly, J. Panes, A. Salas, D. Haller and T. Hofmann (2021). "Development of a Highly Sensitive Ultra-High-Performance Liquid Chromatography Coupled to Electrospray Ionization Tandem Mass Spectrometry Quantitation Method for Fecal Bile Acids and Application on Crohn's Disease Studies." J Agric Food Chem **69**(17): 5238-5251.

Reitmeier, S., S. Kiessling, T. Clavel, M. List, E. L. Almeida, T. S. Ghosh, K. Neuhaus, H. Grallert, J. Linseisen, T. Skurk, B. Brandl, T. A. Breuninger, M. Troll, W. Rathmann, B. Linkohr, H. Hauner, M. Laudes, A. Franke, C. I. Le Roy, J. T. Bell, T. Spector, J. Baumbach, P. W. O'Toole, A. Peters and D. Haller (2020). "Arrhythmic Gut Microbiome Signatures Predict Risk of Type 2 Diabetes." Cell Host Microbe **28**(2): 258-272 e256.

Ridaura, V. K., J. J. Faith, F. E. Rey, J. Cheng, A. E. Duncan, A. L. Kau, N. W. Griffin, V. Lombard, B. Henrissat, J. R. Bain, M. J. Muehlbauer, O. Ilkayeva, C. F. Semenkovich, K. Funai, D. K. Hayashi, B. J. Lyle, M. C. Martini, L. K. Ursell, J. C. Clemente, W. Van Treuren, W. A. Walters, R. Knight, C. B. Newgard, A. C. Heath and J. I. Gordon (2013). "Gut microbiota from twins discordant for obesity modulate metabolism in mice." Science **341**(6150): 1241214.

Rios-Covian, D., P. Ruas-Madiedo, A. Margolles, M. Gueimonde, C. G. de Los Reyes-Gavilan and N. Salazar (2016). "Intestinal Short Chain Fatty Acids and their Link with Diet and Human Health." Front Microbiol **7**: 185.

Sadacca, L. A., K. A. Lamia, A. S. deLemos, B. Blum and C. J. Weitz (2011). "An intrinsic circadian clock of the pancreas is required for normal insulin release and glucose homeostasis in mice." Diabetologia **54**(1): 120-124.

Sanna, S., N. R. van Zuydam, A. Mahajan, A. Kurilshikov, A. Vich Vila, U. Vosa, Z. Mujagic, A. A. M. Masclee, D. Jonkers, M. Oosting, L. A. B. Joosten, M. G. Netea, L. Franke, A. Zhernakova, J. Fu, C. Wijmenga and M. I. McCarthy (2019). "Causal relationships among the gut microbiome, short-chain fatty acids and metabolic diseases." Nat Genet **51**(4): 600-605.

Savage, J. H., K. A. Lee-Sarwar, J. E. Sordillo, N. E. Lange, Y. Zhou, G. T. O'Connor, M. Sandel, L. B. Bacharier, R. Zeiger, E. Sodergren, G. M. Weinstock, D. R. Gold, S. T. Weiss and A. A. Litonjua (2018). "Diet during Pregnancy and Infancy and the Infant Intestinal Microbiome." J Pediatr **203**: 47-54 e44.

Schibler, U., J. Ripperger and S. A. Brown (2003). "Peripheral circadian oscillators in mammals: time and food." J Biol Rhythms **18**(3): 250-260.

Schroeder, B. O. (2019). "Fight them or feed them: how the intestinal mucus layer manages the gut microbiota." Gastroenterol Rep (Oxf) **7**(1): 3-12.

Segata, N., J. Izard, L. Waldron, D. Gevers, L. Miropolsky, W. S. Garrett and C. Huttenhower (2011). "Metagenomic biomarker discovery and explanation." Genome Biol **12**(6): R60.

Segers, A. and I. Depoortere (2021). "Circadian clocks in the digestive system." Nat Rev Gastroenterol Hepatol **18**(4): 239-251.

Segers, A., L. Desmet, T. Thijs, K. Verbeke, J. Tack and I. Depoortere (2019). "The circadian clock regulates the diurnal levels of microbial short-chain fatty acids and their rhythmic effects on colon contractility in mice." Acta Physiol (Oxf) **225**(3): e13193.

Singer, J. M. and J. J. Hughey (2019). "LimoRhyde: A Flexible Approach for Differential Analysis of Rhythmic Transcriptome Data." J Biol Rhythms **34**(1): 5-18.

Sooriyaarachchi, P., R. Jayawardena, T. Pavey and N. A. King (2022). "Shift work and the risk for metabolic syndrome among healthcare workers: A systematic review and meta-analysis." Obes Rev **23**(10): e13489.

Stephan, F. K. and I. Zucker (1972). "Circadian rhythms in drinking behavior and locomotor activity of rats are eliminated by hypothalamic lesions." Proc Natl Acad Sci U S A **69**(6): 1583-1586.

Stokes, K., M. Nunes, C. Trombley, D. Flores, G. Wu, Z. Taleb, A. Alkhateeb, S. Banskota, C. Harris, O. P. Love, W. I. Khan, L. Rueda, J. B. Hogenesch and P. Karpowicz (2021). "The Circadian Clock Gene, Bmal1, Regulates Intestinal Stem Cell Signaling and Represses Tumor Initiation." Cell Mol Gastroenterol Hepatol **12**(5): 1847-1872 e1840.

Stokkan, K. A., S. Yamazaki, H. Tei, Y. Sakaki and M. Menaker (2001). "Entrainment of the circadian clock in the liver by feeding." Science **291**(5503): 490-493.

Subramanian, B., S. Gao, M. J. Lercher, S. Hu and W.-H. Chen (2019). "Evolview v3: a webserver for visualization, annotation, and management of phylogenetic trees." Nucleic Acids Research **47**(W1): W270-W275.

Summa, K. C., R. M. Voigt, C. B. Forsyth, M. Shaikh, K. Cavanaugh, Y. Tang, M. H. Vitaterna, S. Song, F. W. Turek and A. Keshavarzian (2013). "Disruption of the Circadian Clock in Mice Increases Intestinal Permeability and Promotes Alcohol-Induced Hepatic Pathology and Inflammation." PLoS One **8**(6): e67102.

Tahara, Y., M. Yamazaki, H. Sukigara, H. Motohashi, H. Sasaki, H. Miyakawa, A. Haraguchi, Y. Ikeda, S. Fukuda and S. Shibata (2018). "Gut Microbiota-Derived Short Chain Fatty Acids Induce Circadian Clock Entrainment in Mouse Peripheral Tissue." Sci Rep **8**(1): 1395.

Tailford, L. E., E. H. Crost, D. Kavanaugh and N. Juge (2015). "Mucin glycan foraging in the human gut microbiome." Front Genet **6**: 81.

Teixeira, T. F., N. C. Souza, P. G. Chiarello, S. C. Franceschini, J. Bressan, C. L. Ferreira and C. Peluzio Mdo (2012). "Intestinal permeability parameters in obese patients are correlated with metabolic syndrome risk factors." Clin Nutr **31**(5): 735-740.

Thaben, P. F. and P. O. Westermark (2016). "Differential rhythmicity: detecting altered rhythmicity in biological data." Bioinformatics **32**(18): 2800-2808.

Thaiss, C. A., D. Zeevi, M. Levy, G. Zilberman-Schapira, J. Suez, A. C. Tengeler, L. Abramson, M. N. Katz, T. Korem, N. Zmora, Y. Kuperman, I. Biton, S. Gilad, A. Harmelin, H. Shapiro, Z. Halpern, E. Segal and E. Elinav (2014). "Transkingdom control of microbiota diurnal oscillations promotes metabolic homeostasis." Cell **159**(3): 514-529.

Thaiss, C. A., N. Zmora, M. Levy and E. Elinav (2016). "The microbiome and innate immunity." Nature **535**(7610): 65-74.

Thompson, G. R. and P. C. Trexler (1971). "Gastrointestinal structure and function in germ-free or gnotobiotic animals." Gut **12**(3): 230-235.

Thresher, R. J., M. H. Vitaterna, Y. Miyamoto, A. Kazantsev, D. S. Hsu, C. Petit, C. P. Selby, L. Dawut, O. Smithies, J. S. Takahashi and A. Sancar (1998). "Role of mouse cryptochrome blue-light photoreceptor in circadian photoresponses." Science **282**(5393): 1490-1494.

Tourlousse, D. M., S. Yoshiike, A. Ohashi, S. Matsukura, N. Noda and Y. Sekiguchi (2017). "Synthetic spike-in standards for high-throughput 16S rRNA gene amplicon sequencing." Nucleic Acids Res **45**(4): e23.

Turnbaugh, P. J., R. E. Ley, M. A. Mahowald, V. Magrini, E. R. Mardis and J. I. Gordon (2006). "An obesity-associated gut microbiome with increased capacity for energy harvest." Nature **444**(7122): 1027-1031.

Turnbaugh, P. J., V. K. Ridaura, J. J. Faith, F. E. Rey, R. Knight and J. I. Gordon (2009). "The effect of diet on the human gut microbiome: a metagenomic analysis in humanized gnotobiotic mice." Sci Transl Med **1**(6): 6ra14.

Ubeda, C., L. Lipuma, A. Gobourne, A. Viale, I. Leiner, M. Equinda, R. Khanin and E. G. Pamer (2012). "Familial transmission rather than defective innate immunity shapes the distinct intestinal microbiota of TLR-deficient mice." J Exp Med **209**(8): 1445-1456.

Ussing, H. H. and K. Zerahn (1951). "Active transport of sodium as the source of electric current in the short-circuited isolated frog skin." Acta Physiol Scand **23**(2-3): 110-127.

Vitaterna, M. H., D. P. King, A. M. Chang, J. M. Kornhauser, P. L. Lowrey, J. D. McDonald, W. F. Dove, L. H. Pinto, F. W. Turek and J. S. Takahashi (1994). "Mutagenesis and mapping of a mouse gene, Clock, essential for circadian behavior." Science **264**(5159): 719-725.

Vitaterna, M. H., C. P. Selby, T. Todo, H. Niwa, C. Thompson, E. M. Fruechte, K. Hitomi, R. J. Thresher, T. Ishikawa, J. Miyazaki, J. S. Takahashi and A. Sancar (1999). "Differential regulation of mammalian period genes and circadian rhythmicity by cryptochromes 1 and 2." Proc Natl Acad Sci U S A **96**(21): 12114-12119.

Voigt, R. M., C. B. Forsyth, S. J. Green, E. Mutlu, P. Engen, M. H. Vitaterna, F. W. Turek and A. Keshavarzian (2014). "Circadian disorganization alters intestinal microbiota." PLoS One **9**(5): e97500.

Voigt, R. M., K. C. Summa, C. B. Forsyth, S. J. Green, P. Engen, A. Naqib, M. H. Vitaterna, F. W. Turek and A. Keshavarzian (2016). "The Circadian Clock Mutation Promotes Intestinal Dysbiosis." Alcohol Clin Exp Res **40**(2): 335-347.

Wahlström, A., Sama I. Sayin, H.-U. Marschall and F. Bäckhed (2016). "Intestinal Crosstalk between Bile Acids and Microbiota and Its Impact on Host Metabolism." Cell Metabolism **24**(1): 41-50.

Wang, H. B., P. Y. Wang, X. Wang, Y. L. Wan and Y. C. Liu (2012). "Butyrate enhances intestinal epithelial barrier function via up-regulation of tight junction protein Claudin-1 transcription." Dig Dis Sci **57**(12): 3126-3135.

Wang, Y., Z. Kuang, X. Yu, K. A. Ruhn, M. Kubo and L. V. Hooper (2017). "The intestinal microbiota regulates body composition through NFIL3 and the circadian clock." Science **357**(6354): 912-916.

Wirbel, J., K. Zych, M. Essex, N. Karcher, E. Kartal, G. Salazar, P. Bork, S. Sunagawa and G. Zeller (2020). "Microbiome meta-analysis and cross-disease comparison enabled by the SIAMCAT machine-learning toolbox." bioRxiv: 2020.2002.2006.931808.

Woller, A. and D. Gonze (2021). "Circadian Misalignment and Metabolic Disorders: A Story of Twisted Clocks." Biology (Basel) **10**(3).

Wu, G., W. Tang, Y. He, J. Hu, S. Gong, Z. He, G. Wei, L. Lv, Y. Jiang, H. Zhou and P. Chen (2018). "Light exposure influences the diurnal oscillation of gut microbiota in mice." Biochem Biophys Res Commun(1090-2104 (Electronic)).

Wu, M., Y. Cai, J. Sun, H. Yang, J. Li, L. Wang, J. Zhang, L. Zhu and L. Xian (2010). "Effects of experimental chronic jet lag on hematological and immune parameters in mice." Biological Rhythm Research **41**(5): 363-378.

Wu, M., Y. Wu, J. Li, Y. Bao, Y. Guo and W. Yang (2018). "The Dynamic Changes of Gut Microbiota in Muc2 Deficient Mice." Int J Mol Sci **19**(9).

Wu, S. E., S. Hashimoto-Hill, V. Woo, E. M. Eshleman, J. Whitt, L. Engleman, R. Karns, L. A. Denson, D. B. Haslam and T. Alenghat (2020). "Microbiota-derived metabolite promotes HDAC3 activity in the gut." Nature **586**(7827): 108-112.

Yamazaki, S., R. Numano, M. Abe, A. Hida, R. Takahashi, M. Ueda, G. D. Block, Y. Sakaki, M. Menaker and H. Tei (2000). "Resetting central and peripheral circadian oscillators in transgenic rats." Science **288**(5466): 682-685.

Yao, Y., X. Cai, Y. Ye, F. Wang, F. Chen and C. Zheng (2021). "The Role of Microbiota in Infant Health: From Early Life to Adulthood." Front Immunol **12**: 708472.

Yoshimoto, S., T. M. Loo, K. Atarashi, H. Kanda, S. Sato, S. Oyadomari, Y. Iwakura, K. Oshima, H. Morita, M. Hattori, K. Honda, Y. Ishikawa, E. Hara and N. Ohtani (2013). "Obesity-induced gut microbial metabolite promotes liver cancer through senescence secretome." Nature **499**(7456): 97-101.

Yu, F., Z. Wang, T. Zhang, X. Chen, H. Xu, F. Wang, L. Guo, M. Chen, K. Liu and B. Wu (2021). "Deficiency of intestinal Bmal1 prevents obesity induced by high-fat feeding." Nature Communications **12**(1): 5323.

Yu, F., T. Zhang, C. Zhou, H. Xu, L. Guo, M. Chen and B. Wu (2019). "The Circadian Clock Gene Bmal1 Controls Intestinal Exporter MRP2 and Drug Disposition." Theranostics **9**(10): 2754-2767.

Zaibi, M. S., C. J. Stocker, J. O'Dowd, A. Davies, M. Bellahcene, M. A. Cawthorne, A. J. Brown, D. M. Smith and J. R. Arch (2010). "Roles of GPR41 and GPR43 in leptin secretory responses of murine adipocytes to short chain fatty acids." FEBS Lett **584**(11): 2381-2386.

Zarrinpar, A., A. Chaix, S. Yooseph and S. Panda (2014). "Diet and feeding pattern affect the diurnal dynamics of the gut microbiome." Cell Metab **20**(6): 1006-1017.

Zhang, R., N. F. Lahens, H. I. Ballance, M. E. Hughes and J. B. Hogenesch (2014). "A circadian gene expression atlas in mammals: implications for biology and medicine." Proc Natl Acad Sci U S A **111**(45): 16219-16224.

Zheng, B., U. Albrecht, K. Kaasik, M. Sage, W. Lu, S. Vaishnav, Q. Li, Z. S. Sun, G. Eichele, A. Bradley and C. C. Lee (2001). "Nonredundant roles of the mPer1 and mPer2 genes in the mammalian circadian clock." Cell **105**(5): 683-694.

Zheng, B., D. W. Larkin, U. Albrecht, Z. S. Sun, M. Sage, G. Eichele, C. C. Lee and A. Bradley (1999). "The mPer2 gene encodes a functional component of the mammalian circadian clock." Nature **400**(6740): 169-173.

Zhong, L. X., X. N. Li, G. Y. Yang, X. Zhang, W. X. Li, Q. Q. Zhang, H. X. Pan, H. H. Zhang, M. Y. Zhou, Y. D. Wang, W. W. Zhang, Q. S. Hu, W. Zhu and B. Zhang (2019). "Circadian misalignment alters insulin sensitivity during the light phase and shifts glucose tolerance rhythms in female mice." PLoS One **14**(12): e0225813.

Supplementary

Supplementary figures

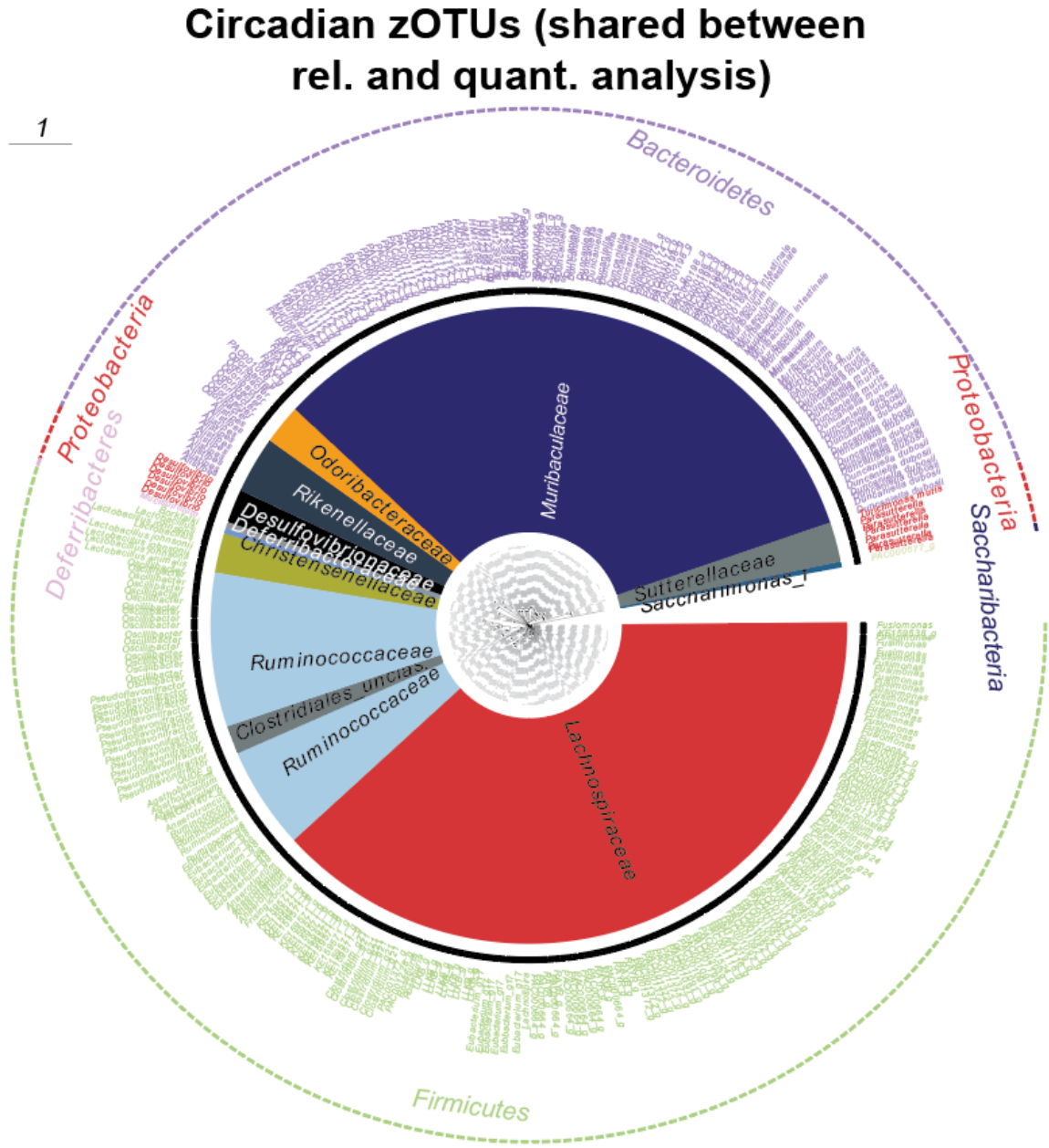

Supplementary figures 1: Circadian zOTUs

Taxonomic tree of circadian zOTUs that are shared between relative and quantitative analysis. Taxonomic ranking is indicated as the phylum level (outer dashed ring), family level (inner circle), and genus level (middle names). Every zOTU is represented by a single branch.

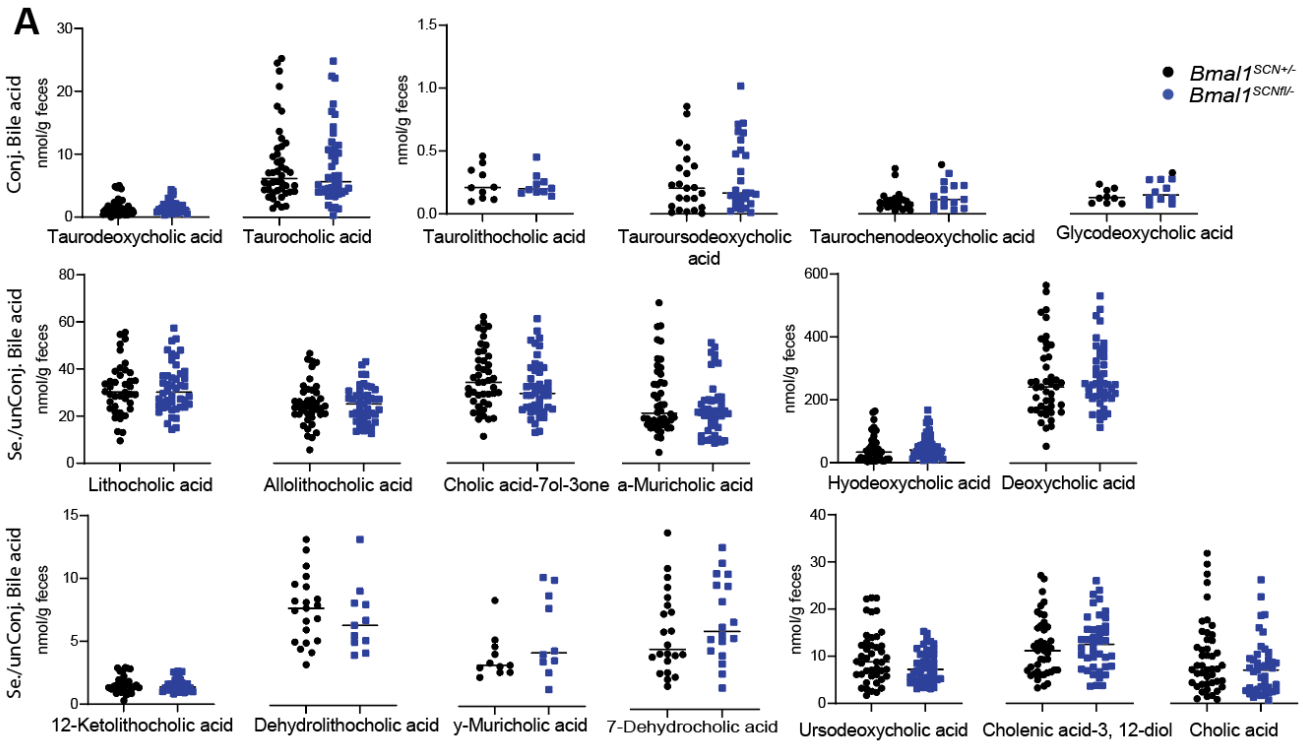

Supplementary figures 2: Lack of central clock induces slight alteration in bile acid concentrations

Fecal bile acid concentration in bmal1$^{SCNfl/-}$ mice and their controls. Bmal1$^{SCNfl/-}$ mice are represented by blue, while the controls are represented by black. N = 48 mice/genotype. Group differences were calculated based on Mann Whitney U test.

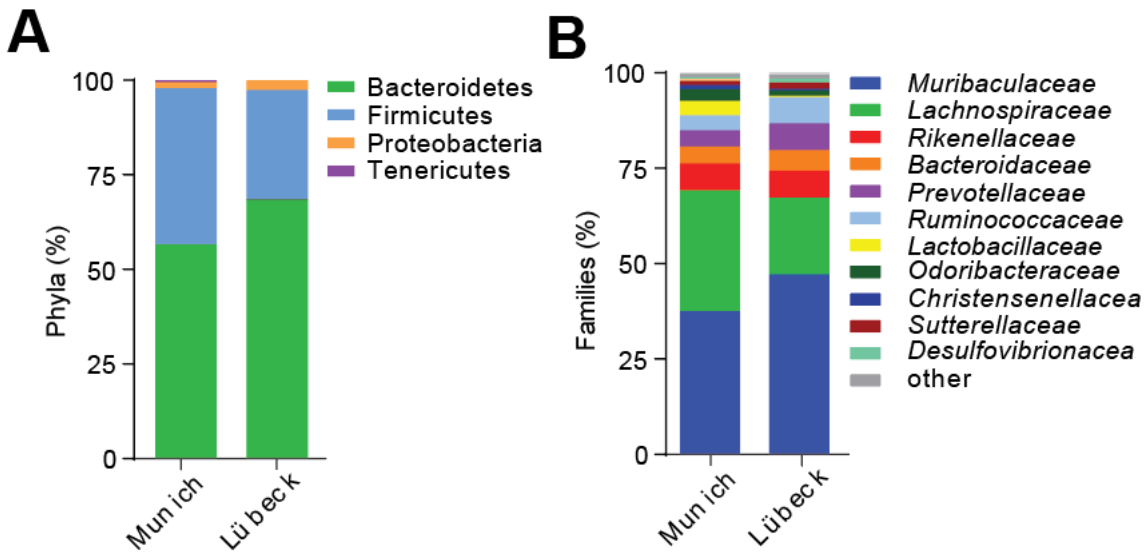

Supplementary figures 3: Different microbial composition between SSW and bmal1$^{SCNfl/-}$ mouse models

(A-B) Microbial composition at the phyla (A) and families (B) level according to relative analysis of fecal microbiota of SSW experiment (performed in Munich) and bmal1$^{SCNfl/-}$ experiment (performed in Lübeck). N = 48 mice/group.

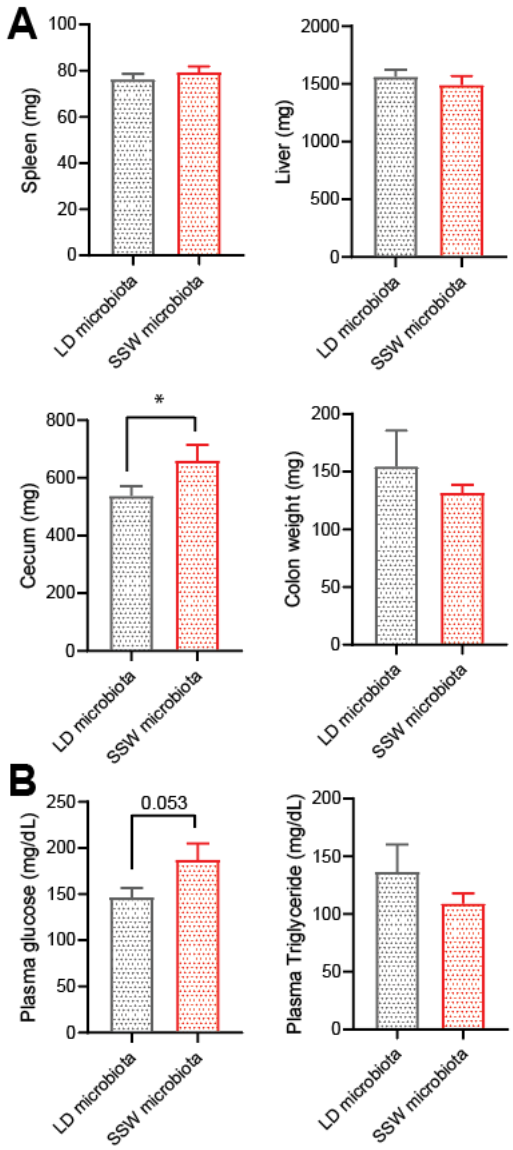

Supplementary figures 4: SSW microbiota has no impact on organ weights, plasma glucose and triglyceride

*(A-B) Bar charts represent organ weights (A), plasma glucose and Triglyceride (B) in germ free (GF) mice receiving SSW and LD microbiota. Red represents GF mice receiving SSW microbiota, while black represents GF mice receiving LD microbiota. N = 12 mice/recipient group. Differences were assessed by Mann Whitney U test. Significance * = p-value ≤ 0.05. Data are illustrated as mean ± SEM.*

List of figures

List of table

List of supplementary figures

Abbreviation

(ANG) Angiogenin

(BMAL1) Brain and Muscle ARNT-Like 1

(CCGs) Clock-controlled genes

(CKI) Casein kinases

(CLOCK) Circadian Locomotor Output Cycles Kaput

(CRY) Cryptochrome

(CT) Circadian time

(DBP) D Site Of Albumin Promoter (Albumin D-Box) Binding Protein

(DCA) Deoxycholic acid

(DD) Constant darkness

(DNA) Deoxyribonucleic acid

(EC) Enzyme commission

(EDTA) Ethylenediaminetetraacetic acid

(EF1A) Elongation factor 1-alpha

(EWAT) Epididymal white adipose tissue

(FABP) Fatty Acid Binding Protein

(FXR) Farnesoid X receptor

(GF) Germ free

(GITT) Gastrointestinal transit time

(GLUT) Glucose transporter

(G. UNIFRAC) Generalized UniFrac distances

(HDAC) Histone Deacetylase

(IBD) Inflammatory bowel disease

(IEC) Intestinal epithelial cells

(IFABP) Intestinal-type fatty acid-binding protein

(IL) Interleukin

(LD) Light-dark cycle

(LGR5) Leucine Rich Repeat Containing G Protein-Coupled Receptor 5

(LPS) Lipopolysaccharides

(MRM) Multiple reaction monitoring

(MUC2) Mucin 2

(NFIL3) Nuclear Factor, Interleukin 3

(NFKB) Nuclear factor kappa-light-chain-enhancer of activated B cells

(NMR) Nuclear magnetic resonance

(OTUS) Operational taxonomic units

(PBS) Phosphate buffer saline

(PER) Period

(PP) Protein phosphatases

(PPARG) Peroxisome Proliferator Activated Receptor Gamma

(QPCR) Quantitative real-time polymerase chain reaction

(RCF) Relative centrifugal force

(REG IIIγ) Regenerating islet-derived protein 3 gamma

(REV-ERBA) Nuclear receptor subfamily 1 group D member 1

(RNA) Ribonucleic acid

(ROR ALPHA) RAR-related orphan receptor alpha

(SCFA) Short-chain fatty acid

(SCN) Suprachiasmatic Nuclei

(SGLT) Sodium/glucose cotransporter protein

(SPF) Specific-pathogen free

(SSW) Simulated shift work

(TLR) Toll like receptor

(TNFA) Tumor necrosis factor alpha

(UPL) Universal Probe Library system

(WCA) Wilkins-Chalgren Anaerobe

(ZOTUS) zero-radius operational taxonomic units

(ZT) *Zeitgeber* time

Acknowledgements

I would like to thank my supervisor and mentor, Dr. Silke Kiessling, for introducing me to this fascinating topic and for her guidance. Moreover, I want to express my gratitude to my supervisor, Prof. Dirk Haller, for his valuable feedback. A special thanks to all members of Haller's group for sharing this journey. In addition, I want to thank our collaborators at Lübeck University, especially Dr. Violetta Pilorz and Prof. Henrik Oster, for their insights and for providing the *bmal1*$^{SCN\ fl/-}$ mouse model.

Special thanks go to the DAAD for giving me the scholarship to complete my studies. I have been so lucky to have such an amazing chronobiology group: Marjolein Heddes, Yunhui Niu, Elezavita Gorbunova and Ziva Fras.

This work would not be possible without the help and encouragement of many great friends and colleagues, especially Mohamad, Amira, Sevana, Silvia, Steffi, Mohsen, Adam, Dorian, Helene, Brita, and Nico

My family, Mohamed, Hend, Rand, and Mahmoud, thank you very much for all the support throughout my life and for giving me a sense of safety from having you. I cannot express how lucky I am to have you.

Publication and presentation

Published manuscript

1- **Altaha, B**., Heddes, M., Pilorz, V., Niu, Y., Gorbunove, E., Gigl, M., Kleigrewe, K., Oster, H., Haller, D. & Kiessling, S. 2022. Genetic and environmental circadian disruption induce weight gain through changes in the gut microbiome. *Molecular Metabolism***,** 101628.

2- Heddes, M.*, **Altaha, B.***, Niu, Y., Reitmeier, S., Kleigrewe, K., Haller, D. & Kiessling, S. 2022. The intestinal clock drives the microbiome to maintain gastrointestinal homeostasis. *Nature Communications*, 13**,** 6068.

Manuscript in preparation

1- Heddes, M., Niu, Y., **Altaha, B.**, Gorbunova, E., Kleigrewe, K., Bruder, J., Meng, C., Haller, D. and Kiessling, S. The intestinal clock controls diet induced obesity by driving the microbiome and balancing host's metabolism. In preparation

2- Niu, Y., Heddes, M., **Altaha, B.**, Birkner, M., Kleigrewe, K., Meng, C., Haller, D. & Kiessling, S. 2023. Targeting the intestinal circadian clock by meal timing ameliorates gastrointestinal inflammation. *bioRxiv***,** 2023.01.24.525433.

Oral presentation

1- European Biological Rhythms Society congress. **EBRS 2022. Zürich, Switzerland.** Heddes, M.*, **Altaha, B.***, Niu, Y., Reitmeier, S., Kleigrewe, K., Haller, D. & Kiessling, S. The intestinal clock drives the microbiome to maintain gastrointestinal homeostasis

2- Emerging Applications of Microbes. **VIB conference 2022. Leuven, Belgium** **Altaha, B**., Heddes, M., Pilorz, V., Niu, Y., Gorbunove, E., Gigl, M., Kleigrewe, K., Oster, H., Haller, D. & Kiessling, S. 2022. Genetic and environmental circadian disruption induce weight gain through changes in the gut microbiome.

Poster presentation

1- European Biological Rhythms Society congress. **EBRS 2022. Zürich, Switzerland.** Heddes, M.*, **Altaha, B.***, Niu, Y., Reitmeier, S., Kleigrewe, K., Haller, D. & Kiessling, S. The intestinal clock drives the microbiome to maintain gastrointestinal homeostasis

2- Emerging Applications of Microbes. **VIB conference 2022. Leuven, Belgium** **Altaha, B**., Heddes, M., Pilorz, V., Niu, Y., Gorbunove, E., Gigl, M., Kleigrewe, K., Oster, H., Haller, D. & Kiessling, S. Genetic and environmental circadian disruption induce weight gain through changes in the gut microbiome.

List of cited publications

1- **Altaha, B**., Heddes, M., Pilorz, V., Niu, Y., Gorbunove, E., Gigl, M., Kleigrewe, K., Oster, H., Haller, D. & Kiessling, S. 2022. Genetic and environmental circadian disruption induce weight gain through changes in the gut microbiome. *Molecular Metabolism***,** 101628.

2- Heddes, M.*, **Altaha, B.***, Niu, Y., Reitmeier, S., Kleigrewe, K., Haller, D. & Kiessling, S. 2022. The intestinal clock drives the microbiome to maintain gastrointestinal homeostasis. *Nature Communications*, 13**,** 6068.

Hiermit erkläre ich an Eides statt, dass ich Hauptautor der zwei oben genannten Publikationen und Studien bin, die in dieser Arbeit wörtlich zitiert wurden.

Ort, den .....

Unterschrift